THÈSE DE DOCTORAT

Spécialité: **Computational Neuroscience**

École Doctorale Informatique, Télécommunications et Electronique

Présentée par

Tianyi LI

Pour obtenir le grade de

DOCTEUR de Sorbonne UNIVERSITÉ

Sujet de la thèse :

Vision, Mutlisensory Integration and Aging in an Integrated Computational Model of Spatial Memory

Soutenue le 13 décembre 2019 devant le jury composé de:

Bruno Gas – Sorbonne Université, Paris, France	Président du jury
Eleni Vasilaki – Université de Sheffield, Royaume-Uni	Rapporteur
Mathias Quoy – Université de Cergy-Pontoise, France	Rapporteur
Mehdi Khamassi – Sorbonne Université, Paris, France	Examinateur
Denis Sheynikhovich – Sorbonne Université, Paris, France	Encadrant de thèse
Angelo Arleo – Sorbonne Université, Paris, France	Directeur de thèse

Abstract

An ever growing body of neuroscientific data is becoming available from various animal species, including humans, due to technological advances in capturing brain signals and behavior linked with them. These increasing amounts of data, together with an unprecedented power and memory capacity of present day computers calls for large scale computational models with the objective of unifying, storing and analysing these data. Moreover, such models allow crosslinking computational studies from various domains and in various levels of neural hierarchy to provide a deeper understanding of neuronal mechanisms underlying various cognitive phenomena and their link with behavior. The objective of this thesis is to develop an integrated model of human behavior in the context of spatial orientation and its deterioration with age.

The problem of spatial cognition is considered as a problem of combining external sensory cues coming from the environment and internal sensory cues coming from self-motion information, with the objective to build a mental representation of surrounding space. A large body of experimental research suggests that this representation is constructed within an intricate network of brain areas residing in the medial temporal lobe, with external sensory input arriving via a "dorsal" visual path originating in early visual areas and passing via the parietal cortex. Aging has been shown to strongly affect medial temporal lobe networks and associated memory-based behaviors, and in particular the creation of mental representations of space.

In this thesis we develop an integrated neural network model of spatial memory by based on anatomical and functional experimental evidence of sensory information processing in the dorsal visual path and medial temporal lobe networks. We use this model to simulate a number of experiments linking human visual functions with spatial orientation behaviors, and propose how visual cues are combined with self-motion input during the construction of mental maps of space. We then test the hypothesis that aging exerts its deteriorating effects on spatial memory via acting on neuromodulatory action in the brain and is linked with reduced novelty processing in the medial temporal lobe. Overall, the work performed during this doctoral thesis provides a first step towards building an integrated computer platform for human behavior simulation and contributes to a better understanding of how spatial representations are built from sensory signals and are affected by aging.

Contents

Abstract **i**

1 Motivation and Objectives **1**

2 Anatomy of Spatial Navigation, Vision & Aging and the Architecture of the Aging Human Avatar **7**

2.1 Spatial navigation 7

2.2 Visuospatial processing in the primate dorsal visual pathway 11

2.3 Spatial representation in rodents 13

2.3.1 Hippocampal formation 14

2.3.2 Head direction cells 19

2.3.3 Grid cells in the dorsomedial entorhinal cortex 20

2.3.4 Hippocampal place cells 22

2.3.5 Firing determinants of place cells 23

2.4 Aging and spatial memory 25

2.5 Aging Human Avatar platform 28

2.5.1 Software architecture 28

2.5.2 Functional architecture 30

3 Computational Model of the Dorsal Visual Pathway **32**

3.1 Introduction 34

3.2 Methods 37

3.2.1 Occipito-parietal input circuit 38

3.2.2 Head direction 39

3.2.3 Parietal transformation network . . . 39
3.2.4 Hippocampal neurons . . . 44
3.2.5 Reorientation network . . . 45
3.2.6 Simulation details . . . 48
3.3 Results . . . 52
3.3.1 Visual and parietal model neurons encode sensory representations in distinct reference frames . . . 53
3.3.2 Spatial coding using temporal accumulation of successive views . 54
3.3.3 Visual responses of hippocampal neurons reflect learning of visual stimuli . . . 58
3.3.4 Top-down hippocampal input in spatial reorientation and memory-based search . . . 59
3.4 Discussion . . . 66

4 Entorhinal-Hippocampal Loop as a Multisensory Integration Circuit 71
4.1 Introduction . . . 74
4.2 Methods . . . 75
4.2.1 Visual input . . . 76
4.2.2 Integration of visual and self-motion input by grid cells . . . 78
4.2.3 Encoding of visual and self-motion input by place cells . . . 80
4.2.4 Simulations . . . 82
4.3 Results . . . 86
4.3.1 Simulation of the merged-room experiment . . . 89
4.3.2 Simulation of the double-room experiment . . . 93
4.4 Discussion . . . 97

5 Modeling the Impact of Aging on the Entorhinal-Hippocampal Network 105
5.1 Introduction . . . 107
5.2 Methods . . . 109
5.2.1 Hippocampal memory recall . . . 110
5.2.2 Encoding of visual and self-motion input by place cells . . . 111
5.2.3 Cholinergic modulation . . . 114

5.2.4 Age-related degradation of cholinergic release 116
5.2.5 Simulations 116
5.3 Results 117
5.3.1 Learning of novel environments by aged rats 117
5.3.2 Age-related effects on the switch between idiothetic and allothetic cues 123
5.4 Discussion 127

6 General discussion **130**
6.1 Thesis summary and conclusions 130
6.2 Contributions of the thesis and related work 132
6.3 Experimental predictions 135
6.4 Limitations and future work 136

A List of contributions **139**

List of Figures

2.1 **Response (egocentric) vs Place (allocentric) learning.** 10
2.2 **Anatomy of the hippocampal formation.** 14
2.3 **Schematic representation the hippocampal formation network.** 16
2.4 **Schematic illustration of grid cells.** 21
2.5 **Software architecture of the AHA platform.** 29
2.6 **Functional architecture of the AHA platform.** 31

3.1 **Anatomy and schematic model of the dorsal visual pathway** 36
3.2 **Implementation of the reorientation network.** 47
3.3 **Properties of neurons in the coordinate-transformation network.** 54
3.4 **Temporal accumulation of successive visual snapshots in the model.** . 56
3.5 **Representation of spatial relations by egocentric (occipito-parietal) and allocentric (parieto-retrosplenial) visual neurons.** 57
3.6 **Visual responses of modeled hippocampal neurons.** 60
3.7 **Simulation of the reorientation experiment.** 62
3.8 **Simulation of memory-based visual search task.** 65

4.1 **Schematic representation of the entorhinal-hippocampal loop model** . 77
4.2 **Multisensory integration in modeled place cells.** 87
4.3 **Multisensory integration in grid cells.** 89
4.4 **Simulation of the merged-room experiment of Wernle et al. (2018).** . 90
4.5 **Place fields in the merged-room experiment.** 92
4.6 **Influence of plasticity and dynamics on grid patterns in the merged-room experiment.** 93
4.7 **Simulation of the double-room experiment of Carpenter et al. (2015)** . 95

4.8 **Evolution of place fields in the double room experiment.** 96
4.9 **Mismatch between the visual and self-motion representations.** 97

5.1 **Model of cholinergic influence in the entorhinal-hippocampal loop.** . 110
5.2 **A model of cholinergic release based on CA1 feedback projection.** . . 114
5.3 **Global place-cell remapping and grid realignment in adult rats** 119
5.4 **Absence of remapping and grid realignment in aged rats** 120
5.5 **Comparison between adult and aged simulated rats** 121
5.6 **Properties of simulated acetylcholine activity in aged and adult rats** . 122
5.7 **The linear track experiment and simulation** 124
5.8 **Mismatch correction between idiothetic and allothetic cues.** 125
5.9 **Cholinergic influence on the transition between self-motion and visual cues.** 126

List of Tables

2.1 **Distinctions between stimulus-response and cognitive navigation strategies** 8

3.1 **Parameters of the dorsal visual pathway model** 49

4.1 **Parameters of the entorhinal-hippocampal loop model** 83

5.1 **Parameters of the acetylcholine-modulated entorhinal-hippocampal loop model.** 117

Chapter 1

Motivation and Objectives

Recent advances in experimental methods of data acquisition provide a wealth of empirical data in various domains of human and animal neuroscience, from detailed characterization of behavior (e.g. oculomotor, navigational or executive) to single cell recordings in different areas of the brain. The unprecedented rate at which these data are collected calls for the need to create large-scale computational models with the aim of data unification, analysis and synthesis. These aims are crucial if computer models are to be used as reliable personalized predictors of human behavior in various situations. Current efforts in various computational research domains address these challenges in different ways. For example, detailed computational models of neural activities during specific behaviors in well-controlled conditions provide elementary building blocks for large-scale cognitive models, but they do not address the issue of how these building blocks work together in an integrated way (Madl et al., 2015; O'Reilly et al., 2010). On the other hand, neurorobotic models address the utility of well-described neuronal mechanisms for the purpose of creating efficient robots with animal- or human-like capabilities, but they usually rely on non-human-like robot-environment interfaces that depend on the robotic platform in question (Sanders and Oberts, 2016; Cox and Krichmar, 2009). Finally, existing large-scale brain models address the computational principles of how brain solves complex tasks but they are usually not interested in how these brain models are embedded into bodies with human-like sensory organs (Kriegeskorte and Douglas, 2018). One approach to overcome the above drawbacks and to combine their advantages is to create computer

simulation platforms that integrate known and experimentally measurable properties of human sensory and cognitive capabilities - human avatars. The general aim of a human avatar model is to serve as a personalized 3D model of a particular human person with sub-models of both sensory organs and high-level associative and mnemonic areas of the brain tuned by available experimental data measured on the same person. The main motivation of this thesis is to make a step towards creating such an integrated human model in the context of spatial cognition. The specific domain of human science where such an integrated model can be of great utility is aging. Aging is an issue with increasing societal impact and it is known to early and profoundly affect spatial orientation capabilities, limiting the elderlies' autonomy and quality of life (Moffat, 2009).

Spatial cognition refers to the ability of the organism to create mental representations of the surrounding environment with the purpose of using these representations for future spatial behaviors. When we visit a city for the first time and take a walk from the hotel, later on we may find ourselves lost, unless we carefully track all the turns and progressions we made, or unless we find a currently visible landmark on a city map. As we gradually become familiar with the new city by daily exploration, we start recognizing streets and buildings encountered before and can eventually generate routes linking different locations in the city event without a map. When that happens, it can be said that we have built a mental representation of the city, or a '*cognitive map*' (Tolman, 1948; Moser et al., 2008; Herweg and Kahana, 2018). While humans, as many other animals, have this cognitive ability to naturally construct spatial representations of surrounding spaces, how a physical environment can be represented in the brain is a long-studied question in neuroscience (Moser et al., 2017).

The question of cognitive map construction can be cast in terms of sensory cue processing. As long as we move through space, we keep interacting with it through various sensory channels that can be classified as either idiothetic or allothetic. *Idiothetic cues* correspond to internal self-motion related cues, generated by body movements. They include proprioceptive information, vestibular sense, and optic flow. These cues are used to track position relative to some origin by integrating them in time, an ability termed "path integration" (Müller and Wehner, 1988; Loomis et al., 1993; Etienne and Jeffery, 2004). *Allothetic*

cues are perceived from the external environment by multiple sensory modalities including vision, audition and olfaction. These cues can be used together with path integration in order to build spatial representations. Primates, including humans, rely most strongly on vision (Epstein et al., 1999; Epstein and Vass, 2014; Ekstrom, 2015), while rodents are much less visual animals. Since the two types of cues provide all available sensory information, the question of the construction of mental representations can be reformulated as the question of how idiothetic and allothetic cues are combined to build them.

Animal behavior in space, and in particular the way they encode the location and direction of important sensory cues during navigation, can generally be described with respect to two spatial reference frames, classified as egocentric (subject-centered) or allocentric (world- or object-centered). In the *egocentric reference frame* positions and directions are defined relative to the subject itself. As long as the subject moves, the position and direction of external cues move together with her or him. On the other hand, in the *allocentric reference frame* positions and directions are defined relative to the external space or landmarks within it and are independent from the subject's current location and heading. Because of this property of being invariant with respect to the subject, position and orientation of sensory cues, remembered with respect to an allocentric reference frame, are believed to contribute to the establishment of cognitive maps of space (Moser et al., 2008; Herweg and Kahana, 2018). A cognitive map can provide information about the location of the subject with respect to external landmarks as well as spatial relations between landmarks. However, since all the information coming via sensory receptors, such as the retina, are defined in an egocentric frame, an important issue is how the brain transforms egocentric sensory cues into allocentric mental representations (Byrne and Becker, 2008). While the primate visual system is one of the most studied in neuroscience, how visual information is transformed on its way to memory structures thought to store cognitive maps is a largely an unresolved question (Ekstrom, 2015).

In **Chapter 3** we propose a spiking neural network model of information processing in the primate dorsal visual path, that is thought to mediate information transfer between visual and mnemonic structures in the hippocampal formation.

The concept of a cognitive map was a purely psychological one until O'Keefe and Dostrovsky (1971) discovered neurons in the hippocampus, termed *place cells*, whose activities are correlated with an animal's location in space. In an influential book the authors proposed that place cell firing represents the position of the animal within the mental map of the environment (O'Keefe and Nadel, 1978). If this mental map is correct (i.e. coherent with the real environment), then place cell activity will also represent a particular place in the environment. Some 20 years after, Taube et al. (1990b,a) described neurons in an area nearby to the hippocampus, called '*head direction cells*', that fire as a function of the head direction of the animal, irrespective of its location. In another 15 years Hafting et al. (2005) discovered yet other neurons, named '*grid cells*', that reside in the entorhinal cortex and fire at multiple spatial locations organized in a hexagonal periodical grid covering the whole area of the experimental environment. Place cells, grid cells, and head direction cells, together with some other neuron types with spatially correlated firing properties (Sargolini et al., 2006), are considered as basic neuronal elements for constructing cognitive maps. Since these neuron types reside in the hippocampus and nearby structures, the hippocampal formation is the principal memory area thought to support cognitive map formation and storage. By successive stages of processing within the entorhinal-hippocampal loop, idiothetic and allothetic cues are thought to be combined by interactive populations of different neuron types to create spatial representations.

In **Chapter 4** we propose a neural network model of multisensory combination between allothetic visual and idiothetic self-motion cues within the entorhinal-hippocampal processing loop. A crucial difference between our model and previous models is the existence of bidirectional dynamic interactions between place cells and grid cells during behavior and the ability to create maps of multi-compartment environments

When we age, our ability of constructing mental maps of space deteriorates. Aging is an inevitable process associated with functional decline in selective aspects of cognitive performance and brain function (Moffat, 2009; Rodgers et al., 2012; Gracian et al., 2013). In particular, the hippocampal formation and spatial navigation functions are extremely vul-

nerable to the influence of aging (Burke and Barnes, 2006). Age-related spatial orientation and wayfinding deficits strongly influence healthy elderlies' life and manifest themselves in various mobility impairments and increased avoidance of novel environments. While there are many hypotheses of aging, neural-level accounts of the role of aging in spatial navigation principally concern synaptic plasticity and neuromodulation (Rosenzweig et al., 2003; Ikonen et al., 2002). While primate and human data on the neural underpinnings of age-related spatial navigation deficits is very limited, electrophysiological and behavioral experiments from aged rodents suggest several principal ways of how age-related changes in the entorhinal-hippocampal processing loop can affect behavior. Despite multiple attempts to describe a conceptual model of neural-level effect of aging, no computational accounts of this process have been given so far.

In **Chapter 5** we propose a neural network model of the effects of aging in spatial navigation. We study the hypothesis that an age-induced dysfunction of cholinergic processing causes synaptic plasticity deficits, which in turn affects neuronal processing in the entorhinal-hippocampal loop.

Thus, if one aims at constructing an integrated model of human spatial cognition for the purpose of studying how age affects spatial memory, which is the main objective of this thesis, one is confronted with the task of integrating the above knowledge in a single modeling platform that we refer to here as Aging Human Avatar (Sheynikhovich et al., 2019). This integrated model is presented in four subsequent chapters. Chapter 2 provides anatomical details of modeled biological networks and some technical details of the Aging Human Avatar platform. As mentioned above, Chapters 3-5 of this thesis focus on three principal questions: *(i)* What are the neural mechanisms supporting the transformation of egocentric visual signals to allocentric representations in the primate visual processing pathway?; *(ii)* How are the allothetic visual and idiothetic self-motion cues integrated together in the entorhinal-hippocampal processing loop during the construction of a mental representation of the multi-compartment experimental environments?; *(iii)* Can age-related behavioral effects, observed in aged rodents, be explained by an impairment

of cholinergic neuromodulatory circuit?

The future Aging Human Avatar platform, of which the basic proof-of-concept is presented in this work, is aimed at simulating a variety of modeled age-related effects on spatial navigation, and at providing a 'transparent' tool to infer new hypotheses cross-linking sensory and cognitive aspects of aging. As in computer simulations presented in the following chapters, the Human Avatar interacts with its 3D environment through multimodal active sensing and locomotion. It perceives the world and acquires spatial representations based on data-grounded models of age-related influences on visual and spatial orientation functions. While this thesis provides only a first step towards creation of such an integrated model, the objective of future implementations is to integrate a large body of knowledge about neural processes underlying human spatial behavior and generate new insights and experimentally testable predictions age-related markers of vision-dependent mobility and autonomy loss. We believe that the issues of visuospatial coordinate transformations and multisensory integration addressed in this thesis provide a necessary prerequisites for the understanding of aging effects on human spatial navigation and creation of detailed computer models of this important cognitive capability.

Chapter 2

Anatomy of Spatial Navigation, Vision & Aging and the Architecture of the Aging Human Avatar

Chapter summary

The aim of this chapter is twofold. First, it presents some details of anatomical structures that are thought to support visuospatial orientation and are modeled in subsequent chapters. In particular, afferent and efferent connections are described for these structures, and their overall connection patterns. In addition, principal neuron types thought to support spatial orientation functions are presented and experimental evidence of age-related effects on these neuron types is reviewed. Second, it presents the Aging Human Avatar platform, a software simulation platform to the development of which this doctoral work has contributed. In particular, the software architecture and main functional modules of this platform are presented.

2.1 Spatial navigation

Spatial navigation is an ability of planning and performing a path from the current position towards a desired location (Gallistel, 1990; Brodbeck and Tanninen, 2012). Two funda-

Navigation type	taxon	locale
Frame of reference	egocentric	allocentric
Learning mode	stimulus-response	place
Dimensionality of trajectory space	1D (route)	2D (map)

Table 2.1: Distinctions between stimulus-response and cognitive navigation strategies

mentally different strategies of navigation can be classified (O'Keefe and Nadel, 1978). *Locale navigation* defines movement as happening from one place to another, where 'place' is an abstract concept defined as a position on the cognitive map of the environment. In contrast, *Taxon navigation* is the one in which goal-oriented movements are defined by a reference to sensory cues external to the subject, e.g. movement in the direction of a landmark or away from it, movement in the direction of a specific odor, movement along a wall, etc. An important difference between these two types, or strategies, of navigation[1] is in flexibility with which different goal-directed paths can be generated. Whereas the taxon navigation learns a specific path and is quite easily disrupted by the change of associated sensory cues, the locale navigation is flexible in the choice of the path from one place to another and is relatively unaffected by the effects of environmental alternations.

Several divisions related to locale/taxon are used in the experimental literature (see Table 2.1), reflected different respect of the two strategies

Egocentric vs Allocentric. As mentioned in Chapter 1, the egocentric frame of reference is defined relative with respect to the subject. The current position of the subject defines the origin of such a reference frame and his or her the current heading defines the reference direction (i.e. 0°). In contrast, the allocentric frame of reference is defined with respect to static sensory cues external to the subject, i.e. independent of the subject's current position and heading (Fig. 2.1c). For example, the center of a recording chamber can serve as the origin of an allocentric reference frame, and direction towards the eastern wall can serve as a reference direction. An important distinction between the goal-oriented behaviors organized in the two reference frames is that knowing the goal position in the egocentric reference frame is sufficient to approach the goal, whereas knowledge of the

[1] A number of different taxonomies of navigation exist that propose further subclasses of either the taxon or locale navigation (see Gallistel (1990); Trullier et al. (1997); Redish (1999); Arleo and Rondi-Reig (2007))

goal's allocentric coordinates can be used only if the current allocentric position of the subject is known as well.

Response vs Place learning. Behavioral experiments dealing with dissociation between different navigation strategies usually describe behavioral decision in terms of response (egocentric) and place (allocentic) strategies (the terms are equivalent to the taxon and locale strategies, but emphasize the result of learning). The response learning strategy[2] amounts to remembering a specific motor response to a set of visual or other sensory stimuli (e.g. turning right in the central junction of a maze), whereas the place strategy requires memory for a location of the food with respect to the extra-maze visual cues. The two strategies can be dissociated by observing human behavior in altered experimental conditions: subjects that learned the response strategy will repeat the same motor response, while those who learned the place strategy will go to the same place (Fig. 2.1b). Such dissociation experiments together with imaging studies provide an insight into the biological mechanisms that implement those strategies (Rodgers et al., 2012; Bécu et al., 2019).

Routes vs Maps. Lastly, the taxon/locale strategies can be distinguished on the basis of trajectories that these strategies generate. The taxon behavior propose movements along a one-dimensional route because each stimulus-response association suggests a particular movement in a particular direction. In contrast, the locale strategy allows for making shortcuts and detours instead of specifying a path how to get from one place to another. Moreover, locale strategy is able to plan paths from novel starting positions, belonged to the cognitive map, to a goal. In contrast, taxon navigation suggest an exact repetition of learned responses and thus unable to generalize paths for novel starting positions not seen during training. The latter distinction has been used to experimentally segregate the two strategies.

This thesis focuses on *place learning* and a construction of neural *maps* of space, as defined above. Moreover, since we are interested in primarily human-like visuospatial behavior,

[2]Sometimes it is also referred to as *stimulus-response* or *cue-response* strategy, when response to a particular visual cue is learned

A

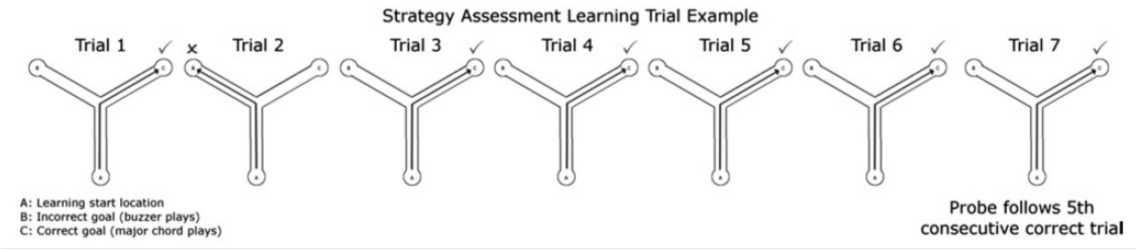

B

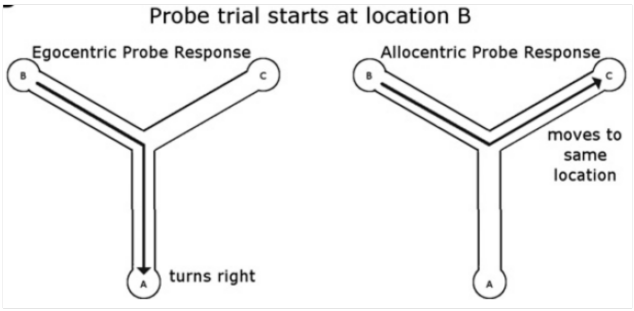

C

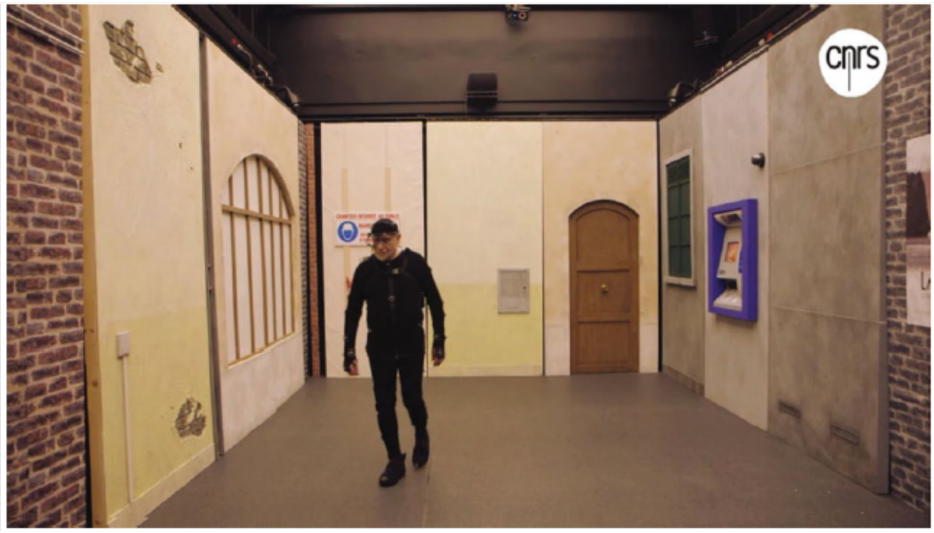

Figure 2.1: (a,b) Experiment dissociating the use of egocentric and allocentric strategies in aged subjects (Rodgers et al., 2012). (a) Training. (b) Probe trial. (c) Testing allocentric learning in an open space. (Bécu et al., 2019).

of which the vision sense is the primary sensory modality, the processing of visual features in the brain is of special importance. It has been proposed that visual information important for spatial navigation is processed in the so-called dorsal visual pathway of the primate visual system, by contrast to the ventral visual pathway concerned with object processing (Goodale and Milner, 1992). While Chapter 3 provides a computational modeling account of the dorsal visual processing, here we briefly review anatomic details of this pathway.

2.2 Visuospatial processing in the primate dorsal visual pathway

Kravitz et al. (2011) reviewed anatomical studies, mainly from primates, addressing visual processing in neural structures leading from early visual areas to the medial-temporal lobe. It was proposed that input visual stream from the retina is first processed by successive stages of low-level visual processing in visual areas V1–V6 and subsequently enters the parietal cortex via occipito-parietal circuit. After that the visual stream is divided into three different pathways: The *parieto–prefrontal pathway* plays a primary role in working and executive memory; The *parieto–premotor pathway* participate in high-level motor control of eye movements, grasping and reaching; Finally, the *parieto–medial temporal pathway* plays a key role in spatial navigation. The parietal–medial temporal pathway is the most complex of the three pathways.

Occipito–parietal circuit. The occipital lobe is believed to be the visual processing center of the primate brain since the large part of the visual cortex is located in it. In particular, the primary visual cortex (V1) receives and converts visual information from the retina (Livingstone and Hubel, 1984). V1 neurons are sensitive to orientation of edge-like visual stimuli, their spatial frequencies and colors (Hubel and Wiesel, 1962). Jones and Palmer (1987) proposed that the two-dimensional Gabor wavelets, which are orientation- and frequency- sensitive image filters, fit well to spatial response of simple cells in V1. In our model described in subsequent chapters we used 2D Gabor filters at different orientations and frequencies to simulate early visual processing. The V1 and subsequent

visual areas (V2, V3, V3A) densely project to V6, mostly concerned with processing motion cues (Galletti et al., 2001). The final stage of the occipito-parietal circuit is the projection from V6 to the posterior parietal cortex, and in particular the caudal part of the inferior parietal lobule (cIPL). Overall, The function of the occipito–parietal circuit is to integrate information from central and peripheral visual fields in egocentric centered representation (Boussaoud et al., 1990).

Parieto-medial temporal pathway. This pathway connects cIPL with medial temporal lobe, including the entorhinal cortex, the hippocampus and parahippocampal structures via direct and indirect synaptic projections. Through the direction projections, the processed visual stream is conveyed: (i) to a small cytoarchitectonic zone between subiculum and CA1 (CA1/prosubiculum) where place cells and head direction cells are contained (Ding et al., 2000; Rockland and Van Hoesen, 1999); (ii) to the posterior parahippocampal areas (Cavada and Goldman-Rakic, 1989); (iii) to the pre- and parasubicular subdivisions of the hippocampal formation. Through the indirect projections, the visual stream is projected to the same target areas as the direction connections, but passing via the posterior cingulate and retrosplenial cortices (Vogt and Pandya, 1987; Morris et al., 1999; Kobayashi and Amaral, 2007; Kondo et al., 2005).

Egocentric-allocentric transformation in the medial-temporal pathway. The occipito–parietal circuit briefly reviewed above provides egocentric (retinotopic or head-fixed) representations of the visual input (Boussaoud et al., 1990; Stein, 1992). More specifically, the posterior parietal cortex is the source of the egocentric information needed for navigation since posterior parietal lesions can also lead to egocentric disorientation (Stark, 1996). On the other hand, extensive evidence suggests that parieto-medial temporal pathway plays a role of translation between the egocentric representations in the parietal cortex and allocentric representations in the medial temporal lobe (Vogt et al., 1992; Maguire, 2001; Byrne et al., 2007). First, allocentric representations, invariant to body movements, were identified in the cIPL and the posterior cingulate cortex, which are potentially useful for navigation and encoding of landmarks locations, since they are anchored with visual cues in the space (Snyder et al., 1998; Mountcastle et al., 1981; Chafee et al., 2007). Second, in monkeys, the peak activity of a subset of cells in the area 7a of the posterior

parietal cortex was modulated by head direction in world-fixed reference frame, suggesting an existence of a world reference representation (Snyder et al., 1998). Third, retrosplenial cortex lesions in humans result in various forms of spatial disorientation indicating that this area plays an important role in the coordination of egocentric heading and allocentric representations of the environment (Maguire, 2001).

Allocentric spatial representation in the human medial temporal lobe Several studies in primates, including humans, suggested the existence of an allocentric representations in the medial temporal lobe, which receives dense projections from the parieto-medial temporal pathway. First, cells selective to spatial location, similarly to rodent place cells, were discovered in the hippocampus and parahippocampal gyrus (including entorhinal cortex) (Ekstrom et al., 2003; Jacobs et al., 2013; Miller et al., 2013; Hazama and Tamura, 2019). Second, studies in humans also identified the existence of grid cells, which fire at multiple spatial locations forming as hexagonal and periodical grid pattern on the environment (Jacobs et al., 2013). Grid-like cells were also observed during exploration of a static visual scenes (Killian et al., 2012). Experimental studies suggested that grid spacing is a function of environment size (Nadasdy et al., 2017). Third, information processing in the human hippocampus is influenced by oscillations, as does rodent hippocampus, but with a lower frequency band (1-3Hz, compared to 8-10 Hz in rodent)(Miller et al., 2018). These lines of evidences suggest that primate representation of space is organized similarly to a rodent one, reviewed below. However, the quantity and quality of primate data is much lower than that in rodents. That is why, while visual processing is modeled based on primate studies, we switch to primarily rodent data in Chapters 4 and 5.

2.3 Spatial representation in rodents

In this section we review the anatomy of the hippocampal formation, an area of mammalian brain where place cells and grid cells are discovered. Then in Section 2.3.3 and Section 2.3.4 we describe basic neurophysiological properties of these neurons, while head direction cells are described in Section 2.3.2.

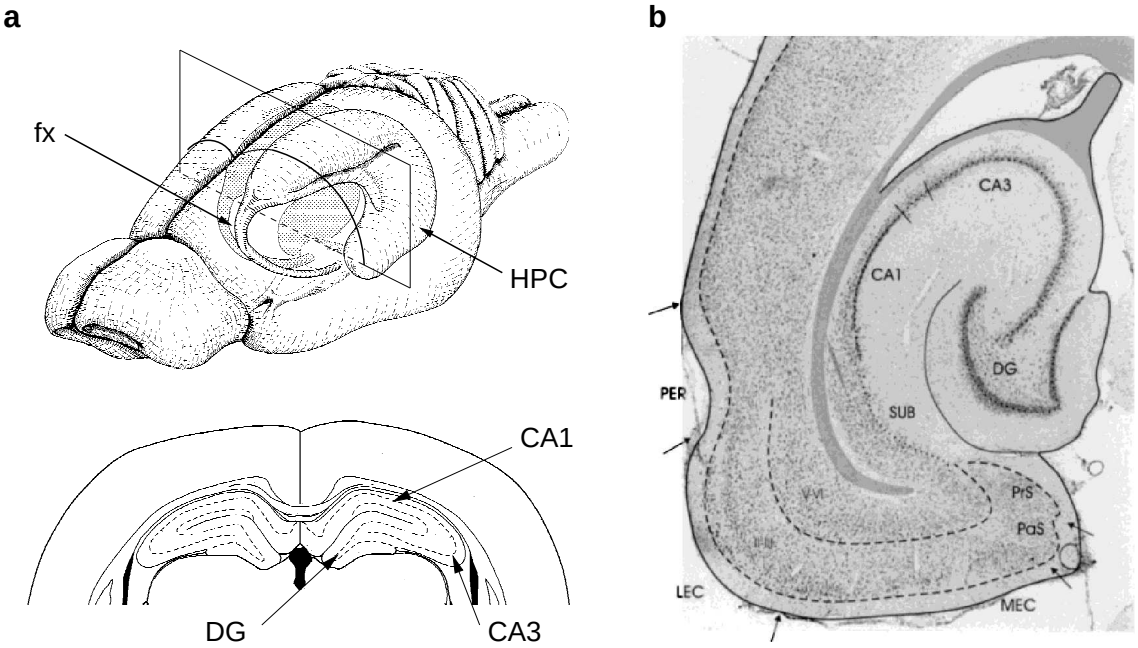

Figure 2.2: Anatomy of the hippocampal formation. (a) The Schematic of rat brain with the hippocampal formation highlighted (Amaral and Witter, 1995) and coronal section of the hippocampus (Praxinos and Watson, 1998). (b) Subregions of the hippocampal formation (Witter et al., 2000). HPC, hippocampal formation; fx - fimbria fornix; DG - dentate gyrus; CA1/CA3 - Cornu Ammonis subregions; SUB - subicilum; PrS - pre-subiculum; PaS - para-subiculum; MEC - medial entorhinal cortex; LEC - lateral entorhinal cortex; PER - perirhinal cortex.

2.3.1 Hippocampal formation

The hippocampal formation (HF) is a limbic brain area which occupies a considerable part of the rat's brain (Fig. 2.2a), contributing to spatial navigation. It contains the entorhinal cortex (EC), the hippocampus (HPC) and the subicular complex (SbC) (Amaral and Witter, 1989, 1995; Andersen et al., 2006).

EC is a target of most higher cortical associative areas. Therefore, HF can operate on highly processed sensory information from all sensory modalities (Burwell and Amaral, 1998; Agster and Burwell, 2009). The hippocampal formation receives afferent connections from subcortical areas through the fornix bundle, particularly cholinergic and GABAergic projections from the medial septum. Cholinergic input targets mainly the excitatory pyramidal and granule cells, as well as inhibitory GABAergic interneurons. GABAergic septal neurons, on the other hand, selectively synapse on GABAergic interneurons only (Freund and Antal, 1988).

There are two main outputs of the HF: One pathway leaves the HF through the subiculum

and projects to subcortical areas. It innervates thalamic nuclei, amygdala and–via the fornix fiber bundle–nucleus accumbens (NA) (Witter, 1993; Legault et al., 2000). A second pathway projects back to the higher cortical areas, and these projections *feed back* to EC (Insausti et al., 1997). Despite that fact that the existence of the hippocampal processing loop has been noted a long time ago (Iijima et al., 1996), this fact has not been accounted from by most of the existing models of hippocampal processing. We address this question in Chapter 4.

EC is the primary sensory input area of the HPC. It can be subdivided into a medial (mEC) and a lateral(lEC) regions. As HPC, it can be further divided into the dentate gyrus (DG) and the Cornu Ammonis (CA). CA contains four subregions, but CA1 and CA3 are the most prominent subregions (Amaral and Witter, 1989, 1995; Andersen et al., 2006). SbC includes the subiculum (Sb), the para-subiculum (paSb) and the pre-subiculum (prSb) (Amaral and Witter, 1989; Andersen et al., 2006). Simplified scheme of internal connectivity between these HF subregions is plotted in Fig. 2.3. As the plot shows, sensory information is processed in two parallel pathways: the first pathway from EC directly projects to CA3 and CA1 via the perforant path (PP) (Hyman et al., 1986; Yeckel and Berger, 1990). The second pathway project EC input to DG via PP as well but then project to the CA3 pyramidal cells via different set of axons called mossy fibers (MF). Pyramidal cells in the CA3 are recurrently connected and project to the CA1 via Shaffer collateral (SC) projections. CA1 projects to the subiculum, and both CA1 and subiculum project via fornix-fimbria system to subcortical areas, particularly nucleus accumbens, and to the deep layers of the EC. (O'Keefe and Nadel, 1978; Amaral et al., 1991; Witter, 1993).

Entorhinal cortex

Entorhinal cortex is a gateway for neural information from a variety of cortical regions entering and leaving the hippocampus. These cortical inputs form a six-layered structure in the EC, classified into two groups: those that terminate in the superficial layers 1-111 and those that distribute to the deep layers IV-VI (Kosel et al., 1981; Witter, 1993; Insausti et al., 1997). A distinction can be made between the medial (MEC) and the lateral (LEC) areas.

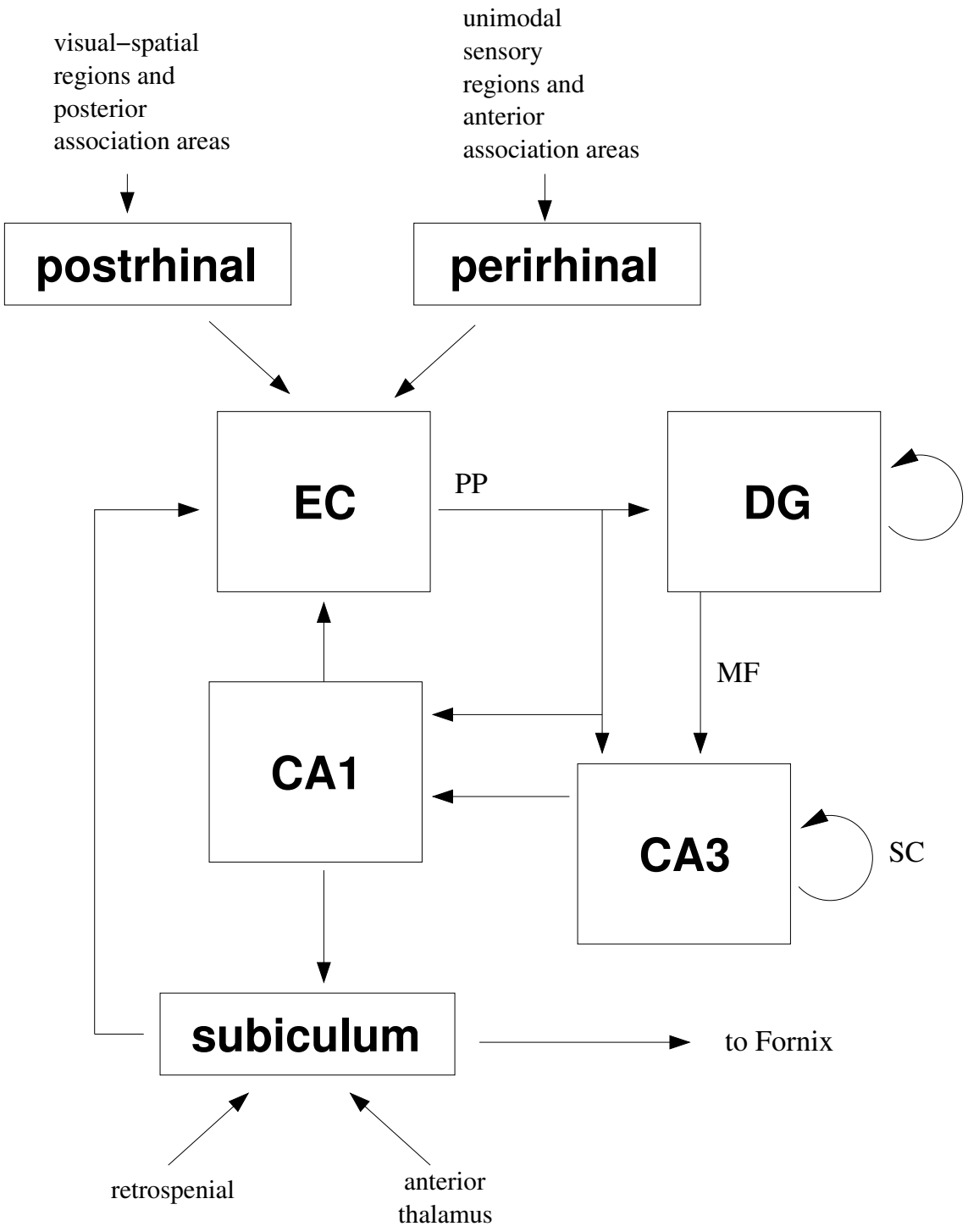

Figure 2.3: Schematic representation the hippocampal formation network. See figure 2.2 for a description of the labels.

Both MEC and LEC receive projections from sensory associative areas (auditory, visual and somatosensory) as well as from the temporal, frontal areas and parietal via postrhinal and perirhinal cortices (Witter, 1993; Suzuki and Amaral, 1994; Insausti et al., 1997; Liu and Bilkey, 1997). Olfactory information from the piriform cortex and olfactory bulb is conveyed directly via perirhinal cortex (Kosel et al., 1981; Witter et al., 1989, 2000). The subiculum and CA1 mainly send their output to MEC, but also to LEC. DG and CA3 are not innervated with EC (Amaral and Witter, 1989; Witter, 1993).

EC cortical efferents target primarily perirhinal, piriform cortices and orbitofrontal, but also innervate parietal, temporal and frontal areas (da Silva et al., 1990; Witter, 1993; Insausti et al., 1997). Via the perforant path, EC forwards multisensory information from its cortical afferents to DG, CA3, CA1 and Sb (Witter, 1993; Andersen et al., 2006). Cells with hexagonal and periodic spatial firing fields (grid cells, see Section 2.3.3) have been discovered in the dorsal MEC. The most dorsolateral band of the MEC provides strongest input to the dorsal part of the hippocampus where place cells (see Section 2.3.4) with sharpest and spatial preferred firing fields were discovered (Fyhn et al., 2004; O'Keefe and Burgess, 1996).

Neurons in the deep regions have connections with neurons in the superficial layer of EC(Amaral and Witter, 1989; Witter, 1993). There is also evidence for strong synaptic innervation from the lateral to the medial region (Quirk et al., 1992).

Dentate gyrus

DG granule cells receive processed sensory input from EC. Granule cells in DG then forward to mossy cells. Mossy cells laterally contact other mossy cells as well as strongly project to CA3 (Claiborne et al., 1986; Hastings et al., 2002). Neurogenesis is occurred in the rat DG throughout the whole life,. Stem cells migrate into the granule layer and differentiate into fully functional and networked granule neurons (Kuhn et al., 1996; Ciaroni et al., 1999; Hastings et al., 2002). Studies suggested that DG contributes to pattern separation, reducing the interference of incoming similiar inputs from EC (Tanila, 1999; Yassa et al., 2011).

Cornu Ammonis or hippocampus proper

The hippocampus proper contains four subregions CA1-CA4, with CA1 and CA3 being the most distinguishable. Place cells with spatially correlated activity (see Section 2.3.4) have been identified in CA1 by O'Keefe and Dostrovsky (1971), later were also discovered in CA3 and DG (Jung and McNaughton, 1993).

The CA3 region receives strong projection from DG via the mossy fibers. Both CA1 and CA3 are innervated by EC via the perforant path (Amaral and Witter, 1989; Witter, 1993; Hastings et al., 2002).

CA1 an CA3 pyramidal cells connect to subiculum via the Shaffer fiber bundle. The angular bundle connects CA1 to EC (perforant path) (Amaral et al., 1991). CA1 projects to the subiculum and the EC (Witter et al., 2000) as well as directly to the nucleus accumbens and septum via fimbria-fornix (O'Keefe and Nadel, 1978).

CA3 neurons laterally project to other CA3 neurons via the Shaffer collaterals (SC). Also via the Shaffer fibers, CA3 connects to CA1 (Amaral and Witter, 1989, 1995). The recurrent collaterals in CA3 are proposed to contribute to pattern completion, the representation in CA3 can be restored when the input is partial or degraded (Stark et al., 2010).

Subiculum

The subicular complex (SC) includes the the pre-subiculum (prSb) and subiculum (Sb), whose dorsal part forms the para-subiculum (paSb) and the post-subiculum (poSb) (Amaral and Witter, 1989, 1995).

The main inputs to Sb are from CA1 and EC (Amaral et al., 1991). The paSb innervates the retrosplenial cortex whereas prSb receive connections from the temporal and parietal lobes, as well as from the thalamic nuclei, which forward into poSb (Burgess et al., 1999).

Sb projects on the nucleus accumbens (NA) and the septal complex via the fornix fiber bundle. Sb is also innervated prefrontal and entorhinal cortex, the thalamus and amygdala. prSb and paSb also project to EC (Amaral and Witter, 1989; Witter, 1993). Within SC,

Sb forward to prSb and paSb and prSb also synapses on paSb (Amaral and Witter, 1989; Witter, 1993).

Theta rhythm

The EEG on hippocampus shows distinct patterns depending on the rat's behavior. During motion (passive or active (Gavrilov et al., 1996)), the EEG presents an oscillation (6–12Hz) called *theta rhythm* (O'Keefe and Recce, 1993; Burgess et al., 1994; Skaggs et al., 1996). Theta rhythm is observed during REM-sleep and sensory scanning as well (Buzsáki, 2002). Except that, firing is synchronized to a *gamma oscillation*(40–100Hz) throughout the entire hippocampal formation (Chrobak et al., 2000; Csicsvari et al., 2003). Subcortical cholinergic and GABA-ergic inputs from the septal region are responsible for generating theta rhythm (Winson, 1978; Buzsáki, 1984; Stewart and Fox, 1990; Miller, 1991; Hasselmo and Bower, 1993; Carpenter et al., 2017). When septal input is inactivated, the place fields of CA3 place cells are disrupted whereas the CA1 place cells are not affected. At the same time, acquisition of place learning tasks is impaired (Brandner and Schenk, 1998) and errors in working memory significantly increase (Mizumori et al., 1989).

While drinking, awake-immobility, eating or in slow-wave sleep, however, the EEG shows large field high irregular amplitude signature, termed *sharp waves*. A high frequency ripple volley (140–200Hz) occurs during each sharp wave event (Chrobak et al., 2000; Chrobak and Buzsáki, 1996). It suggests that theta/gamma waves synchronize input from cortex to hippocampus, whereas sharp ripples/waves modulate output from hippocampus back to cortex (Chrobak et al., 2000).

2.3.2 Head direction cells

A *head direction* (HD) cell is a neuron whose firing activity is correlated with a particular orientation of the animal's head with respect to its environment. A HD cell only emits spikes when the heading of the animal is in its preferred direction regardless the position of the animal in the environment. Therefore, HD cells are believed to encode animal's current heading in an allocentric reference frame (Taube et al., 1990a,b). Taube et al.

(1990b) reported that the preferred firing direction of a HD cell is controlled by allothetic cues. In the experiment, animal foraged in a cylinder room with a salient visual cue on the inside of cylinder wall. After the animal became familiar with the environment, the animal was taken out from the experimental room and disoriented its head direction. Then the animal was placed back to the cylinder with rotated visual cue. The preferred direction of HD cells in the cylinder shifted with the visual cue together (Taube, 1995; Knierim et al., 1998). On the other hand, the preferred firing direction of HD cells is able to be maintained by only integrating idiothetic cues (self-motion related) as the animal moves in the dark environment by turning off the light (Taube et al., 1990b; Goodridge et al., 1998).

HD cells were originally discovered in postsubiculum (Taube et al., 1990a). Then, HD cells were gradually identified in other brain areas within the classical Papez circuit, for example the anterior dorsal thalamic nucleus (ADN) (Taube, 1995), lateral mammillary nuclei (LMN) (Stackman and Taube, 1998), retrosplenial cortex (Cho and Sharp, 2001) and entorhinal cortex (Sargolini et al., 2006). HD cells were also been found in other non–Papez circuit areas, including the lateral dorsal thalamus, the dorsal striatum, the medial precentral cortex, medial prestriate cortex, CA1 hippocampus and dorsal tegmental nucleus (DTN).

2.3.3 Grid cells in the dorsomedial entorhinal cortex

In the layer II of the dorsal part of the MEC (dMEC), neurons are observed with spatial firing fields that resemble hexagonal and periodical grid field distributing over the entire space (Fyhn et al., 2004; Hafting et al., 2005), termed as *grid cell*. The property of these structured grid fields can be quantified with grid orientation, the grid spacing and the grid phase (relative spatial location of the grid field) as illustrated in Fig. 2.4a. For each grid cell, the orientation of the hexagonal grid fields is quantified by measuring the angle between an external reference line and the axis through the fist counter-clockwise vertex of the hexagon (e.g. 0° in the figure). Grid spacing is the distance between two neighboring vertices of the hexagonal grid field, which is the same for all vertices from one grid cell. The spatial phase of a grid cell is defined as a spatial position of the grid field relative with

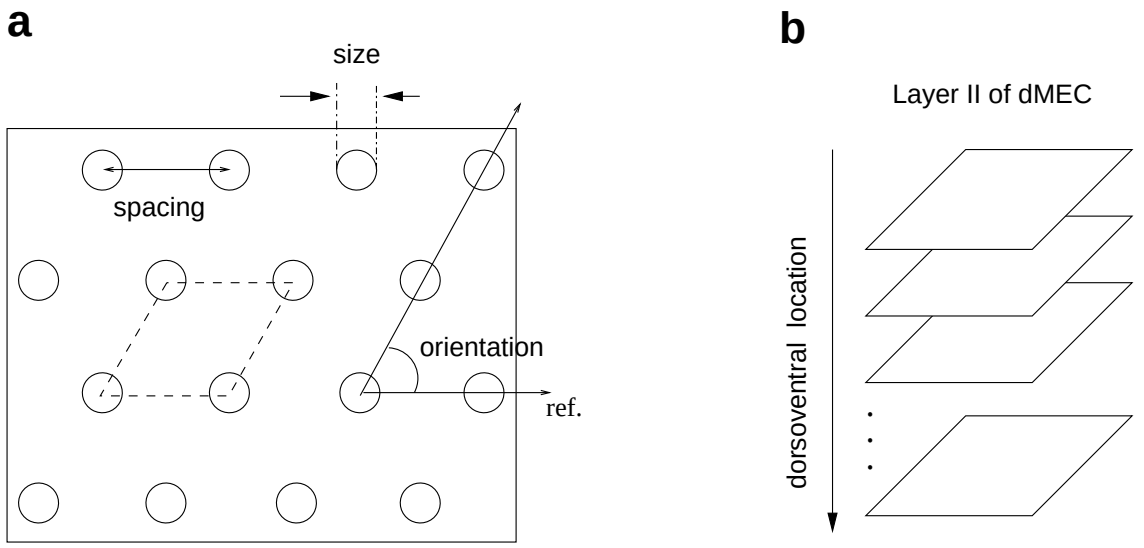

Figure 2.4: Schematic illustration of grid cells. (**a**) Schematic drawing of firing fields of a single grid cell. Large rectangle represents the recording room, circles represent the locations of firing fields. (**b**) The grid cells are organized in different populations along the dorsoventral axis of the dMEC. Cells in each population share the same spacing and orientation (defined as in **a**). The more ventral is the location of a population, the larger is spacing and field size.

the grid field of other grid cell, i.e. it characterizes the mapping of the grid field on the actual environment (e.g. the floor of the experimental room). Each vertex of the grid field is characterized by its size, described in the experiments by the area covered by the central peak of the spatial autocorrelogram using a threshold of 0.2 (Hafting et al., 2005).

The grid cells are topographically organized (Hafting et al., 2005), Fig. 2.4b. Neighbouring grid cells have the same spacing and orientation but different spatial phases, i.e. the firing fields of nearby grid cells have identical orientation, size and spacing, but the grids are offset relative between each other. Hence these grid cells are suggested to belong to a grid-cell population in the following chapters. The grid cells that are far apart (along the dorsoventral axis of the dMEC) differ by field size, grid orientation, grid spacing (i.e. belong to different grid-cell populations). The grid spacing progressively increases from Dorsal to Ventral medial entorhinal cortex (Brun et al., 2008b). But grid orientations differ without any systematic relationship.

Firing fields of grids of individual cells have the following properties (Hafting et al., 2005): (i) The grid pattern is immediately established once upon exposure to a novel environment, i.e. the grid cells fire at the first time the animal passes through the field, both in light and dark situation. (ii) The grid fields are anchored to the allothetic cues in the environment.

If a cue card in the cylinder room is rotated °90, the grid orientation rotate similarly. (iii) The grid field is still persisted after removing the cue card. After initial exposure in the experimental room about 10 min with the lights are on, the grid field were maintained for 30 min in total darkness. However, the majority of cells the darkness period have a weak dispersal of the vertices. (iv) The grid field can be shaped by environmental geometry (Krupic et al., 2015; Stensola et al., 2015).

The model, presented in the Chapter 4, describes a neural network in which neurons have periodic firing fields with hexagonal spatial pattern, similarly to the dMEC grid cells (see Chapter 4). The role of this network is assumed to be the integration of self-motion input over time, i.e. path integration. In contrast to most earlier models, grid cells in our model are influenced by place-cell input from CA1, in according with recent data (Bonnevie et al., 2013).

2.3.4 Hippocampal place cells

A *place cell* is a neuron whose firing activity is associated with the animal's spatial location (O'Keefe and Dostrovsky, 1971). A place cell fires only when the animal is in a specific area of the environment, which defines the place field of the place cell.

Place cells recorded in CA3/CA1 areas of the hippocampus have spatially-tuned place fields which uniformly cover the entire environment, and at any moment only a small proportion of these cells is active. The set of overlapping place fields is suggested to encode a distributed representation of the environment (Wilson and McNaughton, 1993). The shape of place fields can be varied: The firing field can be distributed as a circular two-dimensional Gaussian (Samsonovich and McNaughton, 1997); but it can also be elongated in one dimension (particularly along walls). It is quite rare that a place cell has a place field in several different environments (Kubie and Ranck, 1983), but a place cell can have multiple peaks of activity in one single environment (Muller et al., 1987; O'Keefe and Burgess, 1996; McNaughton et al., 1983). Different with grid cells, topographic relationship is not observed between anatomical structure of the CA3-CA1 populations and environment (O'Keefe and Conway, 1978; Muller and Kubie, 1987; Thompson and Best, 1989)

Except the place property of place cell mentioned above, the CA1 place field is also direction selective (Mehta et al., 1997). When an animal repeatedly ran towards the same direction on a linear track, CA1 place fields, which are initially symmetrical, expand backward with respect to the animal's direction of movement. Such a phenomenon is only observed during the same block of trials, and it disappears the next day. Lesion studies on CA3 and DG suggested that an complete CA3 input to CA1 is not mandatory to maintain the place and directional properties of place cells in CA1 (Mizumori et al., 1989; Brun et al., 2002; McNaughton et al., 1989; Skaggs et al., 1996), it might be because CA1 receives the direct feed-forward projection from the EC (Brun et al., 2008a).

Except CA3/CA1, neurons with spatial sensitive firing were observed in subiculum and the entorhinal cortex as well. Place fields in subiculum is larger than those in the hippocampus proper. In addition, neurons in subiculum has a similar place field topology across several different environments (Sharp and Green, 1994; Sharp, 1997, 1999), and seems that self-motion cues exert control on them (McNaughton et al., 1996). Earlier studies in place-sensitive cells in the EC reported broad single peaked firing fields (Quirk et al., 1992). Recent data (Section 2.3.3) have shown a gradual change from multi-peaked to single-peaked firing fields along the dorsolateral to ventromedial axis of the dMEC.

2.3.5 Firing determinants of place cells

The firing of place cells is highly correlated with the location of the animal. However, place cells are also sensitive to self motion information, visual cues, odor, sound and reward (McNaughton et al., 1983; Markus et al., 1994, 1995).

Sensory information

Place cell activity is influenced by both allothetic and idiothetic inputs, and an extensive of experiments in rodents have studied on the main determinants of place cell firing, as well as the interactions between different sensory information.

Visual allothetic cues. Studies suggest that firing of the place cells mainly relies on visual information (Etienne et al., 1996; Save et al., 2000; O'Keefe and Burgess, 1996;

Markus et al., 1994; Knierim et al., 1998). Visual cues are divided as distal and local visual cues. Distal visual cues exert more control of the firing fields than local cues (O'Keefe and Conway, 1978). Rotation of a cue card on the wall of the experimental room give rise to place field rotation (Muller and Kubie, 1987; Knierim et al., 1995). With the same way of cue controlling, the same experimental result was observed when three objects were placed *at the periphery* of a cylindrical water-maze (Cressant et al., 1999). However, when the same objects were placed *at the center* of the maze, the rotation of objects did not give rise to a rotation of place fields for most of the place cells, suggesting weaker control from local cues than distal cues (Cressant et al., 1999).

Non-visual allothetic cues. Except visual cues, rats can use other allothetic cues to drive the firing of place cells. Odor cues is contributed to the stability of place fields (Lavenex and Schenk, 1996). In addition, blind rats sense the environment by touching with the objects in the environment more often than healthy sighted rats (Save et al., 1998). This behavior allows the rat to correct the error of its internal estimated location (i.e. path integrator) by using tactile information.

Idiothetic cues. The location-sensitive activity of Place cells is still maintained in the absence of visual information, suggested that the self-motion contribute to the firing of place cell. For example, the spatial firing location of place cell was not altered after visual cue was removed (O'Keefe and Conway, 1978; O'Keefe and Speakman, 1987; Quirk et al., 1992); and place cells in visually symmetric environments have asymmetric visual fields (Sharp et al., 1990). In addition, once place cells are established in darkness, their firing are still maintained in the subsequent light situation (Markus et al., 1994). These experimental data suggests that self-motion information may be sufficient to form a stable place code in the hippocampal formation.

Interaction between allothetic and idiothetic cues. Self-motion cues are suggested to update place cell firing (i.e. by path integration, Mittelstaedt and Mittelstaedt, 1980; Etienne and Jeffery, 2004). However path integration results in accumulating errors over time (Knierim et al., 1998). Therefore, it is essential that a re-calibration process based on allothetic cues to maintain an accurate estimation of animal's position (Mittelstaedt, 1983;

Gothard et al., 1996a; Etienne et al., 1996; Save et al., 2000; Redish et al., 2000). Gothard et al. (1996a) further studied the interaction between allothetic and idiothetic cues in the place cell activity with a mismatch experiment with conflicting allothetic and idiothetic cues. They found that the activity of place cell is changed and transit to one of the two when a mismatch is happened between external and internal cues. The determination of the dynamic changes is the degree of the mismatch between the two types of cues. With a similar protocol, Redish et al. (2000); Rosenzweig et al. (2003) suggested that a temporal delay was required to make the transition for place cells. These experimental data indicated that sensory cues dynamically compete to control the firing of place cells.

Influence of environmental geometry

Environmental geometry is generalized from allothetic cues. Extensive experimental data suggested that the place field of place cells is sensitive to geometry information (Muller and Kubie, 1987; O'Keefe and Burgess, 1996). When the rat were sequential tested in a cylinder room then a square room with the same visual appearance, the place fields of the same place cells in the square room are abolished, reshaped or remapped comparing with those in the cylinder room (Muller and Kubie, 1987). In addition, O'Keefe and Burgess (1996) recorded the firing of CA1/CA3 pyramidal cells when rats were exploring four different boxes (a small square; a horizontal rectangle; a vertical rectangle; and a large square). They found out that the shape of place fields of the same place cells in the four different environment are changed. In particular, the place fields of some place cells are either stretched or doubled along the shape changing direction of the box when comparing the small square box with others. Except the geometry of the boundary, geometry of an arrangement of objects also influence the stability of place field. For instance, place fields are poorer controlled by three objects with an equilateral triangle arrangement than an isosceles triangle arrangement (Cressant et al., 1997, 1999).

2.4 Aging and spatial memory

Neurological alterations correlated with aging. Extensive studies suggested that the impairment of spatial memory and navigation is correlated with aging. These deficits

are caused by various age-related neurobiological alterations to the hippocampus: (1) The neural synapses from EC to DG reduced by one-third in aged rats, as shown by measuring the micro-structural features of white matter (Geinisman et al., 1992; Smith et al., 2000; Yassa et al., 2010); (2) Aging place cells in CA3 exhibit hyperactivity (Wilson et al., 2005a) and the increased excitability in CA3 lead to pattern distinguish deficit in a mnemonic discrimination task (Yassa et al., 2011; El-Hayek et al., 2013); (3) Due to the loss of dendrites and synapses, modulation inputs to the hippocampus decrease with aging (Schliebs and Arendt, 2011), including acetylcholine modulation on CA1 and CA3 (Shen and Barnes, 1996; Wilson et al., 2006; Sava and Markus, 2008; Schliebs and Arendt, 2011), dopamine modulation on facilitating synapse plasticity (Abdulrahman et al., 2017), norepinephrine modulation on hippocampal long-term potentiation (LTP) (Luo et al., 2015; Abdulrahman et al., 2017); (4) The rate decline of neurogenesis with aging (Kuhn et al., 1996; Gould et al., 1999); (5) Brain-derived neurotrophic factor decreases with aging in the hippocampus (Tapia-Arancibia et al., 2008); (6) A lower threshold for long term depression (LTD) and a higher threshold for LTP, leading to aging-related impairment of memory maintenance and learning new information (Foster, 1999).

Ag-related reduction of cholinergic modulation. The cholinergic modulation of the hippocampus diminishes with age, as demonstrated by measuring the level of acetylcholine (ACh) processing enzyme due to the loss of dendrites, synapses and ACh neurons (Fischer et al., 1989; Stroessner-Johnson et al., 1992; Sugaya et al., 1998; Schliebs and Arendt, 2011). The attenuated ACh modulation from medial septum to three hippocampal sub-regions (CA1, CA3 and DG) was proposed to cause spatial memory impairments (Shen and Barnes, 1996; Wilson et al., 2006). Studies in humans have also shown the attenuated ACh modulation with aging (Perry et al., 1992). ACh modulation is believed to play an important role in switching of processing states between recall and learning within the hippocampus (Hasselmo et al., 1995). Age-related ACh modulation reduction is thought to decrease the relative impact of novel information in the hippocampus (Hasselmo and Schnell, 1994; Hasselmo and Wyble, 1997) since extensive studies have shown that the ACh release level from the medial septum is associated with novelty (Giovannini et al., 1998; Miranda et al., 2000; Giovannini et al., 2001; Ranganath and Rainer, 2003).

Age-related changes in place-cell activities. Firing activity dynamics of place cells in aged, compared to adult, rats express a number of differences during learning of novel environments. First, extensive studies in aging place cells have shown that CA1 and CA3 cells are less efficient in learning new spatial or task information (Tanila et al., 1997b; Oler and Markus, 2000; Wilson et al., 2003, 2004, 2005a). In these experiments, rats were introduced into a a novel environment, after having learned a previous, control environment. The two environments differed in visual cues present in them. In adults rats, firing positions of place cells in the novel environment were completely different from those in the familiar environment. By contrast, firing fields of place cells in aged rats remained in the same location in both environments. Only after repeated presentation to the novel environment, place cells in aged rats reflected the difference in visual cues. Second, in aged rats, recollection of a spatial representation of an already learned environment was only slightly impaired, compared to the strong effect of age during learning a novel representation. This slight effect was manifested by changes in spatial position of only a small subset of place cells when the animals were replaced into a well learned environment (Rosenbaum et al., 2012; Barnes et al., 1997). Third, synaptic plasticity in the hippocampus is impaired in aged animals (Shen et al., 1997; Burke and Barnes, 2006). When adults rats ran in laps in a rectangular loopy track, firing fields of their place cells became larger in later laps compared to earlier ones. By contrast, the place field expansion effect was absent in aged rats, likely because of an age-related LTP impairment. Fourth, when relying mostly on self-motion cues, place cells in aged rats were equally efficient in creating new spatial representation as those in young rats. In this experiment, rats' behavior was tested in a multi-compartment environment consisting of two identical rooms, thus requiring the rats to use self-motion cues to distinguish between them (Wilson et al., 2005b). Finally, when switching between strategies relying on allothetic and idiothetic cues, age is manifested in strategy-switching impairments (Tanila et al., 1997a; Harris and Wolbers, 2014). Rosenzweig et al. (2003) reported that the transition from using idiothetic to allothetic cues when running back and forth in a linear track is slower in aged than in adult place cells.

In Chapter 5 we put forth a neural-network model of the effects of age on spatial navigation in which we test the hypothesis that age-related reduction of cholinergic activity in the

hippocampal formation causes plasticity impairments that in turn result in the observed cellular and behavioral changes in aged rats.

2.5 Aging Human Avatar platform

Aging Human Avatar platform (AHA) is a modular software platform developed at the Aging, Vision & Action Laboratory, Institute of Vision, Sorbonne University, Paris (Sheynikhovich et al., 2019). As stated in Chapter 1, the overall goal of the platform is to provide a customizable tool for human behavior simulation. A number different people, including myself, contributed to the development of the platform. In this section, the software architecture of the platform is briefly reviewed, with the indication of the specific contributions of the present doctoral work.

The main purpose of the AHA platform is to simulate research experiments in a 3D virtual environment involving a virtual subject (the avatar). The 3D environment (experimentation scene) and the avatar (3D model of a human) can be configured and controlled by the experimenter to carry out custom simulations. AHA Platform is mainly intended to conduct experiments related to the subject's movement, vision and navigation, especially when the effect of the subject's aging is a factor to be considered.

2.5.1 Software architecture

The AHA platform is designed using a modular software architecture, developed by Richard R. Carrillo (University of Granada). It is composed of processing modules, or nodes, which communicate among them to provide an overall processing and simulation. The number of nodes can be adapted to the requirements of each experiment, but at least two nodes are always present (Fig. 2.5): (1) The visualization node, implemented in Unity 3D, (https://unity.com). This node hosts the 3D model of the environment and 3D model of a human. (2) The user interface node, which supports the interface between the user and the platform via Python language interface library. This node also hosts the library that ensures intermodule communication implemented using Robotic Operating System software (ROS, http://www.ros.org). Additional modules, usually providing detailed simulation of

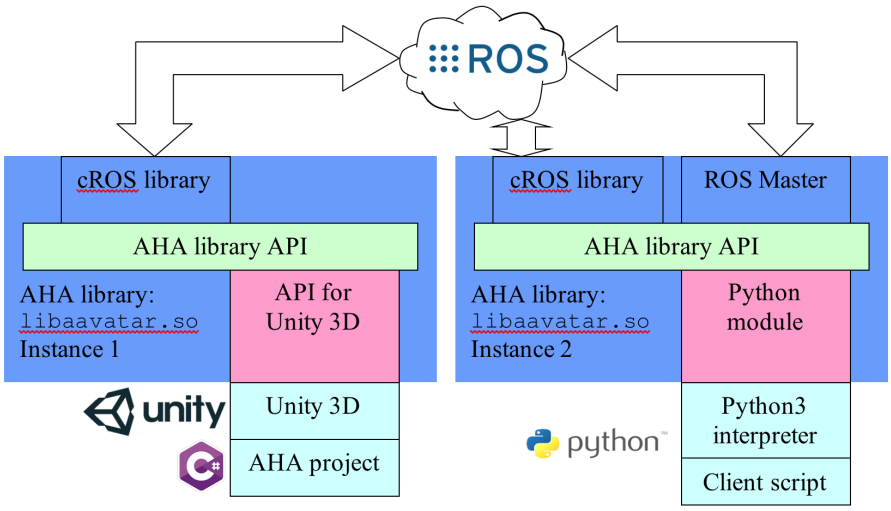

Figure 2.5: Software architecture of the Aging Human Avatar platform. Two main components of the AHA platform are (i) the visualization node, that hosts the 3D simulation environment and the 3D model of the human avatar; and (ii) the user interface node (including ROS master instance and Python module) that supports communication between the user and the platform and between platform modules. The ROS master instance, as well as multiple Python modules simulating various functional components of the avatar (see Section 2.5.2) can either be implemented directly as a part of the Python module or distributed over multiple dedicated computers connecting via TCP/IP.

sensory (such as retina), sensorymotor (e.g. cerebellum) or memory (e.g. hippocampus) areas can be included as additional modules via the Python interface library (see the next section).

Unity 3D is a video game engine developed by Unity Technologies. Unity 3D supports the creation of 2D and 3D games and simulations. It has an intuitive graphical interface that facilitates the creating and edition of projects making its use easier to learn. Its functionality can be extended through assets, which are items that can be included in the project (such as 3D models, textures and character animations). Many of them can be downloaded and easily imported in the project for free from Unity Asset Store, which is a library of assets on the Internet accessible through the Unity 3D interface. However, most of the flexibility of Unity 3D comes from the ability to include C# scripts in the project. These scripts can create, modify and destroy the objects in the scene and control the simulation and visualization.

ROS is not an operating system but middleware conceived for supporting the development of robot applications. These applications can benefit from the ROS network, which are

composed of ROS nodes. One of its main features of ROS is supplying an interface for enabling these ROS nodes to communicate in different ways, such as message passing and remote procedure calls. This communication is carried out through TCP/IP, so the platform nodes can be distributed in a TCP/IP network. The ROS protocol requires that one special node is always present in the ROS network: the ROS Master. This node provides the other nodes with a node-registration service and a parameter dictionary. So, when a normal ROS node starts it registers in the Master. If a node wants to find out the address of a particular node that provides certain service, it queries the Master. This Master node also stores the value of the parameters set by other nodes.

2.5.2 Functional architecture

The functional architecture of the AHA platform in its current implementation includes 3 functional modules (apart from the necessary modules mentioned earlier, Fig. 2.6A): (1) Early visual processing module implementing a detailed models of the retina (Huth et al., 2018); (2) Cerebellar model of vestibular-ocular reflex (Naveros et al., 2019; Luque et al., 2019); (3) Spatial memory module (this doctoral thesis). More specifically, the model of vision-based spatial memory described in Chapter 3-5 can be included as a separate Python module of the AHA platform. Most of the computer simulations in these chapters were run in the Unity environment with the 3D human avatar as the experimental subject (Fig. 2.6B).

A

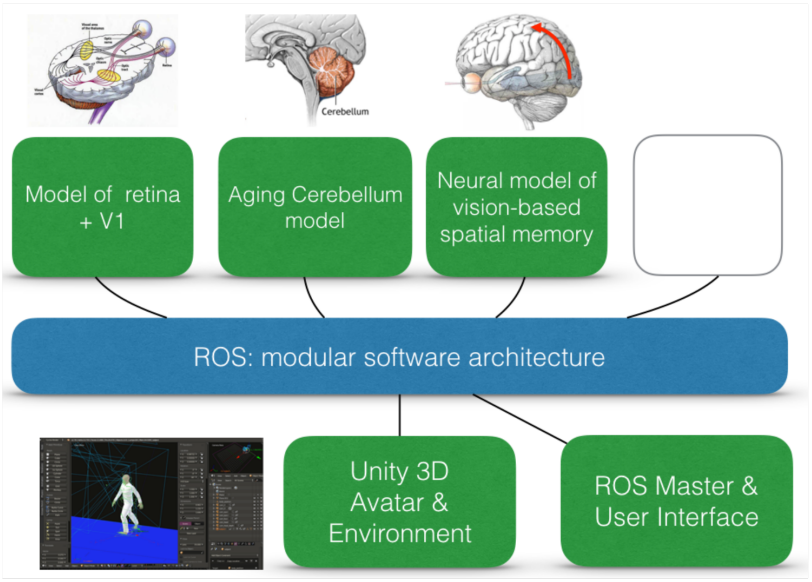

B

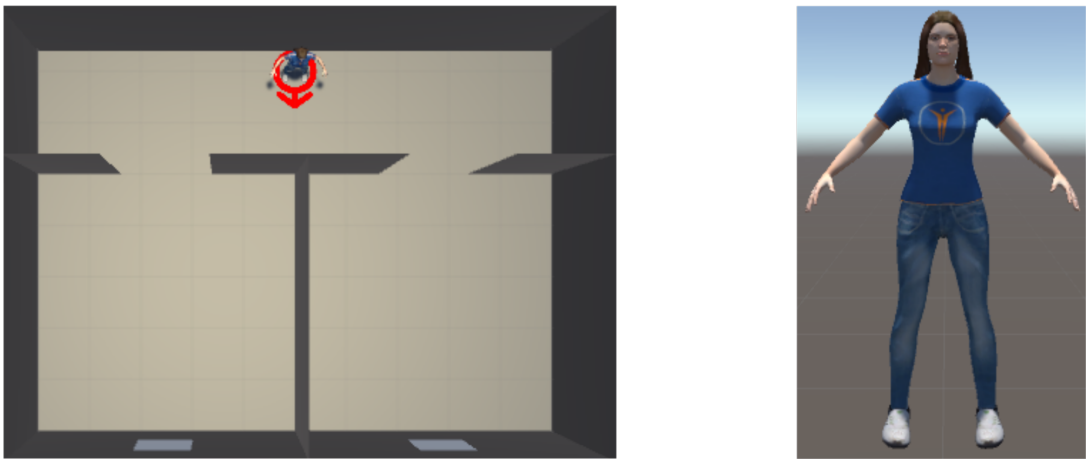

Figure 2.6: A. Currently implemented modules of the AHA platform. B. Simulation environment of the double-room experiment simulated in Chapter 4 (left) and 3D model of a human person (right).

Chapter 3

Computational Model of the Dorsal Visual Pathway

Chapter summary

This chapter presents a computational model of the primate dorsal visual pathway. The model deals with the question of how visual information is converted from an egocentric (retinal or head-fixed) reference frame, in which the information is acquired by the sensory organs and early visual areas, into a world-fixed, allocentric frame of reference. Due to the fact that allocentric representations are subject-invariant, they are thought to be used for spatial memories in the hippocampal formation. In the context of the Aging Human Avatar platform, the coordinate transformation is a necessary step linking visual and mnemonic areas during spatial orientation. The model presented in this chapter is instrumental for the spatial orientation models described in subsequent chapters, as it serves to deliver head-direction independent visual input to the entorhinal-hippocampal processing loop.

This work has been submitted for revision to the eLife journal:

Tianyi Li, Angelo Arleo and Denis Sheynikhovich (submitted) A model of panoramic visual representation in the dorsal visual pathway: the case of spatial reorientation and memory-based search. *eLife*.

Abstract

Primates are primarily visual animals and understanding how visual information is processed on its way to memory structures is crucial to the understanding of how memory-based visuospatial behavior is generated. Recent imaging data demonstrate the existence of scene-sensitive areas in the dorsal visual path that are likely to combine visual information from successive egocentric views, while behavioral evidence indicates the memory of surrounding visual space in extraretinal coordinates. The present work focuses on the computational nature of a panoramic representation that is proposed to link visual and mnemonic functions during natural behavior. In a spiking artificial neuron network model of the dorsal visual path it is shown how time-integration of spatial views can give rise to such a representation and how it can subsequently be used to perform memory-based spatial reorientation and visual search. More generally, the model predicts a common role of view-based allocentric memory storage in spatial and not-spatial mnemonic behaviors.

3.1 Introduction

Recent breathtaking advances in our understanding of rodent hippocampal memory system pave the way for elucidating the organization of human spatial memory (Burgess, 2014; Moser et al., 2017). One major difference between primates and rodents is the role of vision for behavior. Primates are much more visual animals than rodents and understanding the link between primate visual and medial temporal lobe (MTL) memory structures is an important and largely unexplored open question (Meister and Buffalo, 2016). Experimental evidence indicates the existence of functional and anatomical connections between these structures. Functional connections are demonstrated by two principal lines of studies. First, visual behavior is informed by memory as demonstrated by studies of novelty preference in both monkeys and humans (Wilson and Goldman-Rakic, 1994; Manns et al., 2000; Jutras and Buffalo, 2010a). In the novelty preference paradigm, the memory is assessed from looking time: well memorized stimuli are looked at less than novel ones. The specific role of MTL structures in this phenomenon is derived from results showing a decreased novelty preference after MTL lesions or in patients suffering from mild cognitive impairment or Alzheimer's disease, often associated with MTL dysfunction (McKee and Squire, 1993; Crutcher et al., 2009; Zola et al., 2013). In monkeys, restricted lesions of hippocampal and/or parahippocampal cortices also decreased novelty preference (Zola et al., 2000; Pascalis et al., 2009; Bachevalier et al., 2015). Second, the link between visual and MTL structures is manifested in coherent neural activities in the two structures. For example, activity of single MTL neurons is modulated by visual saccades (Sobotka et al., 1997), the onset of visual stimuli strongly affects hippocampal neural responses (Jutras and Buffalo, 2010a) and hippocampal theta oscillations are reset by eye movements (Jutras and Buffalo, 2010b; Hoffman et al., 2013).

Anatomical connections between visual and memory structures have recently been characterized in the novel framework of the occipital–parietal–MTL pathway of visuospatial processing (Kravitz et al., 2011). There are three principal stages of information processing in this pathway (Fig. 3.1A). First, the occipito-parietal circuit processes visual information through visual areas V1-V6 an egocentric (retinal) frame of reference. Successive information processing in these areas is thought to extract visual features of increasing complexity,

including motion and depth cues and relay this information to the parietal cortex. Second, a complex network of interconnected parietal structures relays highly-processed visual cues to support executive, motor and spatial-navigation functions. These structures include the medial, ventral and lateral intraparietal areas (MIP, VIP, LIP) strongly linked with eye movements processing; the middle temporal and medial superior temporal (MT, MST) thought to extract high-level visual motion cues; and the caudal part of the inferior parietal lobule (cIPL), the main relay stage on the way to the medial temporal lobe. The cIPL sends direct projections to the CA1 of the hippocampus as well as to the nearby parahippocampal cortex (PHC). In addition, it sends indirect projections to the same structures via the posterior cingulate cortex (PCC) and the retrosplenial cortex (RSC). Within this complex network, neurons at different neurobiological sites have been reported to code space in a world- or object-centred reference frames (Duhamel et al., 1997; Snyder et al., 1998; Chafee et al., 2007). Moreover, both PCC and RSC have been repeatedly linked to coordinate transformation between egocentric and allocentric frames of reference (Vogt et al., 1992; Burgess, 2008; Epstein and Vass, 2014). Importantly, information processing in this pathway is strongly affected by directional information thought to be provided by a network of head-direction cells residing in several brain areas, including RSC (Taube, 2007). Finally, medial temporal lobe, and in particular the hippocampus, play a key role in constructing an allocentric representation of space in primates (Hori et al., 2003; Ekstrom et al., 2003).

Given functional and anatomical connections between visual and memory structures, the question arises as to the nature of neuronal representations in the dorsal visual path. In addition to the well-established role of parieto-retrosplenial networks in coordinate transformations (Andersen et al., 1993; Snyder et al., 1998; Salinas and Abbott, 2001; Pouget et al., 2002; Byrne et al., 2007), a largely unexplored question concerns the existence of an extra-retinal neural map of the remembered visual space (Hayhoe et al., 2003; Tatler and Land, 2011; Land, 2014). That the task-related visual retinotopic space is remembered has been suggested by studies showing that when asking to recall a recent visual content, eye movements (on a blank screen) closely reflected spatial relations of remembered images (Brandt and Stark, 1997; Johansson and Johansson, 2014). Moreover, preventing subjects from making eye movements decreased recall performance (Johansson and Johansson,

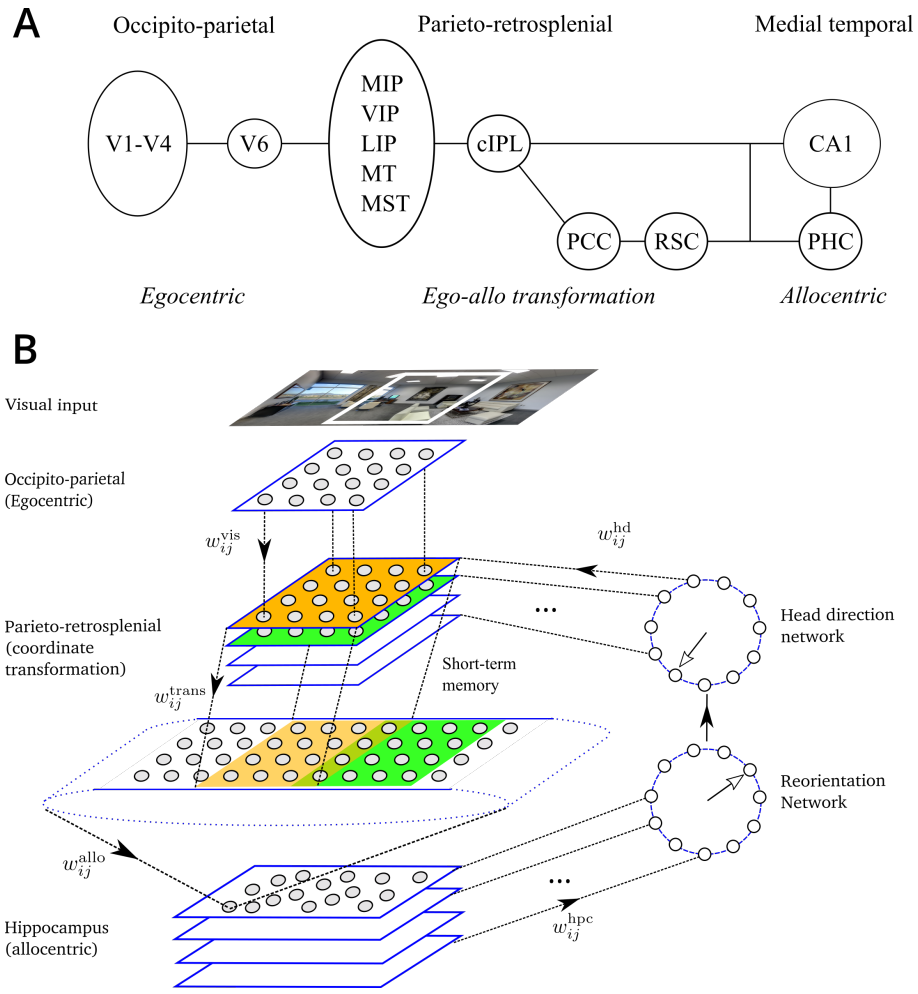

Figure 3.1: A. Dorsal visual pathway of visuospatial information processing in primates (see text for details). B. Schematic representation of the model. Visual features present in the limited visual field constitute the model input. The model network is composed of 6 modules: (1) Occipito-parietal (egocentric); (2) Head-direction network; (3) Parieto-retrosplenial transformation network consists of the coordinate-transformation network and the output layer, which encodes visual features in an allocentric directional frame and spans 2π; (4) Hippocampus; (5) Reorientation network. Projections from the occipito-parietal (visual) areas to the transformation network are topographic. Each head-direction cell activates the corresponding layer of the transformation network. Projections from the different layers of the transformation network to the parieto-retrosplenial output layer are also organized according to head direction: any two layers project topographically to overlapping portions of the output population shifted according to head direction. Synapses between the transformation network and the parietal output network are endowed with short-term memory. Different hippocampal subpopulations project to different neurons in the reorientation network, which in turn corrects head direction signal. Full arrows represent the flow of information in the network. Open arrows represent direction signals in the head direction and reorientation networks.

2014; Laeng et al., 2014). That not only the retinal egocentric space is remembered but also extra-retinal map of surrounding space is stored in memory is demonstrated in studies showing that during natural behavior human subjects direct saccades toward extra-retinal

locations, suggesting that these locations are represented in memory, potentially in an allocentric frame of reference (Land et al., 1999; Hayhoe et al., 2003; Golomb et al., 2011; Melcher and Morrone, 2015; Robertson et al., 2016). Even though suggested by the above studies, the nature of such an extra-retinal map and neural mechanisms underlying its construction and storage are currently unknown.

The present modeling study addresses the question of how such an allocentric representation of surrounding visual space can be constructed and stored by the dorsal visual path – MTL networks. We propose that the existence of such a representation relies on short-term memory linking successive egocentric views and we study how the long-term memory of allocentric visual space can affect behavior in spatial and non-spatial experimental paradigms. In particular, our results suggest that allocentric memory effects during spatial reorientation and memory-based visual guidance tasks can be explained by the existence of such a network.

3.2 Methods

The model is a spiking neuron network constructed to reflect information processing steps thought to be performed by successive stages of neuronal processing in the primate dorsal visual path described above (Fig. 3.1A). To reflect in a simplified way the main processing stages in the pathway, our model of the dorsal pathway is composed of 5 main modules or subnetworks (Fig. 3.1B). First, the module representing information processing in the occipito-parietal circuit essentially applies a set of Gabor-like orientation filters to the incoming visual images, a standard assumption for basic V1 processing. We do not model eye movements, and assume that a retinotopic visual representations obtained at the level of V1 has been remapped, by the time it arrives into the parietal cortex, to a head-fixed representation by taking into account eye position information (Duhamel et al., 1997; Snyder et al., 1998; Pouget et al., 2002). Even though gaze independent, this head-fixed representation is egocentric, or view-dependent, in the sense it depends on the position and orientation the modeled animal (i.e., its head) in space. Second, we model the directional sense by a network of cells whose activity is approximately Gaussian around their preferred orientations (Taube, 2007) and that is sending projections to the parietal cortex (Brotchie

et al., 1995; Snyder et al., 1998). Third, both the activities of the egocentric network and the head direction signal converge onto the network modeling the role of the parieto-retrosplenial network in coordinate transformation. This transformation network uses head direction to convert egocentric visual representations into a head-orientation-independent, or world-fixed representation. This coordinate transformation is done essentially by the same mechanism as the retinotopic-to-head-fixed conversion mentioned above, but in contrast to previous models it does so using low-level topographic visual information. The resulting orientation-independent visual representation is often referred to as spatiotopic, or allocentric, since visual features are determined a world-fixed directional reference frame. Fourth, the allocentric output of the parieto-retrosplenial network arrives to the hippocampus, modeled by a network of cells that learn, by a competitive mechanism, allocentric visual patterns provided by the parietal network. As will be clear from the following, in the context of spatial navigation these cells can be considered as place cells, whereas in a non-spatial context they can be considered as representing memorised visual stimuli. Finally, the reorientation module associates allocentric memories with directional reference frame and feeds back to the head direction cells. The activity of this network represents the correction signal for self-orientation. When the memorized information corresponds to the newly arrived one, the correction signal is zero, whereas in the case of disorientation or in response to specific manipulations of visual cues, it can provide fast adjustment of the self-orientation signal. In the Results section we show that a similar reorientation mechanism can be responsible for behavioral decisions in spatial, as well as non-spatial tasks in primates.

3.2.1 Occipito-parietal input circuit

The occipito-parietal network is modeled by a single rectangular sheet of $N_x \times N_y$ visual neurons, uniformly covering the visual field. In all simulations, except Simulation 6 below, the size of the visual field was limited to $160 \times 100°$, approximately representing that of a primate. The activities of these visual neurons are computed in four steps. First, input images are convolved (using OpenCV `filter2D()` function) with Gabor filters of 4 different orientations $(0, 90°, 180°, 270°)$ at 2 spatial frequencies (0.5 cpd, 2.5 cpd), chosen so as to detect visual features in simulated experiments. Second, the 8 convolution images

are discretized with $N_x \times N_y$ grid, and the maximal response at each position is chosen, producing an array of $N_x N_y$ filter responses. These operations are assumed to roughly mimic retinotopic V1 processing (Heeger, 1992), transformed into a head-fixed reference frame using eye-position information. Third, the vector of filter activities at time t is normalized to have maximal value of unity. Fourth, a population of $N_{vis} = N_x N_y$ Poisson neurons is created with mean rates given by the activity of the corresponding filters scaled by the constant maximal rate A_{vis} (see Table 3.1 for the values of all parameters in the model). For a Poisson neuron with rate r, the probability of emitting a spike during a small period of time δt is equal to $r\delta t$ (Gerstner et al., 2014).

3.2.2 Head direction

The head direction network is composed of $N_{hd} = 36$ Poisson neurons organized in a circle, such that neurons' preferred directions ϕ_k are uniformly distributed between 0 and 2π. The tuning curves of the modeled head-direction neurons are Gaussian with maximum rate A_{hd} and width $\sigma_{hd} = 8°$. Thus, the rate of head-direction neuron k when the model animal's head is oriented in the direction ϕ is given by

$$r_k^{hd} = A_{hd} \exp\left(-\frac{(\phi - \phi_k)^2}{\sigma_{hd}^2}\right) \tag{3.2.1}$$

Such a network generates a Gaussian activity profile centered around ϕ. Our model does not explicitly implement a line attractor dynamics hypothesized to support head direction signal (Zhang, 1996), but it is consistent with it. Head direction cells have been found in several brain areas in rodents and primates (see Taube, 2007, for review), and there is evidence that parietal cortex receives head direction signals (Brotchie et al., 1995).

3.2.3 Parietal transformation network

The parietal transformation network is inspired by previous models (Becker and Burgess, 2001; Byrne et al., 2007) but in contrast to them it operates directly on activities of the Gabor-like visual cells. The transformation of coordinates between the head-fixed and world-fixed coordinates is performed by multiple subpopulations of leaky integrate-

and-fire (LIF) neurons organized as two-dimensional layers of neurons (see Fig. 3.1). Neurons in each layer of the transformation network are in a one-to-one relationship with the visual population and so at each moment t each transformation layer receives a copy of the egocentric (head-fixed) visual input. Therefore, the number of neurons in each transformation layer is equal to N_{vis}. Apart from the visual input, the transformation network also receives input from the population of head direction cells. There is a topographic relationship between the sub-populations of the transformation network and different head directions: each head-direction cell sends excitatory projections to neurons only in one associated layer of the transformation network. Thus, input from head-direction cells strongly activates only a small subset of transformation layers which transmit visual information to the downstream population. More specifically, only the layers which are associated with head directions close to the actual orientation of the head are active. The number of layers in the transformation network is then equal to N_{hd}, giving the total number of neurons in the transformation network $N_{\mathrm{trans}} = N_{\mathrm{vis}} N_{\mathrm{hd}}$.

Thus, in a k-th layer of the transformation network, the membrane potential $v_i(t)$ of the LIF neuron i in is governed by the following equation (omitting the layer index for clarity):

$$\tau_{\mathrm{m}} \frac{dv_i}{dt} = V_{\mathrm{rest}} - v_i + g_i^{\mathrm{ex}}(t)(E_{\mathrm{ex}} - v_i) + g_i^{\mathrm{in}}(t)(E_{\mathrm{in}} - v_i) + R_{\mathrm{m}} I_{\mathrm{ext}} \tag{3.2.2}$$

with the membrane time constant τ_m, resting potential V_{rest}, excitatory and inhibitory reversal potentials E_{ex} and E_{in}, as well as the membrane resistance R_{m}. When the membrane potential reaches threshold V_{th}, the neuron fires an action potential. At the same time, v_i is reset to V_{reset} and the neuron enters the absolute refractory period Δ_{abs} during which it cannot emit spikes. A constant external current I_{ext} is added to each neuron to simulate baseline activity induced by other (unspecified) neurons from the network.

The excitatory conductance in these neurons depends only on the visual input (and thus is independent from k). It is modeled as a combination of α-amino-3-hydroxy-5-methyl-4-isoxazolepropionic acid (AMPA) and N-methyl-d-aspartate (NMDA) receptor activation

$g_i^{\text{ex}} = (1-\alpha)g_i^{\text{ampa}} + \alpha g_i^{\text{nmda}}$ (Murray et al., 2014), that are described by

$$\frac{dg_i^{\text{ampa}}}{dt} = -\frac{g_i^{\text{ampa}}}{\tau_{\text{ampa}}} + \sum_{j\in\{vis\}} w_{ij}^{\text{vis}} s_j(t) \tag{3.2.3}$$

$$g_i^{\text{nmda}} = \frac{\sum_{j\in\{vis\}} w_{ij}^{\text{vis}} s_j^{\text{nmda}}(t)}{1 + 0.22\exp(-0.025 v_i/mV)]} \tag{3.2.4}$$

where the index j runs over input (visual) neurons connected to it, w_{ij}^{vis} are the connection weights and $s_j(t) = 1$ if a presynaptic spike arrives at time t and $s_j(t) = 0$ otherwise. Constant τ_{ampa} determines the time scales of AMPA receptor activation. The parameter s_j^{nmda} is the NMDA gating variable from presynaptic neuron j, modeled as:

$$\frac{ds_j^{\text{nmda}}}{dt} = -\frac{s_j^{\text{nmda}}}{\tau_{\text{nmda}}} + \alpha_s x_j^{\text{nmda}}(2 - s_j^{\text{nmda}}) \tag{3.2.5}$$

$$\frac{dx_j^{\text{nmda}}}{dt} = -\frac{x_j^{\text{nmda}}}{\tau_x} + s_j(t) \tag{3.2.6}$$

where τ_{nmda} and τ_x are the decay time constants of NMDA. The value of constant α_s is 0.2 kHz.

In contrast, the inhibitory conductance depends only on the head-direction cells and ensures that a small subset of transformation layers (i.e. those associated with nearby head directions) are active. To implement it, we employ a simple scheme in which all transformation layer neurons are self-inhibitory, and this inhibition is counteracted by the excitatory input from the head-direction cells. Thus, the inhibitory conductance of the i-th neuron in the k-th layer is given by

$$\tau_{\text{gaba}}\frac{dg_i^{\text{in}}}{dt} = -g_i^{\text{in}} + G_{\text{inh}} + \tau_{\text{gaba}} \sum_{k\in\{hd\}} w_{ik}^{\text{hd}} s_k(t) \tag{3.2.7}$$

where G_{inh} is the constant maximum amount of self-inhibition and w_{ik}^{hd} are the synaptic weights of connections from the head-direction cells. In the current implementation, there is one-to-one correspondence between the head-direction cells and the layers of the transformation network, so $w_{ik} = 1$ only for associated head-direction cell ϕ_k and $w_{ik} = 0$ otherwise.

All layers of the transformation network project to the parietal output population, which codes image features in an allocentric (world-fixed) directional frame. The parietal output population is represented by a two-dimensional neuronal sheet spanning $360 \times 100°$, that is a full panoramic view. It is encoded by a grid of $N_{\mathrm{x}}^{\mathrm{allo}} \times N_{\mathrm{y}}^{\mathrm{allo}}$ neurons. Each layer of the transformation network projects to a portion of the population according to the head direction associated with it associated with this layer (see Fig. 3.1). Since any two nearby layers of the transformation network are associated with head directions shifted relative to each other by $360°/N_{\mathrm{hd}} = 10°$, the overlap between their projections on the parietal output layer is 140°.

Thus, at each moment in time, a spiking representation of the current visual stream (i.e. a spiking copy of the visual input, gated by the head direction cells) arrives to the allocentric neurons spatially shifted according to the current head direction. For example, if two egocentric views (each spanning 160°) are observed at head directions −45° and 45° with respect to an arbitrary north direction, these two views arrive at the allocentric population spatially shifted relative to one another by 90°, so that the activated neurons in the allocentric population span 230°. To ensure that subsequent snapshots are accumulated in time (e.g. during head rotation), the synapses between neurons in the transformation layers and the allocentric population are endowed with short-term memory, implemented by a prolonged activation of NMDA receptors (Durstewitz et al., 2000). Such synapses result in a sustained activity of allocentric output neurons during a period of time sufficient for downstream plasticity mechanism to store information from accumulated snapshots.

The membrane potential of the i-th neuron in the allocentric output population is governed by Eq. 3.2.2 with the synaptic conductance terms determined as follows. First, the excitatory AMPA conductance is given by Eq. 3.2.3 but with the input provided by transformation network neurons via weights w_{ij}^{trans}. Second, the NMDA conductance is described by Eq. 3.2.4, but with the synaptic time scale increased by a factor of 6. This is done to ensure sustained activation of the output neurons upon changes in the visual input. Third, inhibitory input is set to zero for these neurons.

Learning the weights in the transformation network

The connection weights w_{ij}^{vis} from the visual neurons to the parietal transformation cells and w_{ij}^{trans} from the parietal transformation cells to the parietal output neurons are assumed to be learned during development by a supervised mechanism, similar to the one proposed to occur during sensory-motor transformation learning (Zipser and Andersen, 1988; Salinas and Abbott, 1995). In this models it is proposed that when an object is seen (i.e. its retinal position and an associated gaze direction are given), grasping the object by hand (that operates w.r.t. the body-fixed reference frame) provides a teaching signal to learn the coordinate transformation. A similar process is assumed to occur here, but instead of learning body-based coordinates using gaze direction, the model learns world-fixed coordinates using head direction.

More specifically, synaptic weights in the coordinate-transformation network were set by the following procedure. First, the network was presented with an edge-like stimulus at a random orientation and at a randomly chosen location in the visual field. Second, upon the stimulus presentation, the head direction was fixed at a randomly chosen angle ϕ. Third, neurons in the transformation layers associated with the chosen head direction were activated with the average firing rates equal to the rates of the corresponding visual neurons, while neurons in the parietal output layer were activated with the same average rates but shifted according to the chosen head direction (representing the teaching signal). Fourth, the synaptic weights in the network were set according to the Hebbian prescription:

$$w_{ij}^{\text{vis}} = r_i^{\text{trans}} r_j^{\text{vis}} \tag{3.2.8}$$

$$w_{ij}^{\text{trans}} = r_i^{\text{trans}} r_j^{\text{allo}} \tag{3.2.9}$$

where r_i^{vis}, r_i^{trans} and r_i^{allo} are the mean firing rates of the corresponding visual neurons, transformation network neurons and parietal output neurons, respectively. Fifth, the weight vector of each neuron was re-normalized to ensure that the maximum firing rate is below 100Hz. This procedure has been performed for edge-like stimuli at 4 different orientations (corresponding to 4 Gabor filter orientations), placed in the locations spanning the whole visual field and at head directions spanning 360°. Synaptic weights (Eqs. 3.2.8-3.2.9)

were fixed to the learned values prior to all the simulation presented here. No updates were performed on these weights during the simulations.

3.2.4 Hippocampal neurons

As a result of the upstream processing, neuronal input to the hippocampus represents visual features in an allocentric directional frame. Neurons in the parietal output population are connected in an all-to-all fashion to the population of modeled hippocampal cells and the connection weights that are updated during learning according to an spike-timing-dependent plasticity (STDP) rule below. In addition, lateral inhibition between hippocampal neurons ensures a soft winner-take-all dynamics, such that sufficiently different patterns in the visual input become associated with small distinct subpopulations of hippocampal neurons.

Thus, the membrane equation of the i-th hippocampal neurons is given by Eq. 3.2.2. The excitatory conductances are given by Eqs. 3.2.3-3.2.4, but with the input provided by the parietal output neurons via weights w_{ij}^{allo}. Upon the initial entry to a novel environment these weights are initialized to small random values. During learning, the amount of synaptic modification induced by a single pair of pre- and post-synaptic spikes is given by

$$\frac{dw_{ij}^{\text{allo}}}{dt} = G_{\max}\left[a_j^{\text{pre}} s_i(t) - a_i^{\text{post}} s_j(t)\right] \tag{3.2.10}$$

where $s_i(t)$ and $s_j(t)$ detect pre- and post-synaptic spikes, respectively, and

$$\begin{aligned} \frac{da_j^{\text{pre}}}{dt} &= -\frac{a_j^{\text{pre}}}{\tau_{\text{pre}}} + A_+ s_j(t) \\ \frac{da_i^{\text{post}}}{dt} &= -\frac{a_i^{\text{post}}}{\tau_{\text{post}}} + A_- s_i(t) \end{aligned} \tag{3.2.11}$$

The inhibitory conductance of the hippocampal neuron is governed by the following equation:

$$\tau_{\text{gaba}} \frac{dg_i^{\text{in}}}{dt} = -g_i^{\text{in}} + \tau_{\text{gaba}} \sum_{j\in\{\text{hpc}\}} w_{ij}^{\text{inh}} s_j(t) \tag{3.2.12}$$

in which τ_{gaba} determines the time scale of synaptic inhibition as before, and the weights $w_{ij}^{\text{inh}} = W_{\text{inh}}$ are constant and ensure that each hippocampal neuron inhibits all other hippocampal neurons proportionally to its activity.

The hippocampal circuit is complex and consists of several interconnected populations. In our simple model of hippocampal activity we consider only the first stage of hippocampal processing of visual information that is likely to be the CA1, which receives direct projections from the entorhinal cortex, an input gateway to the hippocampus.

3.2.5 Reorientation network

During one continuous experimental trial (e.g. an exploration trial in novel environment or an observation of a novel image on the screen), the reference frame for head direction is fixed and all processing operations in the network are performed with respect to the origin of this reference frame. In particular, an allocentric information stored by the hippocampus as a result of the trial can be correctly used for future action only if the origin of the reference frame is stored with it. Therefore, if in a subsequent trial, the actions to be performed require memory of the previous one, the network should be able to recover the original directional reference (this of course can happen only the visual information received at the start of the trial is considered familiar). Reorientation is the process by which the origin of the stored reference frame is recovered.

Our model of this process rests on the assumption that it is automatic, fast, bottom-up, and does not require costly object/landmark processing. The support for this assumption comes from a large body of reorientation studies in many animal species including primates, showing that object identities are ignored during reorientation (Cheng and Newcombe, 2005). The conditions in which most of the reorientation studies were performed usually are such that there is no single conspicuous point-like cue in the environment that can be reliable associated with a reference direction. For example, in many studies the directional cues come from the geometric layout of the experimental room. Lesion studies in rats suggest that reorientation in such conditions requires an intact hippocampus (McGregor et al., 2004). Furthermore, we propose that this reorientation network is active all the time, in contrast to being consciously "turned on" when the animal "feels disoriented".

Therefore, we expect that its effects can be observed even when no specific disorientation procedure was performed. In particular, we suggest in the Results that a manipulation of objects on the screen can result in automatic corrections of directional sense that can be observed during visual search.

The reorientation network in the model is organized similarly to the head-direction network and consists of N_{re} neurons with preferred positions uniformly distributed on a circle. Therefore, the difference between two nearby reorientation cells is $\Delta\phi = 2\pi/N_{\text{re}}$. The membrane potential of the i-th reorientation neuron is described by the LIF equation (Eq. 3.2.2). Excitatory conductances are described by Eqs. 3.2.3-3.2.4 with the input to the neuron provided by hippocampal place cells via weights w_{ij}^{hpc}. There is no inhibition in the network, and so the inhibitory conductance is set to 0. The ability of the network to perform reorientation is determined by afferent connection weights from the hippocampal cells, which are determined as follows.

Since all allocentric information learned during a trial is linked to the same directional frame, all hippocampal cells learned during the trial are connected to a single neuron of the reorientation network, the one with the preferred direction 0° (Fig. 3.2). The connection weights between the hippocampal cells and the neuron are updated using STDP rule, Eqs. 3.2.10-3.2.11 (this is not essential for the model to work, so that setting the weights to a constant value will give similar results). Once the training trial is finished, N_{re} copies of the learned hippocampal population are created, each corresponding to a separate neuron in the reorientation network. In each copy, all cells have the same input and output weights as the corresponding cells in the original population, but their connection profile is different. In particular, the copy that corresponds to the reorientation neuron with preferred direction $\Delta\phi$ is connected to pre-synaptic cells are shifted by the same angle in the topographically-organized allocentric layer (Fig. 3.2). In machine learning literature, this technique is called “weight sharing” and it allows to achieve translation invariance for detection of objects in images. Here, we apply a similar technique in order to detect familiar snapshots and head direction associated with them.

Suppose, for example, that as a result of learning during a trial, a hippocampal cell is associated with 4 presynaptic cells in the output layer of the transformation network (cells

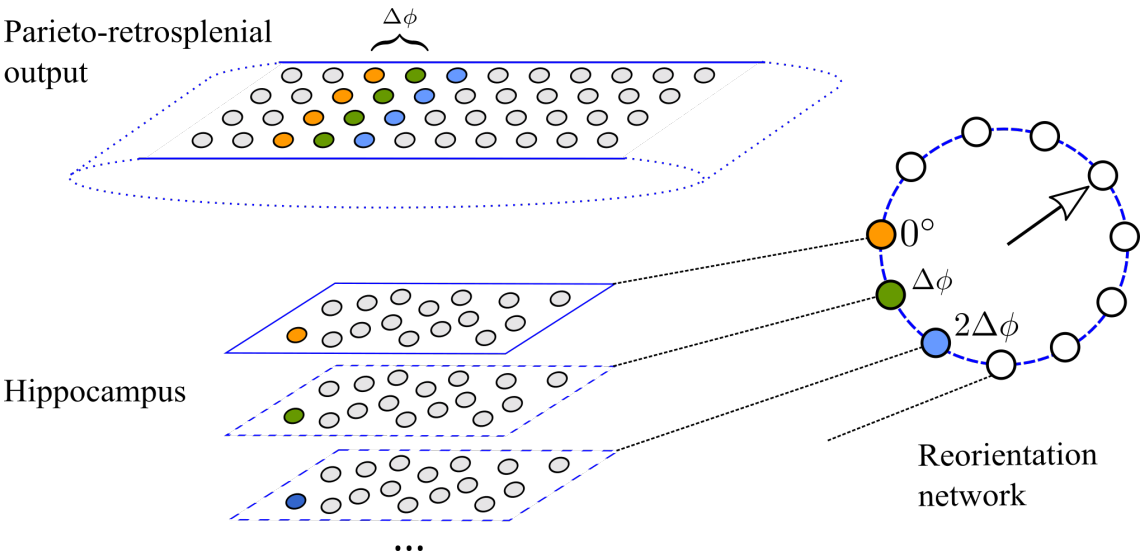

Figure 3.2: Top: the output population of the parieto-retrosplenial network. Bottom: hippocampal cells. The population outlined by full lines is the original population learned during training. As a result of learning, the hippocampal cell shown in orange is connected to the presynaptic cells of the same color (connection weights not shown). All cells in the original population are connected to a single cell (o°) in the reorientation network (Right). The hippocampal populations outlined by dashed lines are copies of the original population that implement weight sharing: the hippocampal cell shown in green (blue) has the same connection weights as the orange cell, but it is connected to pre- and post-synaptic cells shifted by $\Delta\phi$ ($2\Delta\phi$). The number of copies of the original hippocampal population is the same as the number of neurons in the reorientation network.

shown in orange in Fig. 3.2). Suppose further that during an inter-trial interval the head direction network has drifted (or was externally manipulated), so that at the start of the new trial the internal sense of direction is off by $2\Delta\phi$. When the animal sees the same visual pattern again, it will be projected onto the allocentric layer shifted by the same amount (blue cells in Fig. 3.2). This will in turn cause the hippocampal subpopulation that includes the blue cell to be most strongly active, such that the activity peak of the reorientation network signals the orientation error. The reorientation is then performed by readjusting the head direction network to minimize the reorientation error. In the current implementation this is done algorithmically by subtracting the error signal from the actual head direction, but it can also be implemented by attractor dynamics in the head direction layer.

3.2.6 Simulation details

The spiking artificial neural network model described above was implemented using Python 2.7 and Brian 2 spiking neural network simulator (Stimberg et al., 2019). The time step for neuronal simulation was set to 1 ms, while the sampling rate of visual information was 10 Hz, according to the proposals relating oscillatory brain rhythms in the range 6–10 Hz to information sampling (Hasselmo et al., 2002; Busch and VanRullen, 2010). At the start of each simulation, the weights w_{ij}^{allo} and w_{ij}^{hpc} were initialized to small random values (the other weights were trained as described in Section 3.2.3 and fixed for all simulations), see Fig. 3.1B. Parameters of the model are listed in Table 3.1, and the sections below provide additional details of all simulations.

Simulation 1: Egocentric-allocentric transformation

The first simulation was inspired by the study of Snyder et al. (1998), in which monkeys observed visual stimuli at identical retinal locations, but for different orientations of the head with respect to the world, in order to assess whether parietal neurons were modulated by the allocentric head direction. Thus, in this simulation, the head direction angle ϕ was varied from -50° to 50° in 100 sessions. For each trial of a session, the mean rates of the head-direction neurons were calculated according to Eq. 3.2.1 and fixed for the rest of the trial. The stimulus (vertical black bar, width: 10°) was shifted horizontally across the midline of the visual field ($160 \times 100^\circ$) from left to right in 1° steps, such that it remained at each position for 100ms. The neuronal spikes were recorded from the occipito-parietal network, the parieto-retrosplenial transformation network and its output layer, for each stimulus position across 10 trials per session. Mean firing rates were then calculated from these data.

Simulation 2: Accumulation of successive views using short-term synaptic memory

The aim of the second simulation was to illustrate the synaptic mechanism for an integration of successive visual snapshots in time, instrumental for spatial coding. We model a monkey that remains in the same spatial location and turns its head from left to right. Thus, the

Parameter	Value	Description
	Neuron numbers	
$N_x \times N_y$	80×50	Parieto-occipital network size
N_{hd}	36	Head direction network size
$N_x^{allo} \times N_y^{allo}$	180×50	Parietal output layer size
N_{re}	36	Reorientation network size
	Mean amplitudes in the input populations	
A_{vis}	100	Spikes/s., Maximum rate of the parieto-occiptal network
A_{hd}	100	Spikes/s., Maximum rate of the head-direction network
	Parameters of the LIF model	
V_{rest}	-65	mV, Resting potential
V_{th}	-55	mV, Spiking threshold
V_{reset}	-65	mV, Reset potential
E_{ex}	0	mV, Excitatory reversal potential
E_{in}	-80	mV, Inhibitory reversal potential
E_{in}	250	mΩ, Membrane resistance
Δ_{abs}	1^{a-c}, 2^{d}	ms, Absolute refractory period
α	$0.9^{a,b}$, $0.3^{c,d}$	Balance between AMPA and NMDA receptor
τ_{ampa}	5	ms, AMPA receptor time scale
τ_{nmda}	$100^{a,c,d}$ 600^{b}	ms, NMDA receptor time scale
τ_x	2.5	ms, NMDA receptor time scale
τ_m	$10^{a,c,d}$, 20^{b}	ms, Membrane time scale
τ_{gaba}	10	ms, GABA receptor time scale
I_{ext}	20^{a-c}, 40^{d}	mA, External input current
G_{inh}	2	Self-inhibitory conductance
	STDP	
G_{max}	0.05^{c}, 0.1^{d}	Maximal weight change
A_+	0.005	Maximal potentiation amplitude
A_-	A_+ x 1.05	Maximal depression amplitude
τ_{pre}	20	ms, Potentiation time scale
τ_{post}	15^{c}, 17.5^{d}	ms, Depression time scale
	Other parameters	
σ_{hd}	8°	Tuning curve width of hed direction cells
W_{inh}^{train}	1.0	Lateral inhibition weight in the hippocampal population
W_{inh}^{test}	0.1	Lateral inhibition weight in the hippocampal population

Table 3.1: Parameters of the dorsal visual pathway model. The configuration of all the parameters from the model is described in the table. Different neuron populations from the model share common parameters but the value of these parameters is not all the same. In order to distinguish the neural populations, a-d in the second column label neural population: a, Occipito-parietal (egocentric); b, Parieto-retrosplenial transformation network; c, Hippocampus; d, Reorientation network. The parameter share the same value in different neural populations, if its value has no label.

model was presented with a set of 9 successive overlapping views ($160 \times 100°$) taken from a panoramic ($360 \times 100°$) image, 100ms per view. Initial head direction was arbitrarily

set to 0°.

Simulation 3: Encoding of allocentric visual information during spatial exploration

In the third simulation we studied the role of temporal accumulation of visual information for spatial coding. The model ran through a square 3D environment (area: 10×10 m, wall height 6 m)for about 10 min so as to cover uniformly its area. The visual input was provided by a cylindrical camera ($160 \times 100°$) placed at the location of the model animal. At each spatial location 9 successive views of the environment were taken in different directions (as in the Simulation 2). The vector of mean firing rates of the occipito-parietal neurons at a single spatial location and orientation constituted the egocentric population vector. The mean firing rates of the the parieto-retrosplenial output neurons at each location constituted the allocentric population vector (this population vector is independent from orientation as a result of coordinate transformation). To compare spatial information content in the two populations, we first estimated intrinsic dimensionality of the two sets of population vectors. This was performed using two recent state-of-the art methods: DANCo (Ceruti et al., 2014), as implemented by the `intrinsicDimension` R package, and ID_fit (Granata and Carnevale, 2016). For both methods, the principal parameter affecting dimensionality estimation is the number of neighbors for each point in the set that is used to make local estimates of the manifold dimension. Second, we used two different methods to visualize the structure of the low-dimensional manifold: Isomap (Tenenbaum et al., 2000) and t-SNE (van der Maaten and Hinton, 2008). To extract principal axes of the manifold, we used PCA on the data points projected on two principal dimensions provided by the above methods. We chose the parameter values for which the visualized manifold best approximates the original space. We then determined a set of points (i.e. population vectors) that lie close to the principal axes of the manifold and visualized them in the original environment. If the manifold structure corresponds well to the spatial structure of the underlying environment, the principal axes of the manifold should lie close to the principal axes of the environment.

Simulation 4: Visual responses of hippocampal neurons in an image memorization task

This simulation was inspired by the study of Jutras and Buffalo (2010a) in which a large set of novel visual stimuli was presented to monkeys on a computer screen. Neuronal activity in the hippocampal formation in response to the visual stimuli was recorded. One of the results of this study suggested that hippocampal neurons encode stimulus novelty in their firing rates. To simulate this result, we presented to the model 100 novel stimuli randomly chosen from the dataset (http://www.vision.caltech.edu/Image_Datasets/Caltech101). The stimuli (resized to 160×100 pixels) were shown to the model successively in one continuous session (500ms stimulus presentation time + 1000ms inter-trial interval with no stimuli) and the activities of the hippocampal neurons during learning were recorded.

Simulation 5: Spatial reorientation

In this simulation of the experiment of Gouteux et al. (2001), the testing room was a rectangular 3D environment with area 20×10 m and wall height 6m. In the "No cues" task the only visual features in the room were provided by the outlines of the walls. In the other 3 tasks, a square visual cue was presented in the middle of one of the walls with the edge length equal to 1/6 (small cue), 1/3 (medium cue) or 1/2 (large cue) of the environment width. Each task consisted of two phases, exploration and reorientation. During the exploration phase the modeled animal uniformly explored the environment, as in Simulation 3. The reorientation phase composed multiple trials. At the beginning of each trial, the model was placed at one of spatial locations covering the environment in a uniform grid. At each of these locations, 9 successive views were taken. Reorientation performance was assessed in two ways: (i) only the first view at each location was used for reorientation; (ii) successive views accumulated over 60 successive positions were used for reorientation.

Simulation 6: Memory-based visual search

In this simulation we used a dataset of visual images used in the study by Fiehler et al. (2014). This dataset consists of 18 image sets corresponding to 18 different arrangements

of the same 6 objects (mug, plate, egg, jam, butter, espresso cooker). Each set includes a control image (all objects on the table in their initial positions) and images in which one of the objects is missing (target object) and one or more other objects displaced to the left or to the right. In the simulation we used only a subset of all images in a set that included either 1, 3 or 5 of the objects mentioned above displaced either to the left or to the right (referred to as "local" condition in Fiehler et al., 2014), giving rise to 6 experimental conditions. In each condition, there were 18 test images of displaced objects, plus the associated control images. Taking into account the distance between the animal and the screen as well as the size of the image (provided by Fiehler et al. (2014)), we calculated the size of the image in degrees of visual field. We then determined a rectangular portion of the image ($30 \times 15^{\circ}$) that included all objects in initial and displaced positions in all images. The contents of this area served as an input to the model. Thus, in this simulation the spatial resolution of the visual input was higher than in the previous simulations as the visual field of the model was smaller, but the size of the input network was kept the same.

During each simulation trial, the image of objects in initial positions was first presented to the network during 2000 ms and stored by the hippocampal cells. The image of displaced objects (in one of the 6 conditions above) was subsequently presented to the network for the same amount of time and the orientation error was read out from the mean firing rates of the reorientation network.

3.3 Results

We first show that properties of neuronal firing along the simulated neural pathway from the visual cortex to the hippocampus reflect those of biological neurons along the pathway. We then demonstrate how backward projections from the hippocampus to the head direction network, can explain hippocampal influence on head direction during spatial reorientation and memory-based visual search.

3.3.1 Visual and parietal model neurons encode sensory representations in distinct reference frames

We start with a characterization of modeled dorsal-visual path neurons in the case when a simulated animal is assumed to sit in front of a screen and is free to rotate its head (Duhamel et al., 1997; Snyder et al., 1998, for simplicity, we assume that rotation occurs only in the horizontal plane). The firing rate of occipito-parietal (input) neurons and the output parietal neurons as a function of the allocentric position of a visual stimulus (i.e. a vertical bar moving horizontally across the visual field) was measured for two different head directions (Figs. 3.3A,B). For a neuron in the input population, a change in head direction induces the corresponding change of the receptive field of the neuron, since its receptive field shifts together with the head along the allocentric position axis (Fig. 3.3C). In contrast, for a parietal output neuron, a change in head direction does not influence the position of its receptive field, which remains fixed in an allocentric frame (Fig. 3.3D). To show that this is also true on the population level, we measured, for all visual input cells and all parietal output cells, the amount of shift in its receptive field position as a function of head direction shift, while the head was rotated from $-50°$ to $50°$. For cells in the occipito-parietal visual area, the average linear slope of the dependence is close to 1, whereas in the allocentric parietal population the average slope is close to 0 (Fig. 3.3E), meaning that these two populations encode the visual stimulus in the two different reference frames: head-fixed and world-fixed. These properties of model neurons reproduce well-known monkey data showing that different sub-populations of parietal cortex neurons encode visual features in the two reference frames (Duhamel et al., 1997; Snyder et al., 1998).

The receptive fields of the intermediate neurons of the coordinate transformation network exhibit gain modulation by head direction (Fig. 3.3F), as do monkey parietal neurons (Snyder et al., 1998).The hypothesis of reference-frame conversion via gain modulation has been extensively studied in both experimental and theoretical work, in the context of sensory-motor coordination during vision-guided reaching (Avillac et al., 2005; Pouget and Sejnowski, 1997; Salinas and Abbott, 2001). While coordinate-transformation processes involved in the two cases are conceptually similar, the underlying neuronal computations

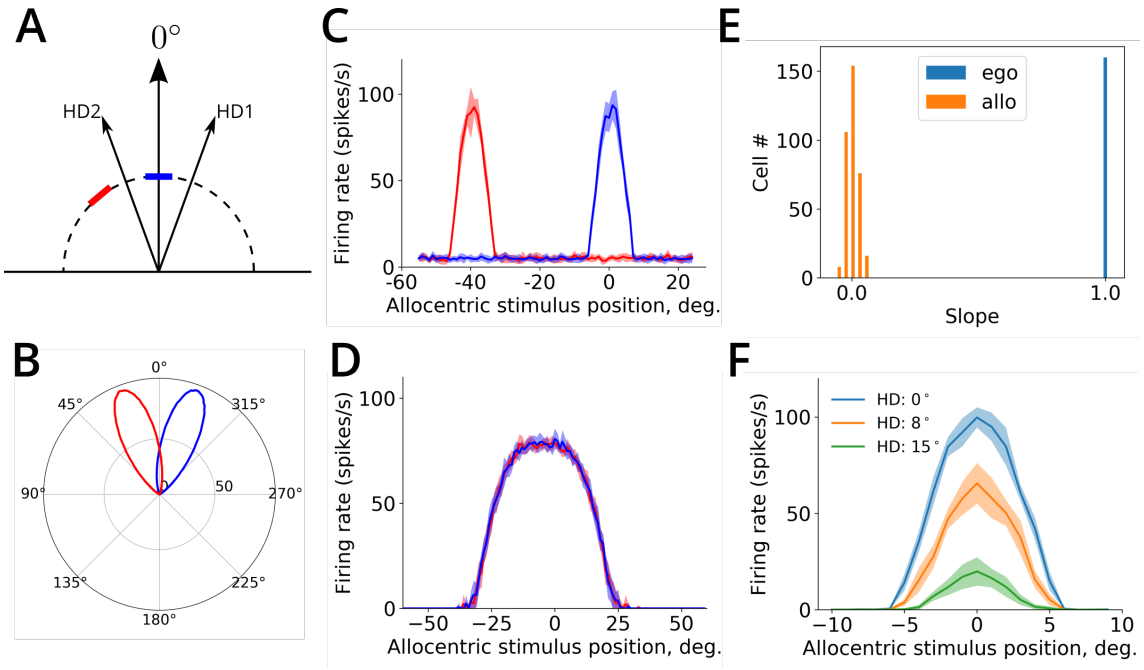

Figure 3.3: A. A schematic representation of the receptive field of one input visual input neuron at two head directions (HD1 and HD2). The position of the receptive field of the neuron is shown by the blue and red bar for HD1 and HD2, respectively. B. The population activity of head direction cells in the model at 20° (HD1) and -20° (HD2). C. Tuning curves of an input visual neuron (±SD) for the two head directions represented in B. D. Tuning curves of an allocentric output neuron for the same head directions. E. Histograms show the distributions of the linear dependence slopes between the shift in the receptive field position and the shift in head direction, for egocentric (in blue) and allocentric (in orange) neuronal populations. F. Transformation network neurons are gain-modulated by head direction. Stimulus tuning curves of the same neuron for three different head directions are shown.

can differ substantially, because the former requires simultaneous remapping for the whole visual field, while the latter is limited to the computation of coordinates for a single target location (i.e. a representation of the point-like reaching target). This difference limits the use of noise-reducing attractor-like dynamics that is an essential component in point-based sensory-motor transformation models (Pouget et al., 2002), because in full-field transformation the information and noise are mixed together in a single visual input stream.

3.3.2 Spatial coding using temporal accumulation of successive views

Because of a limited view field, at each moment in time the simulated animal can directly observe only a restricted portion of visual environment (i.e. a visual snapshot, see Figs. 3.4A,B). That these snapshot-like representations are represented in memory, has

been demonstrated in a number of studies showing viewpoint-dependent memory representations (Diwadkar and McNamara, 1997; Christou and Bülthoff, 1999; Gaunet et al., 2001). Moreover, experimental evidence suggests that visual information can be accumulated from successive snapshots during e.g. head rotation, giving rise to a panoramic-like representation of the surrounding environment that can inform future goal-oriented behavior (Tatler et al., 2003; Oliva et al., 2004; Golomb et al., 2011; Robertson et al., 2016). A candidate neural mechanism for implementing such integration is short-term memory, i.e. the ability of a neuron to sustain stimulus-related activity for a short period of time (Goldman-Rakic, 1995; Constantinidis and Steinmetz, 1996). In our model, this is implemented by sustained firing via prolonged NMDA receptor activation (Fig. 3.4C). Combined with STDP learning rule in the connections between the parietal output neurons and the hippocampus, this mechanism ensures that a time-integrated sequence of visual snapshots is stored in the synapses to hippocampal neurons. In particular, head rotation results in a temporarily activated panoramic representation in the population of output parietal neurons that project to CA1. STDP in these synapses ensures that these panoramic representations are stored in the synapses to downstream CA1 neurons (Fig. 3.4D).

A large amount of experimental evidence suggests that many animal species encode a geometric layout of the surrounding space (Cheng and Newcombe, 2005; O'Keefe and Burgess, 1996; Gouteux et al., 2001; Krupic et al., 2015; Keinath et al., 2017; Bécu et al., 2019). Computational models of spatial representation in rodents link this sensitivity to geometry with a postulated ability of the animal to estimate distances to surrounding walls (Hartley et al., 2000) or to observe panoramic visual snapshots of surrounding space (Cheung et al., 2008; Sheynikhovich et al., 2009), and rely on a wide rodent visual field (320°). That the width of visual field plays a role in geometric processing in humans was demonstrated in the study by Sturz et al. (2013), in which limiting visual field to 50° impaired performance in a geometry-dependent navigation task, compared to a control group. We thus studied whether activities of egocentric and allocentric neurons in the model encode information about the geometry of the environment and whether snapshot accumulation over time plays a role in this process.

To do this, we run the model to uniformly explore a square environment and we stored

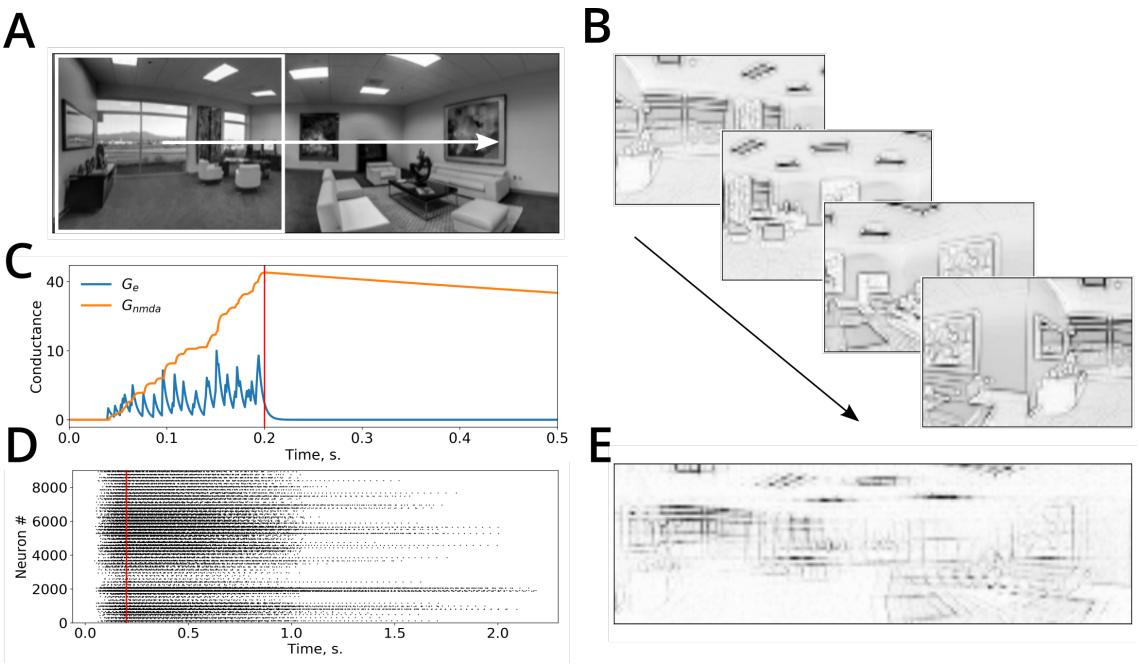

Figure 3.4: A. A panoramic image of an environment superimposed with the visual field of the simulated animal (white rectangle). The white arrow shows the direction of visual scan path. B. Several successive visual snapshots along the scan path shown in A are represented by mean firing rates of the occipito-parietal (egocentric) network. C. An example of the evolution of AMPA and NMDA receptor conductances of parieto-retrosplenial output neurons as a function of time. Stimulus onset: $t = 0$, stimulus offset: $t = 200$ms (red line). D. Raster plot of spiking activities of the output neurons showing short-term memory in this network. An input is presented at time 0 and is switched off at the time shown by the red vertical line. The neurons remain active after stimulus offset due NMDA-receptor mediated short-term memory. E. Synaptic weight matrix of a single hippocampal neuron after learning stores the activity of the parieto-retrosplenial output layer accumulated over several successive snapshots shown in B.

population rate vectors of the egocentric-visual and allocentric-parietal populations at successive time points during exploration. More specifically, for the egocentric population, each population vector corresponded to population activities evoked by the presentation of a single visual snapshot. In contrast, for the allocentric population, each population vector corresponded to a panoramic snapshot obtained by accumulating several successive snapshots during head rotations (see Methods). The visual information content was identical in two sets of population vectors as they were collected during the same exploration trial. Population vectors in each set can be considered as data points in a high-dimensional space of corresponding neural activities. These points are expected to belong to a two-dimensional manifold in this space, since during exploration the model animal moves in a 2D spatial plane. The analysis of the intrinsic dimensionality of both sets indeed shows that it is about 2 (Figs. 3.5A,B). We then applied two different manifold visualisa-

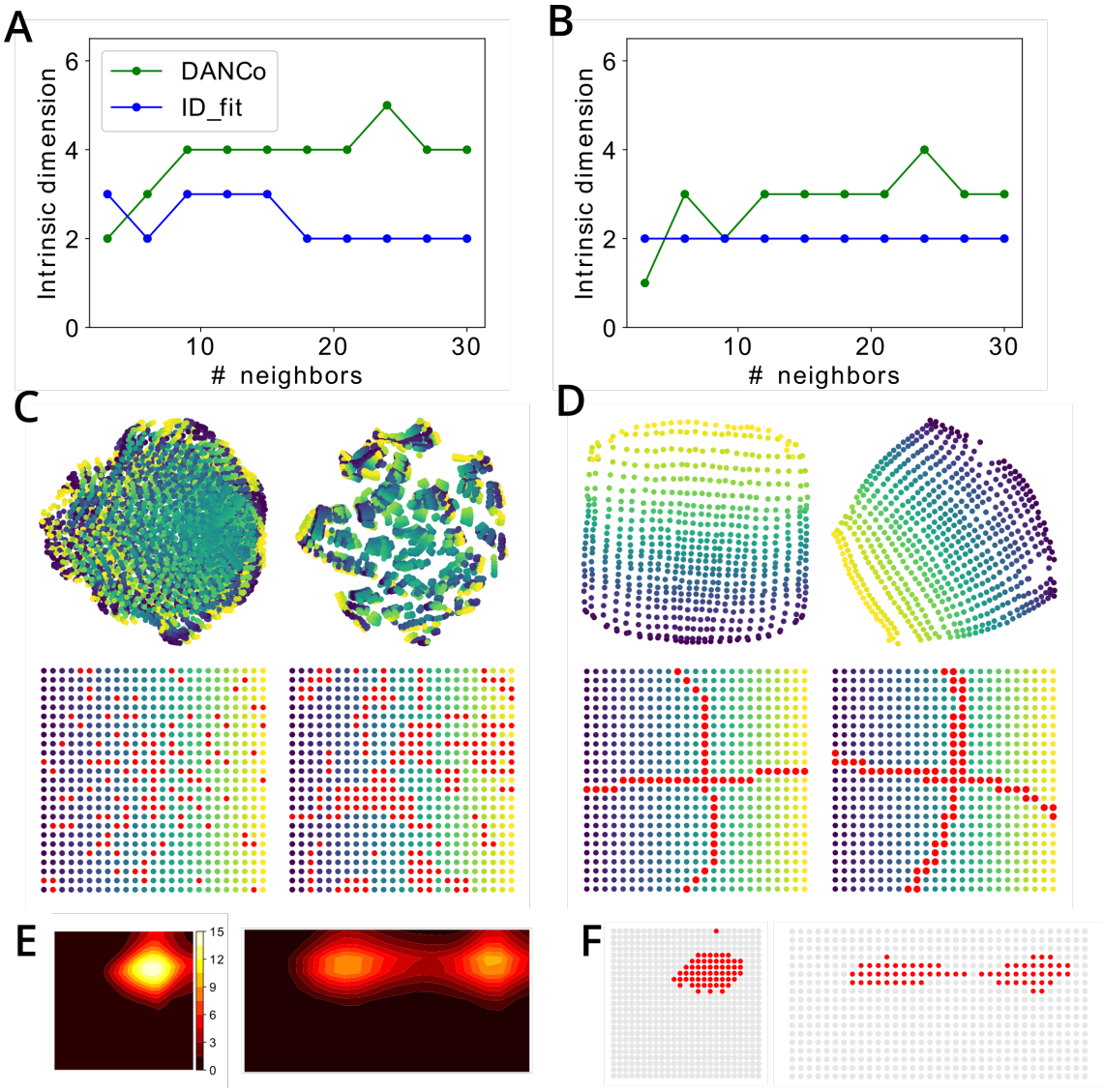

Figure 3.5: A,B. Estimation of intrinsic dimensionality of the set of population vectors in the egocentric (A) and allocentric (B) populations by two different state-of-the-art methods (DANCo and ID_fit). C,D. Top: Projection of the population vector manifolds onto a two-dimensional plane using Isomap (left) and t-SNE (right) algorithms. Color gradient from yellow to blue corresponds to the position at which the corresponding population vector was observed, as shown in the Bottom row. Red dots show population vectors that lie close to the principal axes of the 2D manifold of the principal space. C and D show population vectors of the egocentric and allocentric neuronal populations, respectively. E. An example of the receptive field of one hippocampal neuron after learning the environment before (left) and after (right) extension of the environment along it horizontal axis. F. For the same neuron as in E, red dots show locations in the environment where this neurons is winner in the WTA learning scheme.

tion techniques to see whether the shape of manifold reflects the environment shape (see Methods). We found that when applied to population vectors of the egocentric population, the structure of the manifold did not reflect the layout of the environment (Fig. 3.5C). In

contrast, allocentric population activities reliably preserved geometric information in the spatial organization of the manifold (Fig. 3.5D). Moreover principal axes of the manifold corresponded to the principal axes of the underlying environment only for the population vectors of the allocentric population (bottom row of Figs. 3.5C,D). The extraction of principal axes of an experimental space has been proposed to underlie spatial decision making in several experimental paradigms, including data from humans (Gallistel, 1990; Cheng and Gallistel, 2005; Sturz et al., 2011).

STDP in the connections between the parietal and hippocampal neurons ensures that allocentric spatial views are stored in memory, while lateral inhibition in the hippocampal layer implements a competition such that different hippocampal cells become selective to different localized regions of the visuospatial manifold, which, by virtue of the coherent mapping on the real space, correspond to spatial receptive fields (Figs. 3.5E). When the geometry of the environment is modified, but the memorised allocentric representation remains the same, modeled hippocampal cells express corresponding modifications of their receptive fields (Figs. 3.5E,F), potentially providing a purely sensory basis for the effects of geometric manipulations observed in rats (O'Keefe and Burgess, 1996) and humans (Hartley et al., 2004). These simulations show how the egocentric-allocentric conversion and short-term memory along the modeled dorsal visual pathway can be instrumental in structuring the hippocampal input according to the geometric properties of the surrounding space that were repeatedly shown to affect human navigation (Hermer and Spelke, 1994; Bécu et al., 2019).

3.3.3 Visual responses of hippocampal neurons reflect learning of visual stimuli

The hippocampal memory network is thought to support a large spectrum of memory-based behaviors, and therefore its basic properties should manifest themselves in situations other than navigation. In particular, plasticity and competition, which are proposed to mediate fast hippocampal learning of visual information in our model, occur not only during navigation but also in a passive image viewing paradigm. In the next simulation inspired by the experiment of Jutras and Buffalo (2010a) we used the stationary model to learn

a set of 100 novel images presented in a quick succession (see Methods) and recorded activities of modeled hippocampal neurons. In response to the presented stimuli, some neurons increased their firing rates as a result of STDP (winning neurons), while the rest of the neurons were inhibited (Fig. 3.6A). Even though only a few neurons won the competition for each particular stimulus, some neurons were selective to a larger number of stimuli than others (Fig. 3.6C,D). Therefore, stimulus-averaged firing rates of different neurons expressed either a decrease in the average firing rate (for neurons that were never winners), no change in the average rate (for neurons that were winners for a relatively small number of stimuli), or an increase in the average rate (for neurons that were winners for a relatively high number of stimuli, Fig. 3.6B). There was a larger number of neurons expressed decreased firing rates or no change, than those that increased their average rate (Fig. 3.6D).

Under the assumption that a novelty-detection mechanism (assumed to reside in the hippocampus or elsewhere, but not modeled here) prevents hippocampal firing in response to a repeated stimuli, these results are in accord with the data from a number of studies showing that different subsets of recorded hippocampal neurons either decreased, showed no changes, or increased their activity in response to the presentation of a novel stimulus (Jutras and Buffalo, 2010a; Rutishauser et al., 2006; Viskontas et al., 2006). In these studies of the role of novelty in hippocampal processing, stimulus-averaged elevation of neural activity was considered as an indication of an abstract (i.e. independent of stimulus identity) novelty processing in the hippocampus (Jutras and Buffalo, 2010a; Rutishauser et al., 2006). It is unclear how such an abstract representation of novelty can be reconciled with the role of the hippocampus in navigation. In contrast, our simulation results suggest that elevation or depression of stimulus-averaged firing rate in a neuron may be related to the number of stimuli for which this neuron is winner.

3.3.4 Top-down hippocampal input in spatial reorientation and memory-based search

The population of the hippocampal neurons in the model represents the neural storage of (potentially highly processed) visual information aligned with an allocentric directional

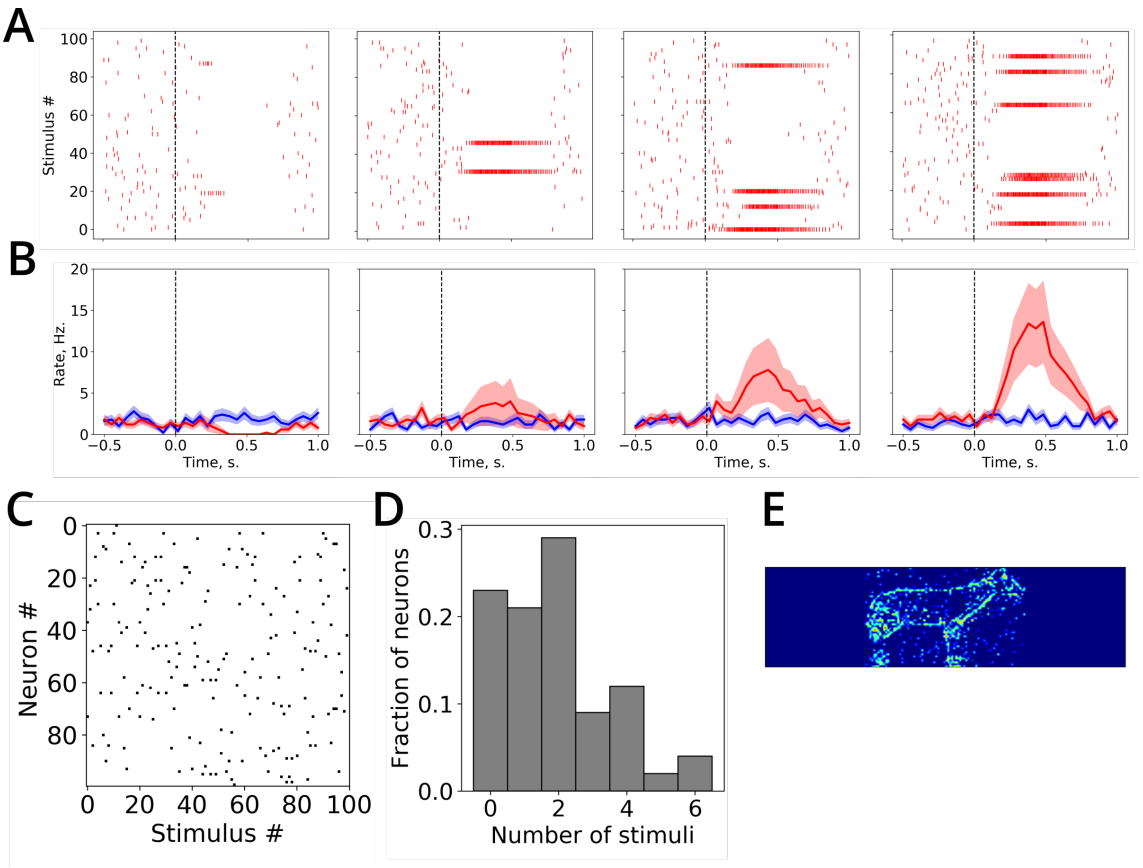

Figure 3.6: A. Spike raster plots for four example neurons in response to presented visual stimuli. B. Stimulus-averaged firing rates of neurons in A (mean ± SEM shown in red), compared to baseline firing rates (shown in blue). The dashed vertical line represents the stimulus onset. C. Black dots correspond to winner neurons among all other neurons (vertical axis) for each of the presented stimuli (horizontal axis). D. The histogram shows the distribution of neurons with respect to the number of stimuli for which they are winners. E. An example of the weight matrix of a hippocampal neuron after learning.

frame by the coordinate transformation network. In this section we show how this neural storage can affect two types of behavior: (i) determination of position and orientation when a disoriented monkey is placed into a familiar environment (Gouteux et al., 2001); and (ii) memory-guided visual target search in an image viewing paradigm (Fiehler et al., 2014). While these two tasks may seem unrelated, we propose that the same neural process, namely a reorientation of the head-direction network based on the comparison between the newly obtained visual information and the contents of the hippocampal allocentric storage, underlies behavioral decisions in these tasks.

Spatial reorientation

In a series of reorientation experiments with monkeys, Gouteux et al. (2001) have shown that these animals relied on both the geometric information (given by the three-dimensional layout of the rectangular experimental space) and non-geometric cues (e.g., landmark objects placed near the walls or corners of the recording chamber). The authors paid specific attention to the influence of landmark size on reorientation behavior. When small objects were placed near one of the walls or in the corners of the room, the monkeys did not use these cues to reorient, and their search pattern was determined based only on the geometric information. Importantly, this was not because the monkeys did not notice the landmarks, since they performed exploratory actions towards them (looked at or touched them). Once the landmark size was increased however, the monkeys successfully used them for reorientation independently of their location and number.

To simulate these data, we tested the model in four reorientation tasks in a virtual three-dimensional rectangular room. In these tasks, either no landmark cues were present in the room, or one visual landmark of three different sizes was placed in the middle of one of the walls (Fig. 3.7A). Each task comprised an exploration phase, during which the model randomly explored the environment, and a reorientation phase. In the reorientation phase the model was initialized with a random heading direction and placed back into the environment learned during the exploration phase at a random location. The performance of the model was assessed from the accuracy of reorientation: we assume that the animal will navigate to the correct corner if it has correctly estimated its initial heading, whereas it will make a navigation error if the reorientation error is high.

Once the information from the initial view reached the hippocampus upon the reentry to the environment, the activity of the reorientation network signalled the orientation error (Fig. 3.7B). This error represented the discrepancy between the initial heading direction and the heading direction most consistent with the allocentric information stored in the projections from the place cells to the reorientation network. The asymmetric shape of the polar plot reflects the influence of the environment's geometric layout on reorientation: for the no-cue condition, the network activity peaked at the correct (0°) and its rotationally opposite (180°) orientations with an identical average amplitude. When the visual cue was

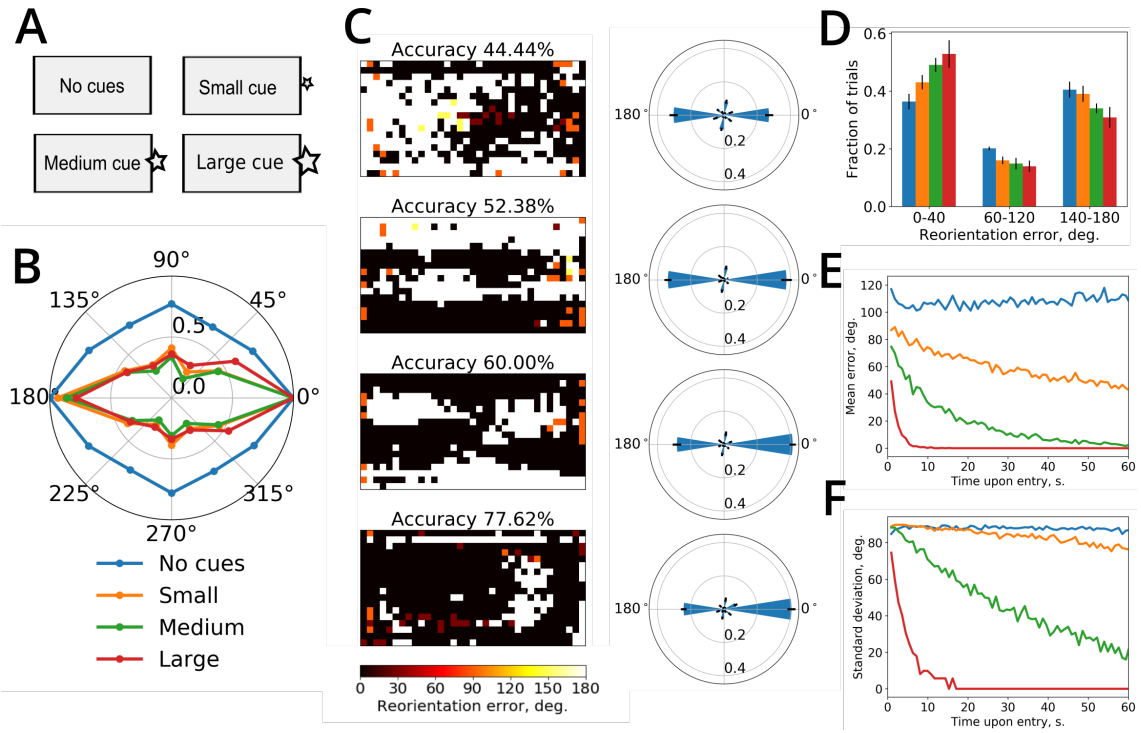

Figure 3.7: A. The experimental environment was a rectangular room (represented by the gray rectangle). The same reorientation simulation was run in four conditions: no visual cues apart from walls of the room, or 1 visual cue at three different sizes (small, medium, large). B. Polar plot of the mean activity of the reorientation network when the simulated animal was placed in various locations in the room. Dots mark the preferred locations of the reorientation N_{re} neurons Colors from blue to red represent 4 experimental conditions. C. Rows from top to bottom correspond to experimental conditions as in A. Left: Reorientation maps show, for each location in the room, the reorientation error committed by the model after seeing only the first visual snapshot from that location (at a randomly chosen head orientation). The pixel color from black to white codes for the absolute value of the reorientation error from 0 to π. Right: polar histograms of reorientation errors (±SD), averaged over 9 random orientations at each location. D. Bar plot shows the distribution of the absolute reorientation errors (±SD) among the approximately correct orientation (0-40°), rotational error (140-180°) and other directions. E,F. Reorientation error mean (E) and its standard deviation (D) when progressively more snapshots were used for reorientation. Color code for D,E,F as shown in B.

present, its size determined the difference between the activity peaks. Therefore, when reorientation was performed from different locations in the environment (based only on the first view taken), the accuracy, measured as the percentage of locations with a correctly determined orientation, was about 50% in the no-cue condition and raised to about 77% in the large-cue condition (Fig. 3.7C, left column). Reorientation maps (Fig. 3.7C, right column) suggest that depending on the position of the orienting cue in the room, some locations in the environment provide better visual information for reorientation than others (shown by white areas in the maps). The histograms of orientation errors (Fig. 3.7C, right

column, and Fig. 3.7D) show that, on average, a larger visual landmark provides a much better reorienting cue than a small one, for which a similar number of correct decisions and rotational errors was observed (Fig. 3.7D). This is due to the fact that orientation is determined essentially by comparing the egocentric view from the initial position with allocentric views stored in synaptic memory, without any explicit landmark identification process. Therefore, influence of small visual cues becomes negligible with respect to gross visual features of the surrounding space (corners, shapes of the walls, etc.). These results are consistent with the hypothesis that reorientation is a fast, bottom-up process based on low-level visual information (Sheynikhovich et al., 2009). Learning landmark identities and their spatial relation to goals can be added by subsequent learning, but may not be taken into account unless their are sufficiently salient compared to other (e.g. geometric) cues present in the environment (Cheng, 1986).

So far the reorientation performance was assessed based only on the first view taken. The reorientation performance is likely to increase if the animal is allowed to accumulated visual information from successive views taken in the same location at different orientations or at different locations, e.g. during initial movements through the environment. This is what happens in the model, since increasing the number of snapshots that are used for reorientation improved its accuracy (Fig. 3.7E,F). In this case we placed the simulated animal at 60 successive positions, while at each position the animal rotated its head to obtain a corresponding panoramic view. The activity of the reorientation network was calculated as a sum of its activities after each successive view. When a large cue was present, the simulated animal obtained an accurate orientation estimate after visiting about 10 successive locations. In contrast, the mean error and standard deviation of reorientation were decreasing much slower for smaller sized landmarks. Thus, our model describes a neural mechanism for spatial reorientation which relies on an allocentric visual information stored in the hippocampal network. This allocentric information feeds into a head-direction-like network, assumed to reside in the retrosplenial cortex, that signals reorientation error and affect the sense of direction via its input to the head-direction system if the brain (Taube, 2007). In addition to providing a mechanistic basis for the reorientation process, which is a necessary part of navigational behavior and whose existence is assumed (either implicitly or explicitly) in a number of computational models of navigation, this

model proposes how reorientation can be performed continuously, i.e. during ongoing spatial behavior.

Memory-based visual search

To illustrate a potential role of the stored hippocampal representation in memory-based visual tasks, we simulated the study of Fiehler et al. (2014). In this study, head-fixed human subjects remembered a visual scene with 6 objects on a table, presented on a computer screen (Fig. 3.8A, top). This encoding phase was followed by 2-s. delay (uniform gray image), and then the subjects were presented with a modified scene in which one of the objects was missing (the target object) and either 1, 3 or 5 other objects displaced horizontally (Fig. 3.8A, bottom). The subjects were required to point to the remembered location of the missing object. If the subjects had used only an egocentric information (i.e. remembered object position with respect to the head), then their performance would have been independent from the displaced objects. The results of this experiment demonstrated in contrast that pointing performance was influenced by the non-target objects, such that shifting a higher number of them induced a larger pointing error. Even though the pointing error was always made in the direction of the object displacement in the image, the size of the error only partially accounted for the veridical displacement of the objects. These data suggest that human subjects combine allocentric (i.e. based on the information from the environment, in this case represented by the visual features associates with displaced objects) and egocentric (i.e. based on the memory of an egocentric location of the target object) information during memory-based search (Fiehler et al., 2014). The neural mechanism of this allocentric correction of the egocentric memory is unknown.

We hypothesized that the influence of allocentric image information observed in this experiment arises as a result of a slight misorientation of the head direction network due to the apparent shift of visual features caused by the object displacement in the attended area of the image. In order to demonstrate this effect, we first presented to the model an image of a control scene with all 6 objects (see Fig. 3.8A, top, for an example). We used, with permission, the same image data set that was used in the experimental study. As input to the network we only used the part of the image near the objects, because in the experiment is was fixated most of the time and because of the evidence that displacement

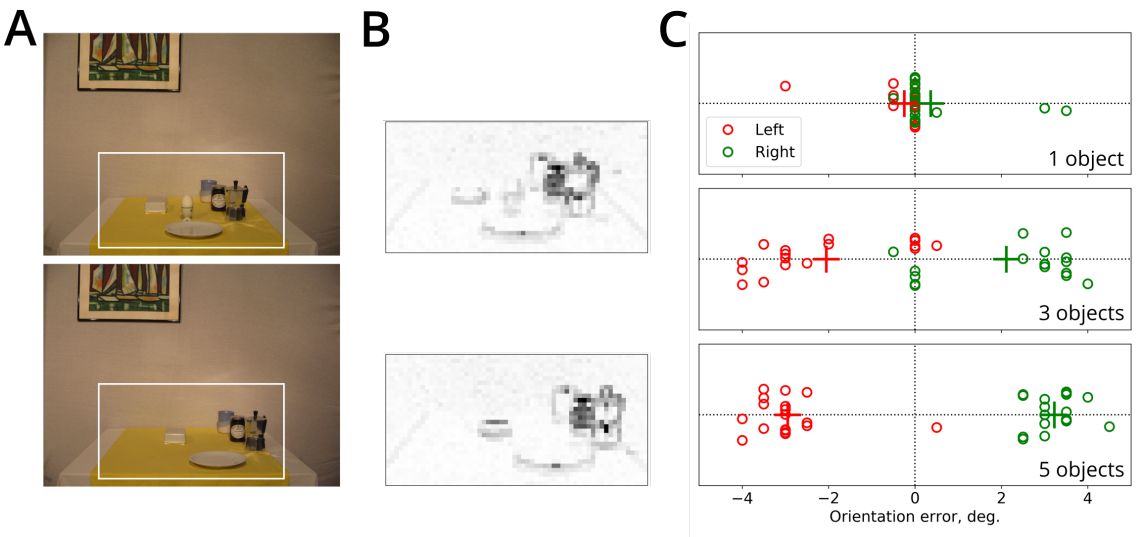

Figure 3.8: A. An example of the remembered (top) and test (bottom) images. In this example, the target object is the egg and 5 non-target objects were shifted to the right in the test image, compared to the encoded image. The white rectangle denotes the part of the image that was provided as input to the network. It corresponds to the part of the image most fixated by the subjects in the experiment. B. Mean firing rates of the egocentric neurons in the model for the encoded and test images shown in A. C. Orientation errors induced in the model by the presentation of the test images with 1 (top), 3 (middle) and 5 (bottom) displaced objects. Horizontal position of each dot corresponds to the maximal activity peak of the reorientation network. Different dots represent different sets of objects in the image dataset. Leftward and rightward displacements are shown in red and green, respectively. Crosses mark the mean displacement value per group. Random jitter along the vertical axis is added for clarity.

of objects outside of this area had no influence on reaching performance (Fiehler et al., 2014). The network converted the visual input of the egocentric layer (Fig. 3.8B) to an allocentric representation according to the actual head direction (set to 0°), which was stored in the synapses between the parieto-retrosplenial output cells and hippocampal cells as before. In this simulation we ignored competition effects, since it was not required to remember multiple images. Second, after the first scene was learned, an image of the scene with one object missing and either 1, 3 or 5 objects displaced (see Fig. 3.8B, bottom) was presented to the model. The orientation error caused by the object displacement can then be read directly from the activity of the reorientation network (Fig. 3.8C). As in the experiment, the number of displaced objects affected the amount of allocentric correction. Since in the test images the displaced objects correspond only to a subset of all visual features, the mean correction only partially account for the object displacement. Thus, as in the case of spatial reorientation, the influence of the allocentric information (in this case represented by low-level features of the presented image) is caused by the comparison

between the stored allocentric and incoming allocentric views, and the resulting activity of the reorientation network that calibrates the head direction signal.

3.4 Discussion

The presented model focuses on the dorsal visual pathway for information processing, generally thought to provide contextual or "where" information to memory structures in the MTL, by contrast to the ventral pathway mediating the processing of object/item representations or "what" information (Goodale and Milner, 1992; Kravitz et al., 2011). The two pathways converge to the hippocampus where both types of information are combined to form the episodic memories. Outputs of hippocampal processing go back to neocortical areas from which the input was originated. In both spatial (e.g. spontaneous novelty exploration) and non-spatial (recollection/familiarity) experimental paradigms the dorsal pathway has been implicated in the recollection of contextual information (e.g. the scene or location where an item was observed) and not in remembering the object identity (see Eichenbaum et al., 2007, for review). These proposals go in line with general properties of neural activities along the dorsal pathway such as PHC and RCS. In particular, fMRI studies that both RSC and PHC are activated by scene processing, with a part of PHC responding equally strongly to images of spatial layouts with or without objects (Epstein and Kanwisher, 1998; Epstein, 2008). RSC was shown to be more strongly implicated in recollection than familiarity (Epstein, 2008) and is proposed to play a specific role in encoding spatial and directional characteristic of landmarks and their stability *independent of their identity* (Mitchell et al., 2018).

In the present work, the selectivity to scenes and spatial layouts, as opposed to objects, during spatial navigation is modeled simply as sensitivity to views (i.e. the total contents of the animal's visual field at one moment in time, usually acquired across multiple fixations, potentially associated with accompanying head movements in natural conditions). Indeed, spatial layout information is often available from a low-frequency representation of a view (Kauffmann et al., 2015, but see Rajimehr et al., 2011), whereas object representations take up a much smaller portion of a view and usually require high-spatial frequency analysis at a localized part of the image during visual fixation. In our simple model, we

represented the contents of a view by a retinotopic-like grid of orientation-sensitive filter responses at just a few spatial frequencies, but a much more complex visual processing can be "inserted" between our input visual layer and the parietal transformation circuit (involving e.g., extraction of salience maps, depth processing, contour extraction, etc). The coordinate-transformation circuit and the rest of the model are agnostic about the nature of features provided to them as input, as long as these features are given in a retinotopic-like head-fixed frame and take up the whole visual field. This last requirement excludes object processing, assumed to be done in parallel in the ventral stream, since object representations are view-independent and assume translation invariance over the visual field (Serre et al., 2005). The relative (i.e. size dependent) sensitivity to objects in our model (see "Spatial reorientation") arises from the fact that large, distal and stable objects (or landmarks) that make up a large portion of a view are considered as part of the layout, and not as identified objects/landmarks. In contrast, relatively small objects, landmarks, or a high-frequency contents of other small localized portions of a view exert contribute only weakly to the overall visual representation. Indeed, they are often overshadowed by gross visual features present in views, such as corners, walls, and other large-scale visual structures during comparison of new and remembered view-based representations (Bécu et al., 2019).

Our model can thus be considered as a model of encoding of contextual information, as opposed to object-related one, and the notion of context is well defined: it is the visual information present in the set of topographically-organized features present in a set of views (that could comprise only one element) and stored in memory after the acquisition phase of a task. This notion of context can be extended to a non-spatial setting (see "Memory-based visual search"): topographically-organized image features present in attended part of the screen and stored in memory provide contextual information with respect to any object-related information stored from the scene (such as the identities of the objects in this experiment). In the absence of reliable object-related information (such as the missing target object), contextual information can be used to drive behavior. The important piece of information that is present in topographic representation of a scene, but is absent in object-related memory, is spatial location. Indeed, one can assign position information within the topographic representation of a view (with respect to an allocentric directional

frame, or with respect to the other features in the view). Therefore, (allocentric) view-based contextual representations can serve as a basis for remembering spatial and directional characteristics of objects or landmarks independent of their identity. Spatial locations in such a contextual representation can serve as "place holders" for specific object/landmark information extracted and stored in the ventral visual stream, or as "pointers" to this information. Such a notion of contextual information is well in line with proposed role of the PHC and RSC in landmark processing (Epstein, 2008; Mitchell et al., 2018).

While the existence of view-based representations in human spatial memory is well established (Shelton and McNamara, 1997; Diwadkar and McNamara, 1997; Christou and Bülthoff, 1999; Garsoffky et al., 2002; Burgess, 2006), the existence of a spatiotopic representation of the surrounding visual space is more controversial. Some proposals reject the existence of such a representation (O'Regan, 1992), some suggest that only a limited number attended features survive beyond one fixation (Rensink, 2000), and some suggest that a feature-rich representation is constructed by accumulating information over time (see Tatler and Land, 2011, for review). For example, some experimental evidence in favor of the latter view comes from studies showing that visual search can be directed to remembered locations in a panoramic scenes and that visual saccades can be programmed to reach previously observed targets outside of the current viewfield (Land et al., 1999; Oliva et al., 2004). These and similar data suggest the existence of a quasi-panoramic representation of surrounding visual cues, accessible for the planning of eye movements, i.e. most likely topographic with respect to the visual space (Golomb et al., 2011; Park et al., 2007; Melcher and Morrone, 2015; Schindler and Bartels, 2013; Robertson et al., 2016). While both egocentric and allocentric representations are stored in memory, they are converted to an egocentric frame whenever possible (Chen et al., 2011). By linking such a panoramic representation with its potential utility for spatial memory and the well known role of the MTL in the storage of allocentric memories, we postulated the existence of an allocentric, visually topographic representation of the surrounding space in the parieto-retrosplenial circuit.

Whereas the allocentric representation in our model is purely visual, the possibility that it could be multisensory can not be excluded (Newell et al., 2005). Loomis et al., 2013

defined a similar representation of surrounding 3D space as a "spatial image" with the following properties: (i) it can be updated during movement with the eye closed; (ii) it exists in all directions; (iii) the information from all sensory modalities converge onto a common, "amodal", spatial image. While our model is directly consistent with the second property, the third one can be implemented by converting spatial locations of egocentric sensory signals at different modalities (e.g. haptic or auditory) into the common allocentric framework. These locations (or placeholders) can then be linked to the detailed representations of sensory experience in sensory-specific areas of the cortex, similarly to the putative links between landmark locations and their high-frequency contents discussed above. The first property can be assured by backward projections from the hippocampus to the allocentric layer (not included in the model), by a mechanism previously proposed to support spatial imagery (Byrne et al., 2007). One obvious candidate for the potential biological locus of the panoramic visual representation is the PPC, since spatiotopic neuronal receptive fields were observed in this area (Snyder et al., 1998; Fairhall et al., 2017). The parahippocampal place area, a scene-selective subdivision of the PHC, while not sensitive to the images of the same scene from different viewpoints (Epstein, 2008), can integrate visual information across saccades to form a representation of a larger scene (Golomb et al., 2011). Finally, RSC and occipital place area were recently shown to mediate the memory of panoramic visual representations (Robertson et al., 2016).

There are two key differences between our model and a previous influential model of spatial memory and imagery (Becker and Burgess, 2001; Byrne et al., 2007, see also Bicanski and Burgess, 2016). First, our model postulates the existence of a quasi-panoramic representation of surrounding visual space, in topographic visual coordinates, as emerging experimental evidence suggests (Melcher and Morrone, 2015; Robertson et al., 2016). We propose that such a representation *(i)* is accumulated from successive views using short-term memory; *(ii)* can be used for planning of eye movements during natural behavior; *(iii)* serves for the storage of object/landmark position and orientation information. In our model, the reference frame for this panoramic representation is allocentric, and only a portion of it, corresponding to the current view field, is explicitly converted to an egocentric visual representation (equivalent to the "parietal window" of Byrne et al., 2007). Second, our model proposes a mechanism of fast bottom-up view-based reorientation of

the head direction system that was either absent (Byrne et al., 2007) or relied on the presence of conspicuous landmarks linked directly to head direction cells (Bicanski and Burgess, 2016). A number of reorientation studies mentioned earlier suggest that this neural process is independent from landmark identities and can be performed in the absence of point-like landmarks. The mechanism we use relies on weight sharing and as such is not, at its present implementation, biologically realistic. The concept of weight sharing has been critical for recent successes of brain-inspired neural networks and is widely used in models of biological networks of visual processing (e.g. Serre et al., 2005; Masquelier and Thorpe, 2007; Bartunov et al., 2018). One possible implementation of our proposed reorientation mechanism would require mental rotation of the stored allocentric representations, while freezing the actual egocentric view in the input layer. Such an implementation would make the model significantly more complex, without changing the underlying computation.

To summarize, the model presented in this work explored the nature of visual representations in the parietal-medial temporal pathway for visuospatial processing and contributed to the open question of the link between visual and memory structures in primates. It proposes that a single, potentially multisensory, representation of surrounding environment is constructed by time-integrated sensory snapshots. This putative representation provides a 3D coordinate space within which positions of localized sensory events can be encoded and which can serve as basis for eye-movement generation in natural conditions. This model thus provides a conceptual framework for linking oculomotor behavior, visual and spatial memory.

Chapter 4

Entorhinal-Hippocampal Loop as a Multisensory Integration Circuit

Chapter summary

This chapter presents a computational model of the entorhinal-hippocampal processing loop, that is thought to support spatial memory functions in mammals. In contrast to the previous chapter focusing specifically on primate data, the present model focuses on rodent data because of a significantly larger amount of detailed behavioral and electrophysiological experimental evidence available. Therefore, the basic assumption here is that the organization of spatial memory in rodents is similar to that in primates. This assumption is supported by experimental evidence demonstrating the existence of primate place and grid cells, as reviewed in Chapter 2. The model of the dorsal visual path described in the previous chapter is used here, the difference being that the visual field is assumed to panoramic, as in rodents. In addition, for the present model we chose a firing rate description of neural activity, instead of a spiking one. These two simplifications greatly reduce the computation time, and allow us to concentrate on learning dynamics in spatial tasks that require many hours of training. The tasks simulated here involve learning of spatial representation of multi-compartment environments with a high degree of visual aliasing, making it possible to assess differential contribution of allothetic and idiothetic cues on spatial learning.

This work has been published in Neural Networks journal:

Tianyi Li, Angelo Arleo and Denis Sheynikhovich (2020). Modeling place cells and grid cells in multi-compartment environments: entorhinal-hippocampal loop as a multisensory integration circuit. *Neural Networks*, 121:37-51.

Abstract

Hippocampal place cells and entorhinal grid cells are thought to form a representation of space by integrating internal and external sensory cues. Experimental data show that different subsets of place cells are controlled by vision, self-motion or a combination of both. Moreover, recent studies in environments with a high degree of visual aliasing suggest that a continuous interaction between place cells and grid cells can result in a deformation of hexagonal grids or in a progressive loss of visual cue control over grid fields. The computational nature of such a bidirectional interaction remains unclear. In this work we present a neural network model of the dynamic interaction between place cells and grid cells within the entorhinal-hippocampal processing loop. The model was tested in two recent experimental paradigms involving environments with visually similar compartments that provided conflicting evidence about visual cue control over self-motion-based spatial codes. Analysis of the model behavior suggests that the strength of entorhinal-hippocampal dynamical loop is the key parameter governing differential cue control in multi-compartment environments. Moreover, construction of separate spatial representations of visually identical compartments required a progressive weakening of visual cue control over place fields in favor of self-motion based mechanisms. More generally our results suggest a functional segregation between plastic and dynamic processes in hippocampal processing.

4.1 Introduction

It has long been accepted that spatial navigation depends crucially on a combination of visual and self-motion input (O'Keefe and Nadel, 1978). Since the seminal work of O'Keefe and Dostrovsky (1971), a neural locus of this combination is thought to be the place cell network in the CA1-CA3 subfields of the hippocampus proper (O'Keefe and Speakman, 1987; Muller and Kubie, 1987; Knierim et al., 1998; Jayakumar et al., 2019), with different subsets of place cells sensitive to self-motion cues, to visual cues or, more often, to a combination of them (Markus et al., 1994; Chen et al., 2013; Fattahi et al., 2018). A more recent discovery of grid cells in the medial entorhinal cortex (mEC) led to the suggestion that the grid-cell network provides a self-motion-based representation of location that is combined with other sensory information on the level of place cells (Fyhn et al., 2004; McNaughton et al., 2006; Hayman and Jeffery, 2008; Cheng and Frank, 2011; Jacob et al., 2019). The grid-cell representation is itself vision-dependent, since various properties of grid cells are affected by changes in visual features of the environment (Hafting et al., 2005; Krupic et al., 2015). Combined with the evidence showing that coherent changes in place-cell and grid-cell representations occur during environment deformation and cue manipulation, these data suggest a bidirectional interaction between these representations at the neural level (Fyhn et al., 2007). While this bidirectional link is always present in normal conditions, it may not be necessary for place cell activities, as shown in a number of lesion experiments (Sasaki et al., 2015; Schlesiger et al., 2018).

The nature of the dynamic interaction between visual and self-motion cues on the level of grid cells has recently been tested in two experiments: in a merged room, formed by removal of a wall separating two visually similar environments (Wernle et al., 2018), and during exploration of an environment consisting of two identical rooms connected by a corridor (Carpenter et al., 2015). Results of the first experiment have shown that firing patterns of grid cells were anchored by local sensory cues near environmental boundaries, while they underwent a continuous deformation far from the boundaries in the merged room, suggesting a strong control of local visual cues over the grid-cell representation (Wernle et al., 2018). Results of the second experiment indicated in contrast that during learning in a double-room environment grid cells progressively formed a global self-

motion-based representation disregarding previously learned local visual cues (Carpenter et al., 2015).

Existing models of the entorhinal-hippocampal system are mostly based on the feed-forward input from grid cells to place cells, with an additional possibility to reset grid-field map upon the entry to a novel environment (Solstad et al., 2006; O'Keefe and Burgess, 2005; Blair et al., 2008; Sheynikhovich et al., 2009; Pilly and Grossberg, 2012), or focus on the feed-forward input from place cells to grid cells (Bonnevie et al., 2013). In addition to be at difficulty at explaining the above results on dynamic interactions between visual and self-motion cues, they are also not consistent with data showing that hippocampal spatial representations remain spatially tuned after mEC inactivation (Brun et al., 2008a; Rueckemann et al., 2016), that in rat pups place fields can exist before the emergence of the grid cell network (Muessig et al., 2015) and that disruption of grid cell spatial periodicity in adult rats does not alter preexisting place fields nor prevent the emergence of place fields in novel environments (Koenig et al., 2011; Brandon et al., 2014).

In this paper we propose a model of continuous dynamic loop-like interaction between grid cells and place cells, in which the main functional parameter is the feedback strength in the loop. We show that the model is able to explain the observed pattern of grid-cell adaptation in multi-compartment environments by assuming a progressive decrease of visual control over self motion, and a plasticity mechanism regulated by allothetic and idiothetic cue mismatch over a long time scale.

4.2 Methods

The rat is modeled by a panoramic visual camera moving in an environment along quasi-random trajectories resembling those of a real rat. The orientation of the camera corresponds to the head orientation of the model animal. The constant speed of the modeled rat is set to 10 cm/s, and sampling of sensory input occurs at frequency 10 Hz, roughly representing hippocampal theta update cycles. The modeled rat receives two types of sensory input (Fig. 4.1). First, self-motion input to the model is represented by angular and translational movement velocities integrated by grid cells in mEC to provide self-motion representation of location, as proposed earlier (McNaughton et al., 2006). Competitive

self-organization of grid cell output occurs downstream from the entorhinal cortex in the dentate gyrus (DG) - CA3 circuit and gives rise to a self-motion-based representation of location, encoded by *motion-based place cells* (MPC). We did not include a specific neuronal population to model DG (see, e.g., de Almeida et al., 2009b). Instead, we implemented competitive learning directly on mEC inputs to CA3. Second, visual input is represented by responses of a two-dimensional retina-like grid of orientation-sensitive Gabor filters, applied to input camera images at each time step. For instance, in featureless rectangular rooms used in most of the simulations below, the only features present in the input images are the outlines of the environment walls (Fig. 4.2A, bottom). Importantly, the 'retinal' responses are assumed to be aligned with an allocentric directional frame further along the dorsal visual pathway (not modeled), the directional frame being set by head direction cells (Byrne et al., 2007; Sheynikhovich et al., 2009). That is, visual input to the model at each spatial location is independent on the head direction that the model rat has upon arriving at that location. The visual input aligned with an allocentric directional frame is assumed to be encoded in the inputs to the hippocampal formation from non-grid mEC cells or from the lateral entorhinal cortex (lEC). Competitive self-organization of these inputs results in a purely vision-based representation of location, encoded by a population of *visual place cells* (VPCs). Both MPCs and VPCs project to CA1 cells that form a conjunctive representation of location in *conjunctive place cells* (CPCs). The CPCs in CA1 project back to the entorhinal grid cells and thus form a recurrent loop, reflecting the anatomy of entorhinal-hippocampal connections (Iijima et al., 1996). Further details of the model components and synaptic learning rules are described in the following sections.

4.2.1 Visual input

Visual snapshots of the environment are produced by a panoramic cylindrical camera representing the model rat visual field (160° x 360°). These snapshots are then encoded by the activities of a rectangular sheet of 40×90 neurons uniformly covering the visual field. The activities of visual neurons are computed in four steps. First, input images are convolved with Gabor filters of 4 different orientations $(0, 90°, 180°, 270°)$ at 2 spatial frequencies (0.5 cpd, 2.5 cpd), chosen so as to detect visual features of simulated environments (see Section 4.2.4). Second, the 8 convolution images are discretized with the

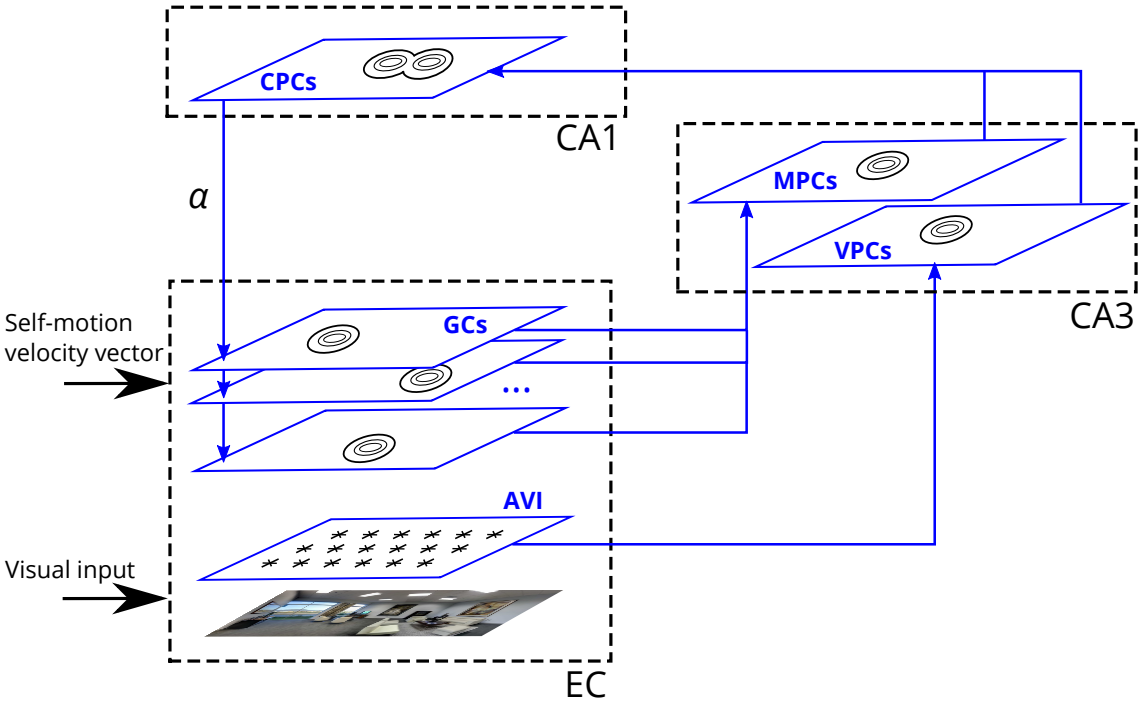

Figure 4.1: Self-motion input is integrated in 5 grid-cell populations of the medial EC (only 3 populations are shown for clarity), and via competitive interactions results in a self-motion-driven space representation in CA3 (encoded by the MPC population). Visual input, represented by the activities of AVI neurons, results in a purely vision-based representation in CA3, encoded by the VPC population. Both MPCs and VPCs project to CA1 where the conjunctive representation of location is encoded in the CPC population. The projection from CPCs in CA1 back to the mEC closes the dynamic hippocampal processing loop and the strength of this projection is determined by the parameter α. The arrows represent the information flow in the network. Small ovals represent subsets of strongly active cells in the corresponding populations (even though strongly active cells are shown in nearby locations in the figure, no particular topographical relations between cells are assumed in the model, apart from the AVI population with a retinotopic neuronal organization).

40×90 grid, and the maximal response at each position is chosen, producing an array of 3600 filter responses. These operations are assumed to roughly mimic retinotopic V1 processing. Third, the filter responses are aligned with a common allocentric directional frame (assumed to be given by the head direction system), such that if the model rat rotates without changing its spatial location, the activities of aligned filters stay constant. This operation implements an egocentric-allocentric coordinate transformation thought to be performed by parietal cortex neurons (Byrne et al., 2007). Fourth, the vector of aligned filter activities at time t is normalized to length unity, giving the final neuronal activities $A_{avi}(t, j)$ of the allocentric visual input cells, with the index j running over all elements of the vector.

4.2.2 Integration of visual and self-motion input by grid cells

The self-motion input is processed by 5 identical neuronal populations (see Fig. 4.1) representing distinct grid-cell populations in the dorsal mEC (Hafting et al., 2005). Each grid cell population is modeled by a two-dimensional sheet of neurons equipped with attractor dynamics on a twisted-torus topology, as has been proposed in earlier models (Guanella et al., 2007; Sheynikhovich et al., 2009; Burak and Fiete, 2009). The position of an attractor state (corresponding to subset of strongly active cells, or *activity packet*) in each grid-cell population is updated based on the self-motion velocity vector. This is implemented by the modulation of recurrent connection weights with Mexican hat-like structure (i.e. with short-range excitation and long-range inhibition) according to the model rat rotation and displacement, such that the activity packet moves across the neural sheet according to the rat movements in space (Guanella et al., 2007). The only difference between different grid-cell populations is that the speed of movement of the activity packet across the neural sheet is specific for each population, resulting in a population-specific distance between neighbouring grid fields and field size (Hafting et al., 2005). As long as each location in an environment corresponds to a distinct combination of positions of the activity packets, the population activity of all grid cells encodes the current position of the animal in the environment (Fiete et al., 2008). The exact implementation of the attractor mechanism governing grid-cell network dynamics is not essential for our model to work.

In addition to the recurrent input from other grid cells in the same population, each grid cell receives input from the CPC population which represent conjunctive visual and self-motion representation (described in detail later), and the relative strength of these two inputs is controlled by the parameter α. At a relatively high value of this parameter, the position of the activity packet in each grid-cell layer is strongly influenced by the hippocampal input, leading to an overall stronger effect of visual information. At a low value of α, the position of the attractor states is determined exclusively by the self-motion input.

Thus, the total synaptic input to grid cell i at time t is (omitting grid cell population index for clarity)

$$I_{gc}(t,i) = \alpha I_{gc}^{cpc}(t,i) + (1-\alpha) I_{gc}^{gc}(t,i) \tag{4.2.1}$$

where the external input from CPCs and the recurrent input from other grid cells are determined by

$$I_{gc}^{cpc}(t,i) = \sum_{j=1}^{n_{cpc}} A_{cpc}(t-1,j) W_{gc}^{cpc}(t,i,j) \tag{4.2.2}$$

$$I_{gc}^{gc}(t,i) = \sum_{k=1}^{n_{gc}} A_{gc}(t-1,k) W_{gc}^{gc}(t,i,k) \tag{4.2.3}$$

Here, $A_{cpc}(t,j)$ is the activity of j-th CPC at time t (described below) and $A_{gc}(t,k) = I_{gc}(t,k)$ is the activity of k-th grid cell (we use linear activation function for grid cells).

Feedforward synaptic connections from CPCs are initialized by small random values and updated during learning according to a standard Hebbian learning scheme:

$$W_{gc}^{cpc}(t,i,j) = W_{gc}^{cpc}(t-1,i,j) + \eta_{gc}^{cpc} A_{gc}(t,i) A_{cpc}(t,j) \tag{4.2.4}$$

followed by explicit normalization ensuring that the norm of the synaptic weight vector of each cell is unity.

Recurrent synaptic connections between grid cells are constructed such as to ensure attractor dynamics, modulated by velocity vector (Guanella et al., 2007). More specifically, the connection weights between cells i and j is a Gaussian function of the distance between these cells in the neural sheet. This connection weight is modulated by the self-motion velocity vector, such that the activity packet moves across the neural sheet according to the direction and norm of the velocity vector, with a proportionality constant that is grid-cell population specific. These proportionality constants were tuned such that the grid spacing across different grid cell populations were between 42 cm and 172 cm. Grid-cell firing patterns were oriented 7.5° with respect to one of the walls of an experienced experimental enclosure (Krupic et al., 2015).

4.2.3 Encoding of visual and self-motion input by place cells

As mentioned above, the model includes three distinct populations of place cells (Fig. 4.1). First, VPCs directly integrate allocentric visual inputs and project further to CA1. We putatively assign VPC population to CA3 where a competitive mechanism based on recurrent feedback can result in self-organization of visual inputs, the resulting spatial code further transmitted to to CA1. The model of this pathway is based on the evidence that stable spatial representations were observed in CA1 after complete lesions of the mEC containing grid cells (Brandon et al., 2014; Schlesiger et al., 2018). Second, MPCs directly integrate input from grid cells and in the absence of visual inputs the activity of these cells represents purely self-motion-based representation of location. These cells represent CA3 place cells, acquiring their spatial selectivity via a competitive mechanism based on mEC inputs. Third, CPCs that model CA1 pyramidal cells, combine visual and self-motion inputs coming from VPC and MPC populations, respectively. Crucially, CPCs project back to the grid cell populations, modeling anatomical projections from CA1 back to the entorhinal cortex forming a loop (Iijima et al., 1996; Slomianka et al., 2011) and controlled by the parameter α as described above.

Vision-based place cells. VPCs acquire their spatial selectivity as a result of unsupervised competitive learning implemented directly on the allocentric visual inputs (see Section 4.2.1). Thus, the total input to a VPC i at time t is given by

$$I_{vpc}^{avi}(t,i) = \sum_{j=1}^{n_{avi}} A_{avi}(t,j) W_{vpc}^{avi}(t,i,j) \tag{4.2.5}$$

where $A_{avi}(t,j)$ is the activity of j-th Gabor filter aligned with the allocentric directional frame. To compute output activities $A_{vpc}(t,i)$ of the VPC cells, *(i)* a subset of maximally active cells is selected that includes all cells with the total input higher than the top E_{vpc}-th percentile of all activities in the population (where E_{vpc} is a parameter, see Table 4.1); and *(ii)* the activity of the cells included in the subset is rescaled to have values from 0 (for the cell with the minimal input) to 1 (for the cell with the maximal input). For the rest of the cells the activity is set to zero. A biologically plausible way to perform such a scheme using γ-oscillation-mediated inhibition was proposed by de Almeida et al. (2009a) who

termed this selection scheme “E%-max winner-take-all”.

Synaptic weight updates according to the Hebbian modification rule (Eq. 4.2.4) are then implemented for the connection weights between the allocentric visual input cells and VPCs. As a result of the competitive learning, different cells become sensitive to constellations of visual features observed from different locations (independently from head direction).

Motion-based place cells. MPCs read out grid cell using a competitive learning scheme identical to that used for the VPCs above but applied to the grid-cell inputs (with parameter E_{mpc} determining the proportion of highly active cells). As a result, a small subset of MPCs is linked to strongly active grid cells at each location of the environment and thus MPC population activity represents the position of the model animal encoded by grid-cells (Solstad et al., 2006; Sheynikhovich et al., 2009).

Conjunctive place cells. Both VPCs and MPCs project to CPCs, that model CA1 pyramidal cells sensitive to both visual and self-motion cues. The total input to a conjunctive cell is:

$$I_{cpc}(t,i) = I^{vpc}_{cpc}(t,i) + I^{mpc}_{cpc}(t,i) \tag{4.2.6}$$

with

$$\begin{aligned} I^{vpc}_{cpc}(t,i) &= \sum_{j=1}^{n_{vpc}} A_{vpc}(t-1,j) W^{vpc}_{cpc}(t,i,j) \\ I^{mpc}_{cpc}(t,i) &= \sum_{k=1}^{n_{mpc}} A_{mpc}(t-1,k) W^{mpc}_{cpc}(t,i,k) \end{aligned} \tag{4.2.7}$$

Again, a E%-max winner-take-all scheme is applied to compute the activities A_{cpc}. The following Hebbian weight update rule is used to adjust synaptic weights of afferent CPC synapses:

$$\begin{aligned} W^{vpc}_{cpc}(t,i,j) &= W^{vpc}_{cpc}(t-1,i,j) + \eta^{vpc}_{cpc} A_{cpc}(t,i) \mathcal{H}(A_{vpc}(t,j) - \theta) \\ W^{mpc}_{cpc}(t,i,j) &= W^{mpc}_{cpc}(t-1,i,j) + \eta^{mpc}_{cpc} A_{cpc}(t,i) \mathcal{H}(A_{mpc}(t,j) - \theta) \end{aligned} \tag{4.2.8}$$

where $\mathcal{H}(.)$ is the Heaviside step function ($\mathcal{H}(x) = 0$ for $x < 0$, and $\mathcal{H}(x) = x$ otherwise) and θ is the presynaptic activity threshold.

Due to the attractor dynamics in mEC grid cells, a subset of strongly activated CA1 cells induces a shift of the activity packets in a downstream grid-cell layers towards the position of former. The size of the induced shift on each cycle of theta is determined by connection strengths between participating cells and on the value of α. The shift of the activity packets in grid cell layers will in turn modify the subset of active CA3 cells, inducing changes in CA1 cells and ultimately grid cells, closing the loop. In the absence of visual input, activity packets in these interconnected populations settle at a global stable state of the loop/attractor dynamics and hence all code for a single spatial location in the environment, which can be considered as a representation of the animal's location based on self-motion input. When visual input is present, the loop dynamics is biased towards the visual position encoded in the VPC population. Thus, the feedback strength in the loop determines the extent to which visual input influences place cell activities in the model.

4.2.4 Simulations

Virtual environments for the three simulations presented in this paper were developed with Unity (`www.unity3d.com`). In Simulation 1 (Figs. 4.2 and 4.3) the environment was a rectangular room 2×1 m with featureless gray walls. In Simulation 2 (Figs. 4.4-4.6), the experimental environment was modeled as a square arena 2×2 m. During training, it was separated into two rooms by a wall at the center of the environment. The experimental arena was located inside a bigger environment (4×4 m) with four salient visual cues (large circles) on each wall. In Simulation 3 (Figs. 4.7-4.8), the environment consisted of two identical rooms 1×1 m connected by a corridor (0.5×2 m). The height of the walls was 0.6 m.

Twenty different animals were simulated, which means that the whole training-testing sequence in the simulations below was repeated 20 times and the data was averaged. In all simulations, VPCs were learned from the simulation environment before the training of the place cells and grid cells. Model parameters are listed in Table 4.1.

Parameter	Value
α	0.03 (Sim.1), 0.04 (Sim.2), reducing from 0.04 to 0.005 (Sim.3)
η_{vpc}^{avi}	0.01
η_{cpc}^{vpc},η_{cpc}^{mpc}, η_{gc}^{cpc}, η_{mpc}^{gc}	0.0025
E_{vpc}	15%
E_{mpc}	20%
E_{cpc}	30%
θ	0.75

Table 4.1: Parameters of the entorhinal-hippocampal loop model.

Simulation 1

Training The model was trained for 25 minutes (15000 time steps) by moving quasi-randomly in the experimental environment.

Testing Synaptic weights were fixed, and activities of all the cells in the model were recorded in the following three experimental conditions. In the 'light' condition the full model was run to randomly explore the environment. In the 'passive translation' condition, the exploration was performed as in the 'light' condition, but the velocity input vector to the grid cell populations was set to $(0, 0)$. In the 'dark' condition, the model was run with visual cues turned off (i.e., uniform gray images were presented as visual input). Next, the trained model was run to cross the environment from left to right in the 'light' and 'dark' conditions as before, but with the speed gain in the grid cell populations modulated as described in the Results.

Simulation 2

In the original experiment (Wernle et al., 2018), the rats were trained in rooms A and B alternately for several days (see Fig. 4.4A for a schematic representation of the experimental environment). After that, the partition wall was removed and rats explored the merged room during a 45 min trial. Up to 9 such trials were performed daily in different animals. The simulation described below was designed to mimic this experimental protocol.

Training The model was trained separately in room A and then in room B for 30 minutes, which was sufficient to learn stable grid and place fields. Synaptic weights were then fixed to the learned values.

Testing In the main experiment, simulated neural activities were recorded while the model rat randomly explored the merged room for 1 h, with $\alpha = 0.04$. Two additional experiments were then performed. First, to test the influence of synaptic plasticity on the results of the main experiment, synaptic weights were updated as during training while the model rat additionally explored the merged room for 1h. Second, to test the influence of the strength of the feedback loop, the model rat was run in the merged room for additional 20 one-hour trials. The value of α was decreased linearly from 0.04 to 0.005 across trials.

Sliding correlation The sliding correlation heat maps for grid-cell firing patterns were calculated as described in Wernle et al. (2018). The size of the sliding correlation window was defined based on the grid spacing of the cell. The window moved from the top left to the bottom right corner in the grid field maps of the environment A|B (i.e. before the wall removal) and AB (i.e. after the wall removal). At each window location, the portion of the grid maps in the environments A|B and AB, outlined by the sliding window, were correlated with each other.

Displacement vector analysis Displacement vectors were calculated as described in Wernle et al. (2018). To obtain a displacement vector for one grid cell, the experimental environment was divided into 4×4 blocks (50×50 cm each). In each block, the vector corresponding to the shift of grid fields in the environment AB relative to that in the environment A|B was calculated. The vectors were sorted into the corresponding blocks based on the grid field location in the training environment and the mean over all vectors was computed. To analyze displacement vector lengths, the environment was divided into 8×8 bins. The vectors were then sorted into the corresponding bins based on the original grid field location in the training environment, and the mean vector length was computed.

Simulation 3

In the original experiment (Carpenter et al., 2015), rats foraged for food pellets during up to 20 daily experimental sessions in the experimental environment schematically shown

in Fig. 4.7A. Each session consisted of 2 trials, 40 min each. The two trials were identical, and were only needed to check for uncontrolled local cues possibly used by rats to identify the two compartments. At the beginning of each trial the rat was placed in the corridor between the two compartments facing the north wall and freely explored the environment. The simulation described below was designed to mimic this experimental protocol.

Training During training, the model was placed in the center of the corridor and then explored the complete environment quasi-randomly for 1 h. This learning period approximately represents a single training session of the original experiment. Eight such training sessions were performed, such that the strength of the feedback loop α decreased from 0.04 (first session) to 0.005 (last session) with step 0.005.

Testing After each training session, the weights were fixed and neural activity was recorded as the model rat explored the environment for 1 h.

Global and local fits The firing rate maps of modeled grid cells were fit with ideal local and global grid patterns using the procedure described in Carpenter et al. (2015). First, grid spacing was identified by correlating the firing pattern with 30 ideal firing grids. Each ideal grid pattern is a product of three cosine gratings

$$f(\vec{x}) = A[1 + \cos(k_1(\vec{x} + \vec{c}))][1 + \cos(k_2(\vec{x} + \vec{c}))][1 + \cos(k_3(\vec{x} + \vec{c}))]$$

with peak firing rate A, wave vectors $\vec{k}_1$, $\vec{k}_2$ and $\vec{k}_3$ and phase offsets $\vec{c} = (c_x, c_y)$. The wave vectors are defined as $\vec{k} = (\frac{2\pi}{\lambda}cos(\varphi), \frac{2\pi}{\lambda}sin(\varphi))$, where $\lambda = \frac{\sqrt{3}}{2}G$ is the grating wave length, G is the grid spacing and φ is the grid orientation. The 30 ideal grid patterns were created with grid spacing evenly distributed between 30 and 170 cm. Since the grid orientation in the model is set to 7.5°, φ in the three wave vectors is equal to 7.5°, 127.5° and 247.5°, respectively. Spatial cross-correlograms were computed between the recorded firing rate map and the ideal grid patterns over a range of spatial phase offsets. The grid spacing of the recorded firing pattern is then set to that of the ideal grid pattern with the highest correlation. Second, a local and global fit with the identified grid spacing was computed for the recorded firing rate map. The local fit was performed using two grid patterns

(one per room) with the same phase offset. The global fit was performed using only one grid pattern with continuous phase across the two rooms. The Pearson product-moment correlation between the recorded firing rate map and the local and global grid patterns were computed over a range of phase offsets. The highest correlation with the local and global model was identified as the value of local and global fit, respectively.

4.3 Results

Since the early experiments testing the influence of visual and self-motion cues on place cell activity, it was clear that different subsets of place cells are controlled by these cues to different degrees, with some cells being controlled exclusively by one type of cue (Markus et al., 1994; Chen et al., 2013; Aronov and Tank, 2014; Fattahi et al., 2018). In the model we conceptualized these differences in VPC, MPC and CPC neural populations, representing purely vision-dependent, motion-dependent and multisensory place cells. Thus, after the model has learned place fields by moving quasi-randomly around a virtual rectangular box (Fig. 4.2A), VPCs had fields only in a 'light' condition, i.e. in the presence of visual cues (Fig. 4.2B, top row). This was true even if motion-based cues were absent, as in a passive transport through a virtual maze (Chen et al., 2013). Conceptually, these cells represent the ability of hippocampal circuits to form self-organized representations of location even in the absence of grid-cell input from the mEC (Hales et al., 2014; Brandon et al., 2014; Schlesiger et al., 2018). In contrast, MPCs had place fields both in the light and dark conditions, but not during passive translation (Fig. 4.2B, middle row). Finally, CPCs were active in all the three conditions since they combine both types of input (Fig. 4.2B, bottom row).

In contrast to VPCs that are completely independent of self-motion cues and encode stable visual features of the surrounding environment, MPCs and CPCs are influenced by both visual and self-motion input, by virtue of their loop-like interactions through the grid cells. To assess the relative influence of vision and self-motion on the activity of these cells in a situation of sensory conflict, we decreased the gain of self-motion input to grid-cells while the model animal crossed the environment from left to right (Fig. 4.2C). This decrease in gain was applied only to the horizontal component of motion, i.e. the horizontal component

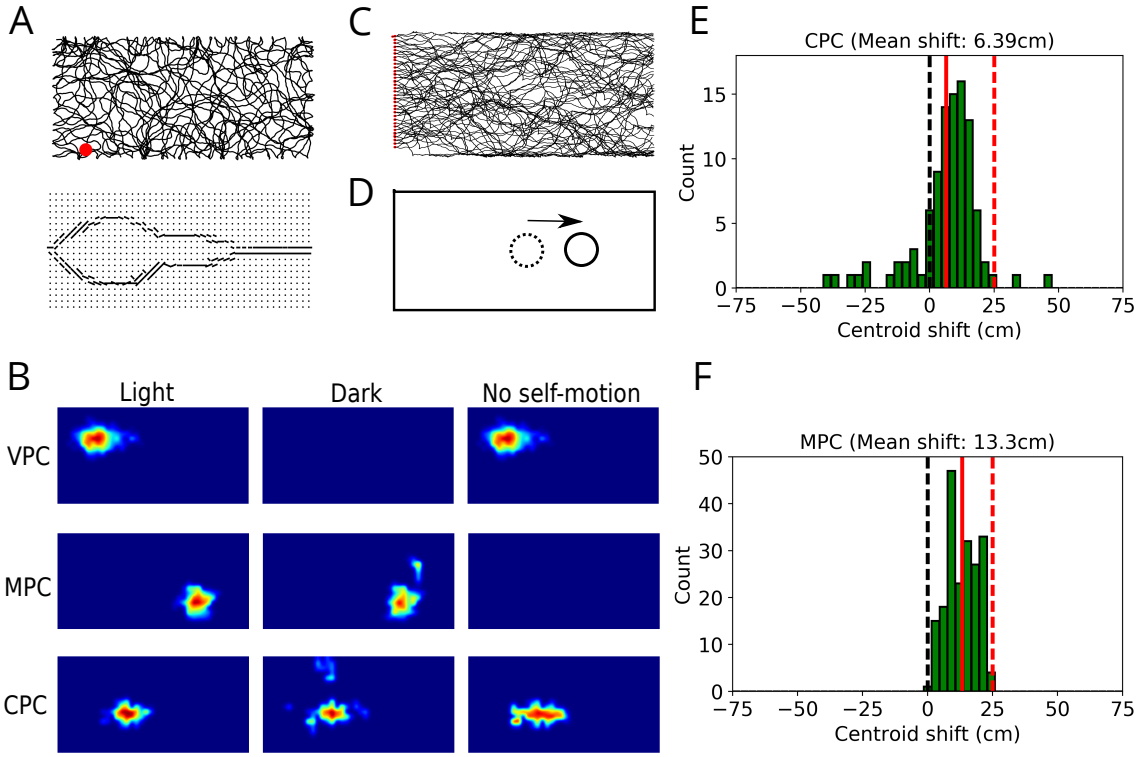

Figure 4.2: A. An example of the trajectory of the modeled animal in a rectangular environment (top) and the visual input to the model (bottom) from the location marked by the red dot. In the bottom plot, the dots represent the grid of Gabor filters, and lines represent the orientations of the most active filters. Visual input at each location is independent from head direction. B. Firing fields of VPCs (top row), MPCs (middle row) and CPCs (bottom row) in simulated 'light' condition (left column), 'dark' condition (middle column) and during passive translation (right column). C. Trajectories of model animal crossing the rectangular environment from left to right. The red dots denote the starting positions. D. When the model rat crosses the environment from left to right, self-motion position estimate (dotted circle) is behind the visual position estimate (full circle) in the conditions of decreased speed gain, leading to a forward-shift of receptive fields. E,F. Forward-shift of receptive fields in the population of CPCs (top) and MPCs (bottom). Full red lines represent the mean shift in the population. Dashed red lines represent the shift due to purely self-motion input.

of the self-motion velocity vector was set to $3/4$ of the baseline value. Such a modification is similar to a change in the gain of translation from real-to-virtual movement in a virtual corridor (Chen et al., 2013), but implemented in a two-dimensional environment instead of a linear track. The change in gain resulted in a forward-shift of receptive fields of MPCs and CPCs relative to their position in baseline conditions and the size of the shift was smaller than what would be predicted from purely self-motion integration (Figs. 4.2E,F), expressing the correction of self-motion position code by visual cues.

To illustrate the loop dynamics in this simple example, consider the case when the model

animal crossed the middle line of the environment moving from left to right (Fig. 4.2D). The integration of pure self-motion input over time provides an estimate of the current position that is *behind* the actual position due to the decrease in speed gain. As a result, the place field of a purely self-motion dependent cell should shift *ahead* of the animal by the amount an amount proportional to the gain factor (shown red dashed line in Figs. 4.2E,F). However, when visual cues are available, the VPC population activity encodes the visual position estimate that is in independent of gain changes. As a result of the dynamic loop-like interaction, the VPC activity induces a forward shift of the activity packet in the grid-cell populations towards the visually identified location, and the size of this shift is controlled by the parameter α. Grid cells would similarly affect the MPCs, and then CPCs, closing the loop. Therefore, in the presence of conflicting cues, place fields shifted to an intermediate position between the self-motion and visual estimates, as shown by the distributions of place-field centroids in the MPC and CPC populations (Figs. 4.2E,F). A similar effect of conflicting cues on place fields was experimentally studied by Gothard et al. (1996a) and subsequently simulated in several computational models (Samsonovich and McNaughton, 1997; Byrne et al., 2007; Sheynikhovich et al., 2009). However, in the present model the parameter controlling the interaction between the visual and self-motion cues is cast in terms of the strength of the entorhinal-hippocampal loop.

To illustrate the same multisensory integration mechanism on the level of grid cells, we conducted another simulation in which the horizontal velocity gain was only transiently decreased when the model animal crossed a specific portion of the environment (Fig. 4.3A). In this case of a transient cue conflict, grid patterns were locally deformed in that firing fields near the zone of decreased gain shifted forward relative to control conditions, reflecting the sensory conflict (Figs. 4.3B). Near the borders of the environment, where the speed input was identical to the baseline conditions, grid pattern remained stable. The same effect on the level of the whole population of grid cells was quantified by the analysis of displacement vectors (Fig. 4.3C) and by sliding correlation maps (Fig. 4.3D, see Section 4.2.4 for details of this analysis). These results suggest that local modifications of grid patterns can be induced by conflicting sensory representations, similarly to what has been observed in a recent experiment by Wernle et al. (2018). As mentioned in the Introduction, these observations are at odds with results of an earlier experiment (Carpenter

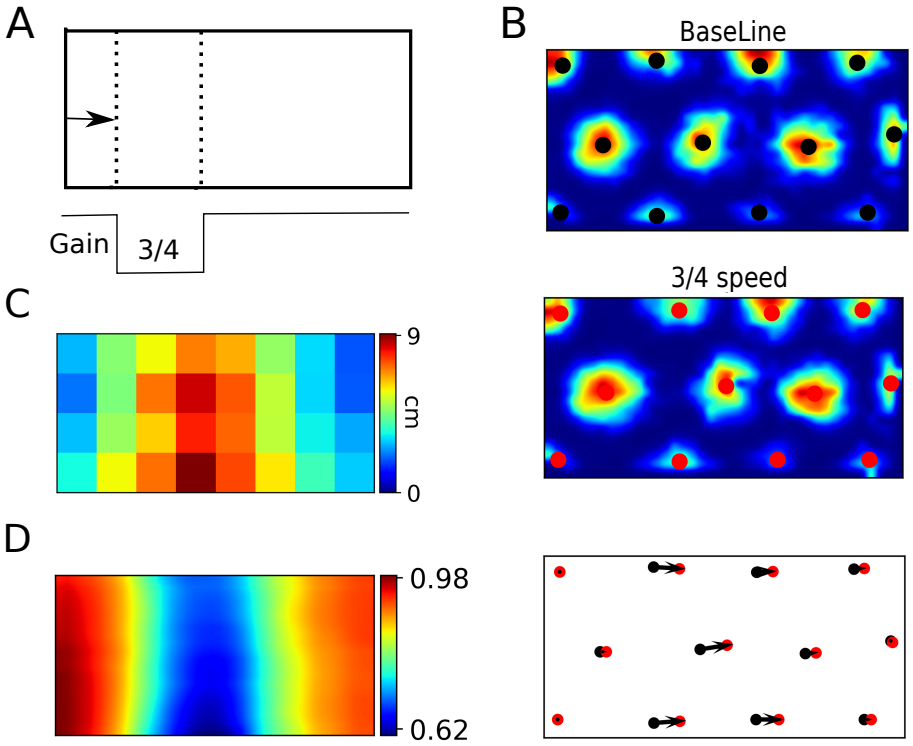

Figure 4.3: A. The speed gain was transiently decreased to 3/4 of the normal gain when the model animal approached the portion of the environment marked by the dotted lines. B. An example of firing pattern of a grid cell in the conditions of normal speed (top) and with transiently decreased speed gain (middle). The black and red circles represent the centers of firing fields in the baseline condition and during decreased gain, respectively. The shift of firing fields is quantified by displacement vectors shown by the black arrows (bottom). C. Color map of the mean displacement vector lengths in different portions of the environment. D. Color map of mean sliding correlation over all grid cells.

et al., 2015) that studied adaptation of grid-cell patterns during construction of a spatial representation in an environment consisting in two identical rooms connected by a corridor. In the following sections we present simulations of the two experiments in an attempt to explain the conflict between them and to understand neural mechanisms responsible for apparently different patterns of grid-cell adaptation in the two experiments.

4.3.1 Simulation of the merged-room experiment

Wernle et al. (2018) studied the integration between visual and self-motion cues by recording grid cells in two adjacent rectangular compartments initially separated by a wall (see Fig. 4.4A). The two compartments were located inside a larger environment equipped with distal visual cues. The wall was subsequently removed and grid cells were recorded while the rat foraged in the merged room. The authors observed that at locations

far from the removed wall grid cells conserved their firing patterns, while at locations near those previously occupied by the wall grid fields shifted so as to form a continuous quasi-hexagonal pattern (Wernle et al., 2018).

Simulation results from the previous section suggest that the observed local deformation of the grid pattern can result from the local visual deformation caused by wall removal. To verify that our model can reproduce these results, we recorded activities of simulated grid cells and place cells cells in experimental conditions similar to those in Wernle et al. (see Section 4.2.4). More specifically, in the training phase the model learned place fields separately in two virtual rooms *A* and *B* (Fig. 4.4A) located inside a bigger room with distal visual cues (not shown), such that learned representations of the two rooms were different after the initial exploration. In the testing phase, the wall was removed, the synaptic weights were fixed and neural activity was recorded while the model rate explored the merged room. We observed that after wall removal, grid fields near distant walls remained at the same location as during training, while those near the former wall location shifted towards it (Fig. 4.4B), as in the experiment. The same phenomenon on the level of the whole population was quantified by the analysis of displacement vectors (Fig. 4.4C) and by sliding correlation analysis (Fig. 4.4D).

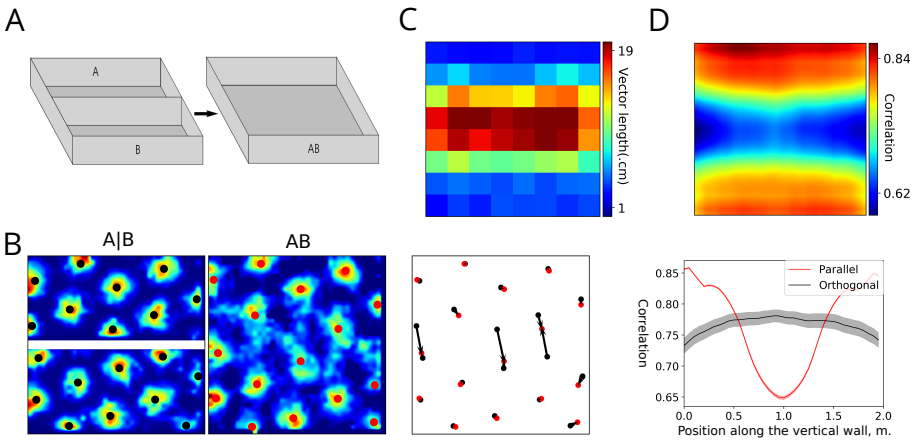

Figure 4.4: A. The training environment with two separate rooms, referred to as room 'A|B', and the testing environment, referred to as merged room 'AB'. B. Firing fields of an example grid cell in the training (left) and testing (middle) environments, as well as firing-field displacement vectors calculated in the testing environment (right). C. A color map of mean vector lengths. D. Top plot: A color map representing the mean sliding correlation over all grid cells. Bottom plot: the correlation profiles at the center of the environment along two cardinal directions.

Thus, the low-correlation band near the location of the removed wall was induced in the

model by changes in visual input in the merged environment, which affected place coding via VPC activities. Local visual features at the locations distant from the removed wall were similar in the corresponding locations of the original environments A and B, since visual patterns formed by the closest walls and extramaze cues remained largely unchanged after the central wall removal. Therefore, VPCs activities at these locations during testing were very similar to those during training (Fig. 4.5A), leading to the same grid pattern at these locations. However, at the locations close to the removed wall, the combined effect of stable distal cues and modified proximal wall cues resulted in an extension of VPC receptive fields over the previous location of the removed wall. Such changes in visual receptive fields induced local corrections of grid cell activity by shifting grid-cell activity packets towards the center, resulting in local deformations of grid-cell firing patterns similar to those observed during gain modification experiments. These deformations in turn affected place fields of MPCs and CPCs, by shifting place fields of the cells near the removed wall towards it (Figs. 4.5B,C). The results suggest that local deformations of grid fields can be explained by the same correction mechanism as the one studied in the previous section, but in which local sensory conflict is induced by changes in the visual input instead of changes in self-motion gain.

Two principal neural processes affect the formation of spatial representation in our model: while the acquisition of new spatial representations crucially depends on synaptic plasticity, the dynamic interaction between visual and self-motion cues is mediated by neuronal dynamics. We therefore tested the contribution of these two processes to the observed results. The influence of plasticity was assessed by letting the model learn during testing in the merged room, while that of neuronal dynamics was tested by progressively decreasing the strength of the loop (i.e. decreasing the control of vision over self-motion cues) in the absence of synaptic plasticity. The results of these manipulations can be summarized as follows. First, when learning was allowed during testing and the testing trial in the merged room was sufficiently long, the particular correlation pattern (see Fig. 4.4C,D) was broken and a new representation was formed as a result of learning (Figs. 4.6A-C), unlike what was observed by Wernle et al. In particular, the newly formed global pattern was aligned with only one of the walls, resembling the results of Carpenter et al. (2015) addressed in the following section. Moreover, learning of the new representation was faster when the

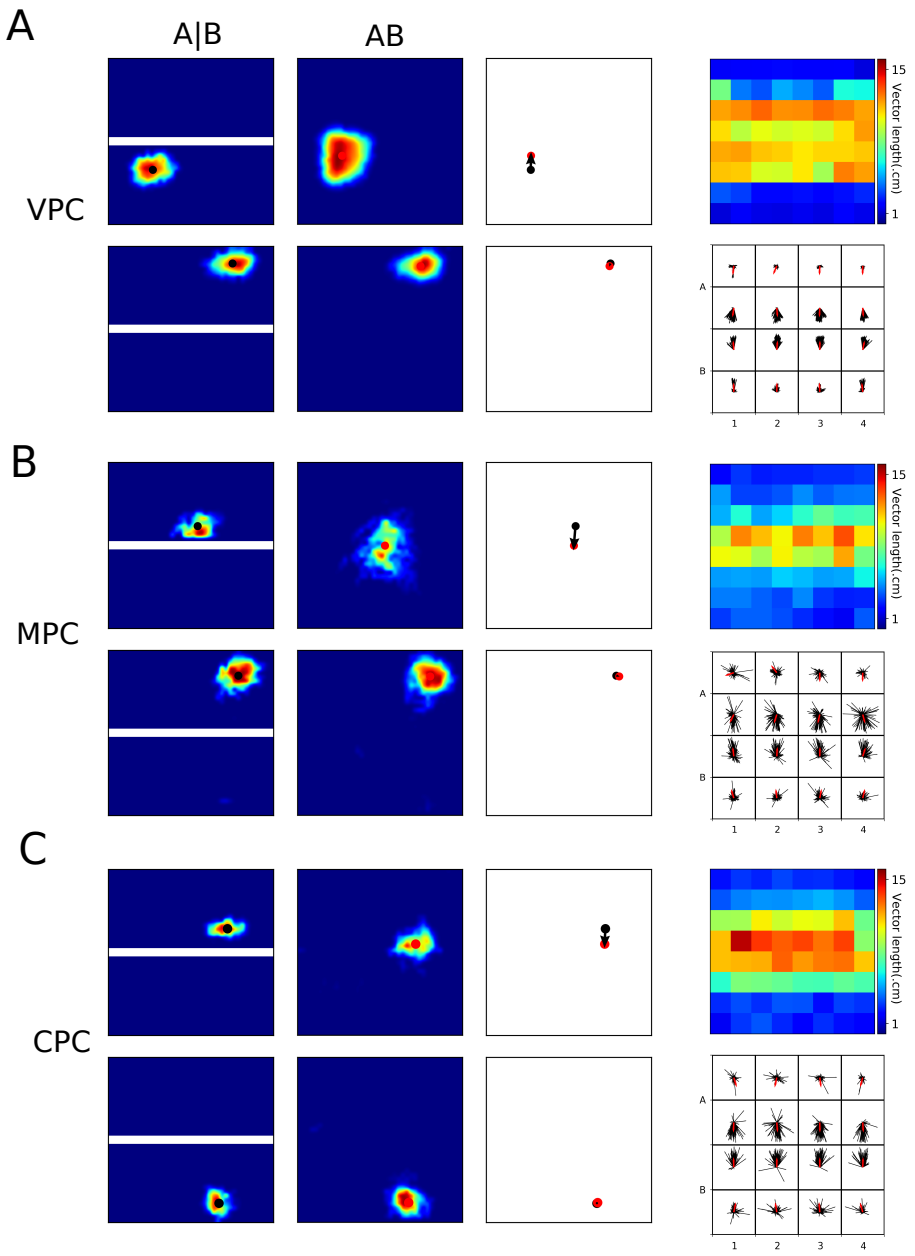

Figure 4.5: A. Left: receptive fields of two VPCs in the training and testing environments, either close to the removed wall (top) or distal from it (bottom). Middle: displacement vectors of the cells on the left. Right: color map of displacement vector lengths for all cells (top) and all displacement vectors with their mean direction shown in red (right). B,C. Receptive fields and displacement vectors for MPCs (B) and CPCs (C). Refer to A for details.

control of visual cues (controlled by α) was low (not shown), since slower dynamics favors the learning of new connections between self-motion-based and visual representations. Second, the decrease of α across separate sessions (with plasticity turned off) resulted in widening of the low correlation band (Fig. 4.6D). This modification of the correlation pattern is explained by the fact that under a weak control of place fields by vision, it takes

longer for the visual cues to correct self-motion.

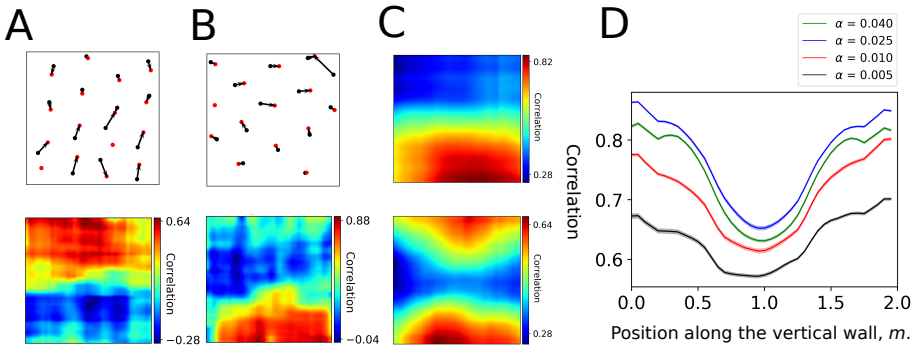

Figure 4.6: A,B. Displacement vectors (top) and corresponding sliding correlation maps (bottom) of two example grid cells after learning in the merged room. C. Averaged over many grid cells, sliding correlation maps can result in two different mean correlation patterns. D. Mean correlation along the direction perpendicular to the removed wall for different values of the the strength α.

4.3.2 Simulation of the double-room experiment

In the experiment of Carpenter et al. (2015), grid cells were recorded in rats during foraging in an experimental environment consisting of two rectangular rooms (A and B) connected by a corridor (Fig. 4.7A, see also Carpenter et al., 2015). The two rooms were rendered as similar as possible in their visual appearance in order to favor visual aliasing. The rats were released in the corridor and explored the whole environment for 80 minutes across up to 20 daily sessions. If local visual cues are the only determinants of grid cell activity, grid cells were expected to express identical hexagonal firing patterns in the two rooms, reflecting the same visual appearance of the rooms. However, since the animal is free to move between the rooms, self-motion cues can be used to spatially disambiguate them. Thus, if self-motion cues contribute to grid-cell firing, grid cells were in contrast expected to form distinct firing patterns in the two rooms. The results of this experiment revealed that both external and internal cues influence neuronal activity, but in a temporally-organized fashion. In particular, grid cells had similar firing patterns in the two rooms during early exploration sessions, suggesting that local visual cues of the two rooms initially had a strong influence on grid-cell activities. As the number of sessions increased however, grid cells progressively formed a global hexagonal pattern extending over the whole environment suggesting a progressive contribution of self-motion cues. One consequence of the creation of the global representation was that local firing patterns

in the two rooms progressively became more and more dissimilar despite the fact that visual cues remained the same. This can be interpreted as a progressive loss of control of local visual cues over grid-cell activities. These results are thus in conflict with the data from the merged-room experiment by Wernle et al. considered earlier, since in that experiment local visual cues near the distant walls kept their control of nearby grid fields for up to 9 consecutive sessions.

What could be the reason for the differences in learned grid-cell representations in the two experiments? Suppose that, in the conditions of the double-room paradigm, the rat first enters room A, such that initial associations between self-motion and visual cues are established in that room. The key question is whether or not a new representation for the subsequently entered room B will be formed, despite its identical visual appearance with room A (note that in the following we refer to any initially experienced room as room A, independently on which actual room was visited first in the simulations). Results of the previous section suggest that a weaker control of visual cues combined with synaptic plasticity leads to the formation of such a new representation. To verify this hypothesis, we ran our model in the conditions of Carpenter et al. experiment (see Section 4.2.4), and we progressively (i.e. session by session) decreased the strength of the hippocampal-entorhinal feedback loop (without disabling synaptic plasticity). As the feedback strength controls the influence of visual input in our model, we expected that this procedure will result in the construction of a global representation on the level of grid cells when the strength of the loop is sufficiently low. This was indeed the case as the global fit was high when the loop strength was set to low values (small α), and, conversely, the local fit was high for a strong loop (Figs. 4.7B,C, both of these measures were calculated in the same way as in the study by Carpenter et al., 2015, see Section 4.2.4).

The local representation in early sessions is a consequence of the fact that representation of only one of the rooms is learned, so that once the model rat enters the second room, grid-cells activities are quickly reset by vision to the representation of the first (or, in terms of Skaggs and McNaughton (1998), the representation of room A is "instantiated" upon the entry to the room B). In this case both MPCs and CPCs had identical firing fields in the two rooms (Fig. 4.8A). This was quantified in the model by computing the spatial correlation

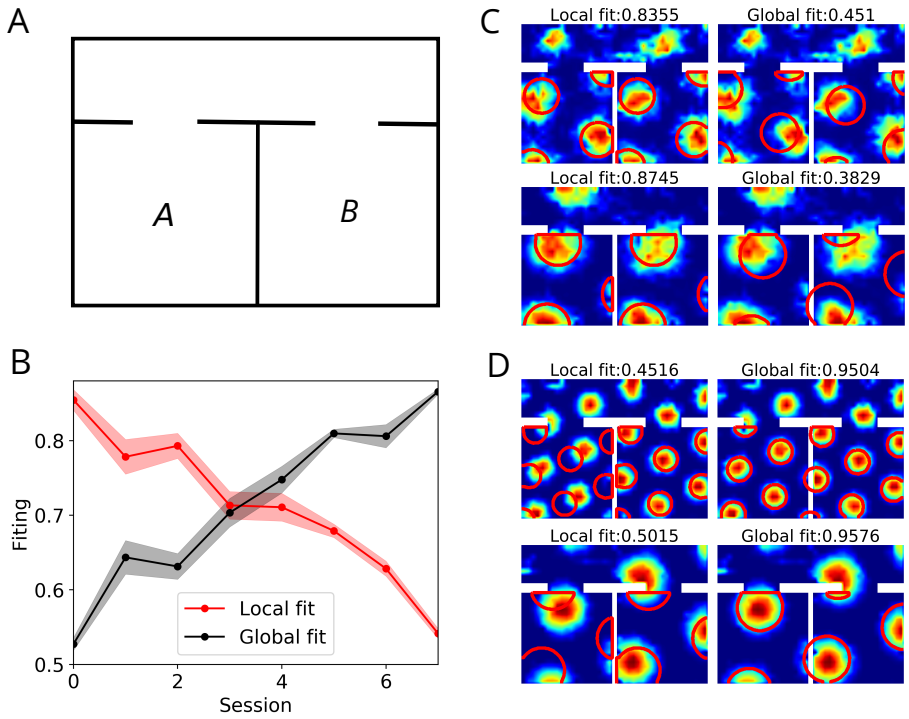

Figure 4.7: Simulation of the double-room experiment of Carpenter et al. (2015). A. Top view of the experimental environment with two visually identical rooms (*A* and *B*). B. Population estimates of the local fit (red) and global fit (black) as a function of session number (see C and D for examples). The value of parameter α decreased from 0.04 to 0.005 across sessions. C,D. Examples of firing rate maps of 4 different grid cells (rows) with superimposed ideal grid patterns according with the highest local (left column) or global (right column) fit. In each row the same firing map is shown twice. In early sessions (C) identical ideal grid patterns in the two rooms fit the data better than a single global hexagonal pattern: local fit is higher than the global fit. In late sessions (D) the reverse is true. The local and global fit was assessed from grid cell firing patterns in the rooms only (not in the corridor).

between place fields of each cell in the two rooms (correlation of 1 corresponds to identical place fields). On the level of the whole population, the mean place-field correlation is high for a strong feedback loop (early sessions, large α, Fig. 4.8B). The transition to a global representation in later sessions results from newly formed synaptic associations between MPCs in CA3 (that are under a strong influence of self-motion input from grid cells), and CPCs in CA1 that are driven by vision. Synaptic plasticity at these connections is favored by a decreased hippocampal input to the EC, leading to a stronger reliance on self motion. The development of such a new representation is reflected in lower place-field correlation on the level of MPCs and CPCs (late sessions, small α, Fig. 4.8B). Note that purely vision-driven VPCs always have identical place fields in the two environments (not shown).

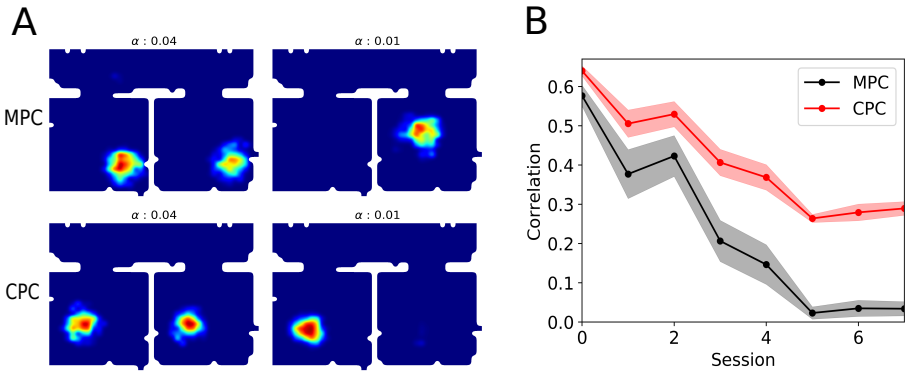

Figure 4.8: A. An example of MPC (top) and CPCs (bottom) place field during early learning sessions (left column, high α) and late sessions (right column, low α). In early sessions a majority of place cells have similar place fields in the two rooms, whereas in late sessions a majority of place cells have a place field only in one of the rooms. B. Spatial correlation between place fields of a cell in the two rooms, averaged over all place cells, as a function of session number (or, equivalently, as a function of decreasing value of α.

To summarize, the results of both the merged-room experiment of Wernle et al. (2018) and the double-room experiment of Carpenter et al. (2015) can be explained by the same model under two conditions: First, the hippocampal control over mEC grid cells progressively decreases in a familiar environment in the course of daily sessions (this requirement is crucial to reproduce the result of the second experiment, but, according to our simulations, has only a weak effect in the first); Second, synaptic plasticity is weak or inhibited when rats are placed into the merged room after learning in room A and B, but not when the rats are exposed to a stable double-room environment. What could be the reason for the inhibition of learning in the merged-room, as opposed to the double-room experiment? Analysis of our model offers the following possible explanation: In early sessions of the double-room experiment, a large mismatch between visual (i.e. encoded in VPC activities) and self-motion (encoded by MPC activities) input occurs at the moment of entry to, or exit from, the room B, since the population activity of VPSs "jumps" to reflect the room A cues or the corridor cues, respectively. This jump of population activity can be quantified by the drop in correlation between the projections of VPCs and MPCs in CA3 onto the CPCs in CA1 near the room doors (Fig. 4.9A). In contrast, the mismatch is smaller for the merged-room experiment, since the visual and self-motion cues near the removed wall code for similar spatial positions (Fig. 4.9B). Therefore, it is possible that learning across sessions is regulated by the size of the mismatch between visual and

self-motion cues. Note that statistical characterization of the mismatch in Fig. 4.9 required averaging over many experimental runs and even in our idealized model can not be reliably detected online. This could be a possible reason why building of a global environment representation in Carpenter et al. experiment takes many days. We thus propose that CA1 area or, more likely, its output structures implement a mismatch detection process that can regulate hippocampal synaptic plasticity on the time scale of days.

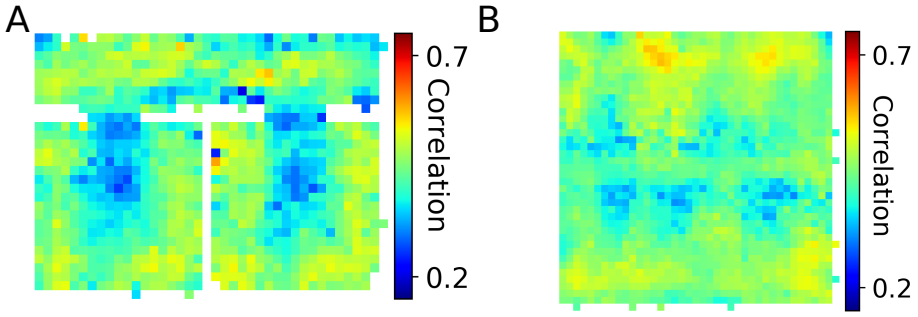

Figure 4.9: A. Mismatch in the double-room experiment. B. Mismatch in the merged room experiment. The colors denote the correlation between VPCs and MPCs projections onto the CPC population.

4.4 Discussion

The presented model is based on two main assumptions: that of a loop-like dynamics in the entorhinal-hippocampal network, and that of an independent visual place-cell representation formed on the basis of hippocampal inputs other than grid cells. Place cells in CA1 receive inputs from spatial (including grid cells) and non-spatial entorhinal cells (Zhang et al., 2013), either via a direct projection from mEC or via an indirect pathway through the DG and CA3. Lesion experiments have shown that either of these pathways can support location-sensitive activity of the hippocampal CA1 neurons (Brun et al., 2002, 2008a). Moreover, even after massive EC lesions CA1 cells retained their spatial selectivity of (Van Cauter et al., 2008), suggesting that such selectivity can result from a large variety of afferent inputs to this structure. Place cells in CA1 project back to the entorhinal cortex both directly and via subiculum (Naber et al., 2001; Kloosterman et al., 2003; Slomianka et al., 2011) and hippocampal input is necessary for grid cell activity (Bonnevie et al., 2013), supporting the loop-like structure of entorhinal-hippocampal interactions (Iijima et al., 1996; Mizuseki et al., 2009).

That a subset of hippocampal place cells can form spatial representations independently from grid cells is supported by a substantial amount of evidence (Poucet et al., 2013). In particular, in rat pups place cells are present before the emergence of the grid cell network (Muessig et al., 2015), whereas in adult rats a disruption of grid cell activity does not prevent the appearance of place cells in novel environments (Brandon et al., 2014). These grid-cell independent place codes retain all principal properties of a self-organized representation in control animals: they can be learned in new environments, they are stable over time, and independent representations are established in different rooms (Rueckemann et al., 2016; Schlesiger et al., 2018). These data suggest the existence of two parallel and overlapping input streams that give rise to hippocampal place sensitivity: the first one integrating spatial inputs from grid cells in the dorsal mEC, likely representing self-motion-based spatial signals (McNaughton et al., 2006); the second one integrating other sensory information to form a grid-cell independent spatial representation in a self-organized manner (Poucet et al., 2015). The differential reliance of place cells on these principal input streams is most clearly manifested in neural responses of these cells to sensory manipulations in virtual linear track experiments (Chen et al., 2013): during passive movement through the track (i.e. with only visual cues available) 25% of cells kept their firing fields unchanged relative to a control condition with both types of cues present; during locomotion in the absence of visual cues (i.e. with only self-motion cues available) 20% of cells did not change their firing patterns; the activity of the rest of CA1 cells was modified to various degrees by cue manipulations (see also Haas et al., 2019). Moreover, recent evidence suggests that CA1 cells responsive to visual and self-motion input are anatomically separated: place cells more responsive to self-motion cues are located predominantly in superficial layers of CA1, while those more responsive to visual cues are found in deep layers (Fattahi et al., 2018; Mizuseki et al., 2011). It was also recently shown that CA1 cells in deep and superficial layers receive stronger excitation from mEC and lEC, respectively, with the amount of excitation being also dependent on the position of the neurons along the longitudinal hippocampal axis (Masurkar et al., 2017). These data further support the existence of functionally different subsets of place cells in CA1, that can either be inherited from similarly segregated cells in CA3 or to be formed directly from non-grid EC inputs to CA1.

Our model is constructed to reflect the above data in a simplified way. While the neural basis for the aforementioned grid-cell-independent code is not clear, we conceptualized it by a population of VPCs, which learn subsets of visual features corresponding to a particular location using simple competitive learning scheme. Similarly to experimental data described above, VPCs form a stable and independent code for different environments as long as visual cues in these environments are stable. It is likely that such a code is formed inside the hippocampus itself based on the inputs either from lEC (Schlesiger et al., 2018) or ventral mEC (Poucet et al., 2013) possibly together with inputs from other structures (Van Cauter et al., 2008), since no location-sensitive code has been observed directly upstream of the hippocampus (Mao et al., 2017). While in its current version our model assumes that VPCs are learned in CA3 and transmitted to CA1, the model can be modified to implement competitive learning in CA1 directly on visual inputs from lEC, bypassing CA3 (Brun et al., 2002). Similarly to a number of attractor-network models of grid-cell activity (Fuhs, 2006; McNaughton et al., 2006; Guanella et al., 2007; Sheynikhovich et al., 2009; Burak and Fiete, 2009; Bonnevie et al., 2013), our model of self-motion-driven activity in GC-MPC populations relies on the assumptions that *(i)* the position of the animal in an environment is represented by the position of the activity packet (i.e., an attractor state of network dynamics) on a 2D neural sheet corresponding to a grid-cell population; and that *(ii)* the activity packet is shifted to precisely integrate the animal's velocity. As long as these assumption hold, our modeling results are independent of the exact neural mechanisms realizing the attractor dynamics and velocity-based shifts of the attractor state (provided that the hippocampal input can influence the attractor state according to Eqs. 4.2.1-4.2.2).

The main contribution of the present model is the proposal that integration of visual and self-motion representations occurs in the EC and is regulated via feedback projections from the CA1. This is in contrast to a long-standing idea that multisensory integration is performed by the attractor network residing in CA3 (McNaughton et al., 1996; Samsonovich and McNaughton, 1997). Our model thus resolves two outstanding issues related to this earlier proposal. The first issue is the existence of separate self-motion-dependent and vision-dependent subsets of cells in CA1/CA3 mentioned above (Chen et al., 2013; Fattahi et al., 2018; Chen et al., 2019; Haas et al., 2019). If CA3 performed the integration of the

two representations as the earlier model suggest, why would they still persist in the downstream CA1? In our model, the existence of the two representations in CA1 are essential for the model to work, since their combined input to the EC is required for multisensory integration. The second issue is the mutual interaction between external/sensory and self-motion-based representations. In earlier models cognitive mapping was essentially performed by a "path integrator" (that is now thought to reside in the grid-cell network) and the role of visual input was only to occasionally reset it and to prevent error accumulation. As discussed above, it is now clear that external sensory inputs can self-organize into a stable and persistent representation and that neural mechanisms supporting such a representation appear earlier during development than the putative path integration system. It is thus possible that the two representations exist in parallel and interact with each other. Here we propose how such an interaction can be performed by the entorhinal-hippocampal processing loop. We believe that studies of grid cells and place cells in environments with visually similar compartments provide an important line of experimental evidence as to the modes of interactions between the two representations, since in these studies the two types of information are put in direct conflict. Previous models that addressed mutual relations between place cells and grid cells (Guanella et al., 2007; Rennó-Costa and Tort, 2017) focused on other aspects of such relations. While our model postulates the important role of hippocampal CA1 representation in the correction of cumulative error at the level of grid cells, it does not exclude the involvement of other possible mechanisms of error correction. For example, it has been recently proposed that border cells, experimentally observed in mEC, correct grid-cell activity near environmental boundaries (Hardcastle et al., 2015). It is not clear how such a boundary-related processing can affect grid cells far from boundaries, for example in the conditions of experimental studies simulated in the present work. In addition, it is not clear whether the boundary-based error correction occurs independently of the hippocampal input, as proposed by Hardcastle et al., or via the hippocampal processing loop, in which case it will be a particular case of the model proposed here. The relative contribution of different mechanisms, if they exist, will potentially be determined by the features of the environment, such as the presence of distal cues, objects and boundaries.

An important parameter of our model is the strength α of the feedback projection from

CA1 to EC, reflecting the efficacy of neural information transmission between the two areas (Colgin et al., 2009; Bonnevie et al., 2013). The progressive construction of a global representation in our simulation of the double-room experiment required a progressive decrease in the value of this parameter. By slowing down the dynamical correction of motion-based entorhinal-CA3 representation by vision, it allowed synaptic plasticity in afferent CA1 synapses to form new associations between a visual representation of the rooms (encoded in the VPC activity) and the motion-based representation, and hence to disambiguate the two rooms. Ultimately then, whether a global representation was learned or not is determined by the relative time scales of two processes: *(i)* dynamical correction of EC attractor states and corresponding CA3 representations by external visual cues and *(ii)* synaptic plasticity at afferent CA1 synapses. The interplay between the two processes can in principle be governed by several neuronal mechanisms, including neuromodulatory influences on plasticity and neural dynamics (Hasselmo et al., 1995) and/or on oscillation coherence (Colgin et al., 2009). While in our simulations α was manually decreased across sessions, the model could be extended to automatically adjust its value. One possibility would be to link the value α to novelty processing: upon initial exposure to an environment the novelty signal is high (potentially reflecting the absence of learned connections between motion-based and vision-based representations), while it should progressively decrease as these connections are learned and motion-based CA3 representation take precedence over external sensory inputs (Hasselmo et al., 1995). Another possibility is to consider the hippocampal loop processing as a network to implementing statistical inference and prediction (Bousquet et al., 1997; Penny et al., 2013): in a novel environment, prediction about future incoming sensory inputs is poor (high prediction error); as learning progresses this error decreases reflecting a better statistical model of the environment. These considerations suggest that a global representation must eventually arise after a sufficiently long exposure to an environment. This was not however the case in the merged-room experiment. Indeed, under the hypothesis that grid cells express hexagonal firing patterns as a consequence of attractor dynamics with circular weight matrices (McNaughton et al., 2006), the local translocation of grid fields at the center of the merged environment must result from a dynamic correction mechanisms, since synaptic plasticity between place-cell and grid-cell networks would necessarily lead to the emergence of a

coherent (global) grid-cell representation. One possible explanation for this discrepancy is that the testing period in the merged room (up to 9 daily sessions) was not long enough, as rats in the double-room experiment expressed clearly global grid patterns after at least 10 testing sessions (Carpenter et al., 2015). Another possibility suggested by the analysis of the model is that the learning process is also regulated by the size of the mismatch between visual and self-motion-based representations.

A number of experiments studied place fields dynamics in environments consisting of two or more visually identical compartments (Skaggs and McNaughton, 1998; Tanila, 1999; Fuhs et al., 2005; Paz-Villagrán et al., 2006; Spiers et al., 2015; Grieves et al., 2016). The objective of these experiments was to check whether path integration can be used by animals to distinguish between compartments and to assess the extent to which visual cues control path integration information. Earlier experiments provided evidence for a partial (Skaggs and McNaughton, 1998) or a nearly complete (Tanila, 1999) remapping when rats travelled between two similarly looking compartments, suggesting that path integration can be used to distinguish between them. A major difference between experimental setups in these latter experiments was that the two compartments in Skaggs and McNaughton (1998) were oriented in the same way, whereas in Tanila (1999) there was a 180° difference in their orientation. A follow-up experiment (Fuhs et al., 2005) has demonstrated a key role of angular, but not linear, path integration in the complete remapping observed by Tanila et al. 1999. However, Fuhs et al. did not observe partial remapping in conditions very similar to those of Skaggs and McNaughton (1998), as most cells had identical place fields in the two compartments. More recent experiments with multiple visually identical compartments confirmed the importance of angular path integration for remapping (Spiers et al., 2015; Grieves et al., 2016, see also Paz-Villagrán et al., 2006), and suggested that a larger amount of time (about 2-3 weeks) is necessary to build separate representations for visually identical rooms connected by a corridor (Carpenter et al., 2015).

In our simulations, we assumed that head direction system provides a correct orientation information (i.e. relative to an arbitrary fixed reference orientation) at any moment in time, and so the visual input to the model is always aligned to the common directional frame in all environments (in the experiment of Carpenter et al. a common directional frame could be

provided by the corridor cues, whereas it was provided by distal extramaze cues in Wernle et al. experiment). As a result of competitive learning, synapses to visual place cells learn visual features observed at a location where these cells were recruited. Therefore, a place is visually "recognized" (i.e. the visual place cell wins the competition and strongly fires) if the previously learned visual features are observed in the same allocentric direction (independently of any path integration signal). If, however, the visual features are observed at an orientation very different from the learned one (e.g. in a room rotated by 180°) the cells will not be activated (unless visual features are rotationally symmetric) and new visual cells will be recruited, in agreement with Fuhs et al. (2015) study. At smaller rotation angles, the model predicts that place cells will be activated to a higher degree, depending on the autocorrelation width of the learned visual snapshots (Grieves et al., 2016, 2018). That the head direction system can maintain a fixed orientation in the presence of visual cue rotation is supported by experimental evidence (Jacob et al., 2017, see also Paz-Villagrán et al., 2006).

The ability (or inability) of the hippocampal representations to express partial remapping has been discussed in view of the multichart model (McNaughton et al., 1996; Samsonovich and McNaughton, 1997). This model predicted that if rats could learn room identities despite their similar visual appearance, place-field representations of the two rooms would be orthogonal (different charts are active in different rooms), whereas they would be identical in the opposite case (the same chart is active in both rooms). Partial remapping observed by Skaggs and McNaughton (1998) contradicted this hypothesis, as some cells had identical fields in the two rooms, while other cells and different place fields, suggesting that two charts could be active at the same time. In similar experimental conditions Fuhs et al. (2005) observed no partial remapping for unclear reasons, but suggested that the map of one compartment was somehow "extended" to the second one, instead of loading a new map. Our results contribute to this question in two ways. First, we argued that learning of a new representation is under control of a putative neural mismatch detection mechanism. In the experimental conditions of the two above studies, the largest amount of mismatch occurs upon the door crossing, and so the number of door crossings experienced by the rat may be an important parameter with respect to learning. While in Skaggs and McNaughton (1998) the rats were freely moving between the compartments during a trial,

in Fuhs et al. (2005) the number of transitions between rooms was limited to 2 per trial, potentially affecting the results. Second, our results provide a neuronal mechanism for the map observed map extension, i.e. progressive learning of a global representation.

Our results lead to a number of testable predictions. First, VPC in the model acquire representation of only one compartment (among two or more identically looking ones). We thus predict that a subset of place cells, that do not rely on self-motion signals (e.g. such as those observed in Chen et al., 2013) and potentially located in the deep sublayer of CA1 pyramidal layer (Fattahi et al., 2018), will persist through learning and will have repetitive place fields even when a global representation has been learned. Second, learning of separate neuronal representations of different compartments (i.e. progressive remapping) will require the formation of new associations between CA3 cells and CA1 cells preferentially from the superficial sublayer of pyramidal cells. Third, place cells that remap first should have place fields closer to the door, since for these cells the difference between visual and motion-based inputs is largest. Finally, as the width of the low-correlation band (Fig. 4.6D) is proposed to be related to the strength of the visual cue control over path integration, it is predicted that stronger reliance on path integration will result in a wider band. This might occur for example in aged animals, in which a stronger reliance on path integration (or, conversely, an weaker control by visual cues) has been observed (Tanila, 1999; Rosenzweig et al., 2003).

Chapter 5

Modeling the Impact of Aging on the Entorhinal-Hippocampal Network

Chapter summary

The present chapter extends the entorhinal-hippocampal processing model described in Chapter 4 by considering how aging may affect spatial memory. In particular, we focus on the neuromodulatory account of aging by studying how age-relate cholinergic deficits can affect synaptic plasticity and memory in the hippocampal formation. This model provides a first, to our knowledge, neurocomputational account of age-related effects in the hippocampal formation during spatial behavior. In the context of the Aging Human Avatar platform it provides a basic framework of studying how various age-related impairments can affect spatial memory and navigation.

The publication of the results of the present chapter is under preparation.

Abstract

Aging is correlated with spatial memory impairments and thought to be caused by neurobiological alterations in hippocampal memory circuits. A recurring idea in conceptual models of aging links age-related changes in cholinergic modulation of the hippocampal formation with synaptic plasticity deficits in this area. Neurophysiological experiments with aging rodents show that place cells in aged rodents exhibit a variety of differences compared with those in young or adult ones. In particular, place cells in aged animals are impaired in creating spatial representations of novel environments, as shown by reduced spatial remapping of these cells. Moreover, the transition from idiothetic to allothetic cues, when these cues provide conflicting information about spatial location, is slower in aged animals. Despite a large amount of data from aged rodents, the neurocomputational nature of age-related effects underlying differential place cells dynamics as a function of age remains an open issue. In this work we extend our previous model of entorhinal-hippocampal circuit of spatial information processing (Li et al., 2020) by including age-regulated cholinergic modulation of hippocampal input to the entorhinal cortex. The extended model is tested in two simulated experiments addressing the learning of a novel environment and a switch from self-motion to visual cues. Our modeling results suggest that age-induced attenuation of acetylcholine release leads an to excessive recall of stored allocentric memories, mediated by entorhinal recurrent networks, in contrast to classical theories implicating the dentate gyrus in this process. Moreover, this age-related impairment is proposed to play a key role in the control of visual information influence on multisensory integration in the entorhinal-hippocampal circuit.

5.1 Introduction

A large body of experimental evidence suggests that aging is associated with an impairment of spatial orientation ability. On the neural level, aging is thought to affect neuronal processing in brain areas that support spatial memory, and in particular the hippocampal formation. Multiple neuron types in this area were shown to mediate formation of spatial memories, including place cells and grid cells (O'Keefe and Nadel, 1978; Fyhn et al., 2004; McNaughton et al., 2006). While grid cells are generally thought to support path integration, i.e. representation of location based on idiothetic cues (Cheng and Frank, 2011; Fyhn et al., 2004; Hayman and Jeffery, 2008; Jacob et al., 2019; McNaughton et al., 2006), place cells are sensitive to both visual and self-motion cues and are therefore thought to encode location by combining idiothetic and allothetic cues (Chen et al., 2013; Fattahi et al., 2018; Markus et al., 1994; Hafting et al., 2005; Krupic et al., 2015).

Multiple age-related effects were observed when comparing firing activities of place cells in adult and old rats in experiments testing the effect of cue manipulations on spatial memory. When a geometric layout of the experimental space is altered, landmarks are displaced or objects are removed, place cells in adult rats express spatial remapping: changes in visual cues are reflected in changes in the position of place-cell firing fields. In contrast, when the same cue manipulations are experienced by aged rats, their place fields are abnormally maintained at a constant location between the novel and familiar environments (Tanila et al., 1997a,b; Oler and Markus, 2000; Wilson et al., 2003, 2004, 2005a). Thus, on the level of place cells, aging is reflected in the inability of encoding visual cue changes and a tendency of recalling from a previous spatial representation. In contrast to the differences between aged and adults rats observed during visual cues manipulations, when visual cues remained the same but *self-motion cues* differed between the novel and familiar environments, place cells in both old and adults rats reflected these changes with equal efficiency (Wilson et al., 2005b). In another experimental paradigm testing the interplay between allothetic and idiothetic cues in aging, neural activities in young and old rats were compared during running back and forth on a linear track (Rosenzweig et al., 2003). When the starting position on the track was manipulated (while leaving all the surrounding visual cues on their stable locations), place cells in young rats

quickly switched from idiothetic to allothetic cues, while those in old rats maintained firing based on path integration. These results go in line with human experiments showing that aged subjects have difficulties in switching from an egocentric to an allocentric strategy when navigating in a virtual city (Harris and Wolbers, 2014).

Neurocognitive aging is associated with a wide range of changes in neural networks supporting spatial orientation, both within and outside of the hippocampal formation across species (Leal and Yassa, 2015; Lester et al., 2017). In view of an enormous complexity of a general analysis of these changes aimed at finding principal causes of age-related decline in spatial behavior, one approach is to focus on a small set of candidate hypothesis and explore, using computational modeling, their potential consequences on neural activity and behavior. If a large part of available experimental evidence can be explained by this set of hypotheses, these can be further analysed in order to arrive to a reduced minimal model of age-related effect on spatial memory. Such a core set of proposed neural-level mechanisms of age-related decline includes the effect of age on synaptic plasticity (Burke and Barnes, 2006), age-related abnormalities in cholinergic activity within the hippocampal formation (Shen and Barnes, 1996; Ikonen et al., 2002; Schliebs and Arendt, 2011) and deficits in pattern separation (Rosenzweig et al., 2003; Gracian et al., 2013). In the present work we focus on the first two of these hypotheses and we explore the idea that age-related changes in cholinergic modulation affect plasticity, in turn causing the observed neural and behavioral changes. Cholinergic modulation of CA1/CA3 circuits by the medial septum declines significantly with age (Shen and Barnes, 1996; Schliebs and Arendt, 2011), and this decline has been repeatedly related to novelty processing (Giovannini et al., 1998; Miranda et al., 2000; Giovannini et al., 2001; Ranganath and Rainer, 2003). In addition, a long-held view is that cholinergic modulation controls the state switches of hippocampal processing between recalling from a previously stored spatial representation or learning a new spatial representation (Hasselmo et al., 2002; Sava and Markus, 2008). In a behavioral study, the impairment of spatial learning in old animals was related to cholinergic deficits, as young rats with acetylcholine lesions were not able learn a new spatial representation in a novel environment similarly to old rats (Ikonen et al., 2002).

Despite the fact that synaptic plasticity deficits and impairments of cholinergic processing have been repeatedly related to age-related decline in spatial memory, how they affect spatial information processing in the entorhinal-hippocampal network of place cells and grid cells has not been studied. Earlier computational models addressed the effect of cholinergic reduction in a non-spatial context of learning of simple patterns (Hasselmo and Schnell, 1994; Hasselmo et al., 1995). A conceptual model by Wilson et al. (2006) proposed that age-related deficits in learning novel environments is caused by excessive pattern completion by the CA3 auto-associative network and reduced pattern separation in the hippocampal DG/CA3 (Rosenzweig et al., 2003), both linked to reduced cholinergic modulation, but no description of associated neural mechanisms has been provided.

The present work extends our previous model of spatial information processing in the entorhinal-hippocampal loop (Li et al., 2020, see also Chapter 4) by including cholinergic modulation mechanisms. The release of acetylcholine in this extended model is controlled by novelty, representing the difference between the actual and stored entorhinal activity. Acetylcholine in turn dynamically modulates the interaction between entorhinal grid cells and hippocampal place cells, and hence the relative influence of allothetic (visual) and idiothetic (self-motion) cues. Thus, the feedback regulation of cholinergic modulation switches between learning of novel environments and recall of familiar ones.

5.2 Methods

The neural architecture of the model is similar to the one presented in Chapter 4. In particular, the inputs and neuronal populations in the entorhinal-hippocampal processing loop are organized as before (Fig. 5.1). More specifically, visual inputs, grid-cell network, motion-based place cells, vision-based place cells and conjunctive place cells are described by AVI, GC, MPC, VPC and CPC populations respectively. The following sections present the differences between the aging model and the one described in Chapter 4. In the following we refer to equations from the previous chapter where appropriate and give the new expressions when needed.

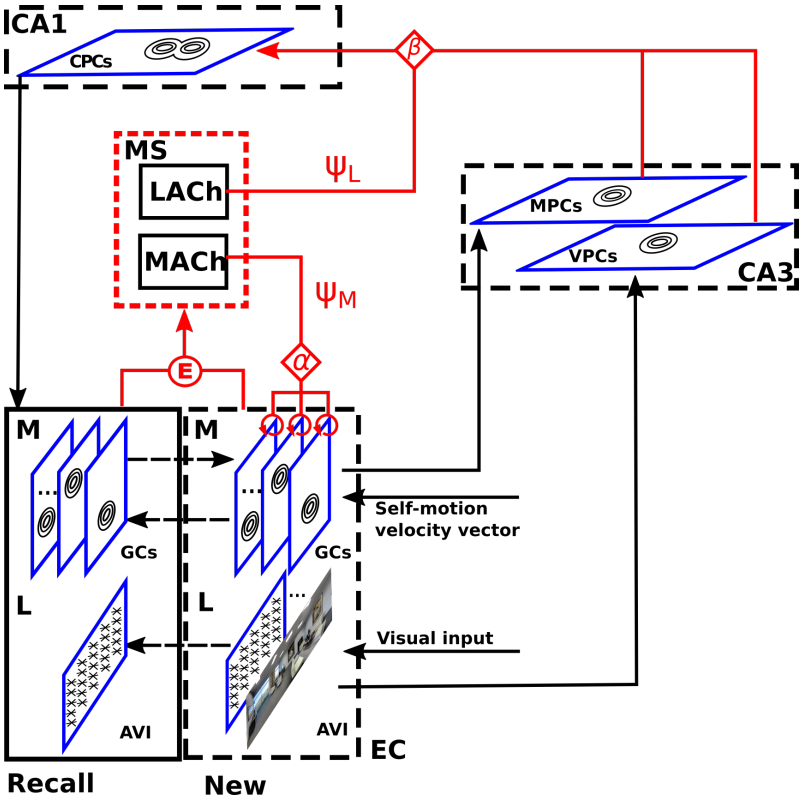

Figure 5.1: Schematic representation of the model. Self-motion input is integrated by GC populations in mEC and results in a self-motion-driven space representation in CA3 (encoded by the MPC population). New visual input, represented by the activities of AVI neurons, results in a purely vision-based representation in CA3, encoded by the VPC population. The GC populations and AVI neurons represent the current sensory signals, and associated activities in the loop (shown by the dashed black boxes). MPCs and VPCs project to CPCs in CA1, and the relative strengths of their projections are controlled by the parameter β. The projection from CPCs back to the EC closes the dynamic hippocampal processing loop, and induces the recall of previously stored information in the GC and AVI neurons (shown by the solid black box). The difference between the current and recalled information represents novelty signals, that control medial-septal (MS) cholinergic release (shown by the dashed red box). The mEC-induced (mACh) and lEC-induced (lACh) cholinergic activities (ψ_m and ψ_l) regulate the dynamics of the hippocampal loop by modulating the parameters α and β, respectively. The arrows represent the information flow in the network.

5.2.1 Hippocampal memory recall

As mentioned in Fig. 5.1, the feedback projection from CPCs to the EC induces memory recall of previous encoded information in the GC and AVI neurons. The recalled information about GC and AVI neurons are determined by the winner neuron from CPCs as

below:

$$I_{avi}^{cpc}(t,i) = \sum_{j=1}^{n_{cpc}} V_{cpc}(t-1,j) W_{avi}^{cpc}(t,i,j) \tag{5.2.1}$$

$$I_{gc}^{cpc}(t,i) = \frac{\sum_{j=1}^{n_{cpc}} V_{cpc}(t-1,j) W_{gc}^{cpc}(t,i,j)}{\max_{j} V_{cpc}(t-1,j) W_{gc}^{cpc}(t,i,j)} \tag{5.2.2}$$

where W_{gc}^{cpc} and W_{avi}^{cpc} are the feedback synapses from CPCs to GC and AVI neural populations, initialized with zero value. The learning of the two synapses are introduced in 5.2.2 (Conjunctive place cells). $V_{cpc}(t-1)$ is a winner vector, computed from the activity of CPCs as below:

$$V_{cpc}(t,j) = \begin{cases} 1, & \text{if } j == \arg\max_{k} \left[A_{cpc}(t-1,k)\right] \\ 0, & \text{otherwise} \end{cases} \tag{5.2.3}$$

Here, $A_{cpc}(t-1,k)$ is the activity of k-th CPC at time t and $V_{cpc}(t,j)$ is a vector representing the CPC winner neuron. In our model, the CPCs input to EC $A_{cpc}(t-1)$ is simplified to a winner vector from biological population coding. The recalled information about AVI neurons is only conveyed to medial septum cortex but not summed to influence the current visual input (see the section 5.2.3). In contrary, the recalled information of GCs is conveyed to medial septum cortex and summed to the current gird cell activities (see the section 4.2.2 and 5.2.3).

5.2.2 Encoding of visual and self-motion input by place cells

Synaptic modification - recruitment learning. The model is required to learn from multiple environments and morphing linear track, respectively. It is known that winner take all(WTA) with hebbian learning(HL) gives result to catastrophic forgetting issue in sequential learning (McCloskey and Cohen, 1989). For instance, a neuron, associated with a location in a cylinder room, would forget the memory of this location, if the neuron be a winner neuron in a new environment i.e. square room. Therefore WTA-HL is not the appropriate modification rule in the model. In order to overcome the memory forgetting issue, selecting a winner neuron is replaced by recruiting a new neuron to learn the input.

The recruitment learning happens when the maximal neural activation of all recruited post-synaptic neurons is lower than threshold value. The activation value of recruited neuron is computed at time step t as below:

$$A_{post}(t,i) = \sum_{j=1}^{n_{pre}} A_{pre}(t,j)W^{pre}_{post}(t,i,j), \quad \text{where i} \in \{0,...n_r\} \tag{5.2.4}$$

$$\tag{5.2.5}$$

Where the activity of each recruited neuron $A_{post}(t,i)$ is computed when receiving pre-synaptic activity $A_{pre}(t,j)$. Then the post-synaptic neuron activity is compared with a threshold as below.

$$\eta_r(t) = \begin{cases} 1, & \text{if } \max_k(A_{post}(t,k)) \leq \theta \\ 0, & \text{otherwise} \end{cases} \tag{5.2.6}$$

$$\tag{5.2.7}$$

Here $\eta_r(t)$ indicates whether do recruitment learning by comparing with the threshold value σ. The synaptic modification of $W^{pre}_{post}(t,n_r,j)$ from input to recruited neuron n_r is computed as follow:

$$W^{pre}_{post}(t,n_r,j) = W^{pre}_{post}(t-1,n_r,j) + \eta_r(t)A_{pre}(t,j) \tag{5.2.8}$$

$$n_r = n_r + 1 \tag{5.2.9}$$

If recruitment learning happened, the number of recruited neuron n_r is increased if learning is happened. All the neural populations (VPCs, MPCs, CPCs, GCs, AVIs) in the model use this learning rule.

Conjunctive place cells. In the present model, the relative strength of input from VPC and MPC populations to CPCs is controlled by the parameter β (see Fig. 5.1), balancing the relative proportion of visual and self-motion influence in the multimodal spatial representation. The CPCs project back to the EC (recall box in Fig. 5.1), which reinstates population activities of GC and AVI in mEC and lEC. The recalled information of GCs are summed to reset the current activities of GCs, where the parameter α controls the strength

of recall (see the section 4.2.2). The recalled and current information of GCs and AVIs are conveyed to Medial septum to compute the cholinergic release, the processing details are introduced in the section 5.2.3.

Both VPCs and MPCs project to CPCs, that model CA1 pyramidal cells sensitive to both visual and self-motion cues with a parameter β control the relative strength between VPCs and MPCs. The total input to a conjunctive cell is:

$$I_{cpc}(t,i) = \beta I^{vpc}_{cpc}(t,i) + (1-\beta) I^{mpc}_{cpc}(t,i) \tag{5.2.10}$$

with

$$I^{vpc}_{cpc}(t,i) = \sum_{j=1}^{n_{vpc}} A_{vpc}(t-1,j) W^{vpc}_{cpc}(t,i,j) \tag{5.2.11}$$

$$I^{mpc}_{cpc}(t,i) = \sum_{k=1}^{n_{mpc}} A_{mpc}(t-1,k) W^{mpc}_{cpc}(t,i,k) \tag{5.2.12}$$

Again, a E%-max winner-take-all scheme is applied to compute the activities A_{cpc}. The recruitment learning rule is used to adjust synaptic weights of afferent CPC synapses from VPCs and MPCs by assigning the input from VPCs and MPCs as the synaptic strength between the recruited neuron n_r and MPCs and VPCs. The weight assignment equations are listed below:

$$W^{vpc}_{cpc}(t,n_r,j) = W^{vpc}_{cpc}(t-1,n_r,j) + \eta_r A_{vpc}(t,j) \tag{5.2.13}$$

$$W^{mpc}_{cpc}(t,n_r,j) = W^{mpc}_{cpc}(t-1,n_r,j) + \eta_r A_{mpc}(t,j) \tag{5.2.14}$$

where the detail explanation of n_r and η_r was described in the section 5.2.2. At the same time, the recalling synapses from CPCs to gc and mEC are determined by assigning the current grid cell and visual activity as the synaptic strength between recruited neuron and lEC and mEC. The weight assignment equations are listed below:

$$W^{cpc}_{avi}(t,j,n_r) = W^{cpc}_{avi}(t-1,j,n_r) + \eta_r A_{avi}(t,j) \tag{5.2.15}$$

$$W^{cpc}_{gc}(t,j,n_r) = W^{cpc}_{gc}(t-1,j,n_r) + \eta_r A_{gc}(t,j) \tag{5.2.16}$$

5.2.3 Cholinergic modulation

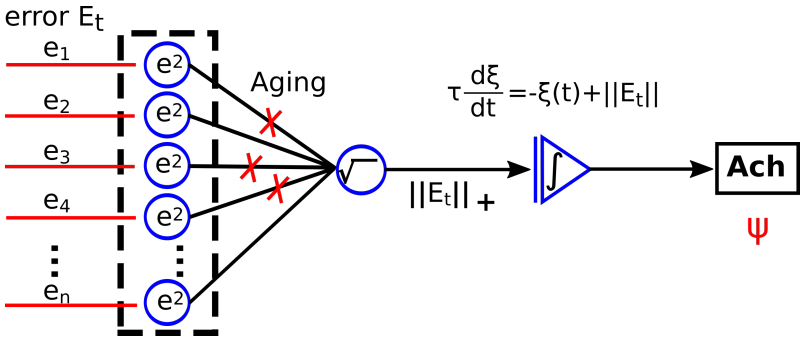

Figure 5.2: A model of cholinergic release based on CA1 feedback projection. The error vector E_t is projected to an MS neuron, which is assumed to compute the norm of the error. The impact of aging on this synapse is modeled by a reduced number of functional connections. The output, integrated with time constant τ, models the cholinergic release. The same computation is performed by mACh and lACh, with different E_t.

In medial septum, the recalled and current information of GCs and AVIs introduced above are compared to compute the error of GCs in mEC (ME) and AVIs in lEC (LE), representing novelty of stimulus. At each timestep ME and LE are accumulated in two neural integrator, respectively. The integrated novel signals (IME, ILE) determine the activity of mEC-induced and lEC-induced acetylcholine neuron (mACh ψ_m, lACh ψ_ι). In turn, mACh is applied to regulate the strength of recalling from CPCs by tuning parameter α. For example, with a higher value of ME, mACh increases and tuning the loop into remapping state. After remapping, the value of ME decreases and the loop turn into a state of recall. Therefore, the feedback regulation of mACh dynamically regulate the state of entorhinal-hippocampal loop. On the other hand, lACh is similar with mACh, but regulate the percentage of the usage of visual information in CPCs through tuning the parameter β. As a result, the neural computing of mACh and lACh modulation on α and β are below:

$$\alpha(t) = b_\alpha - w_\alpha \psi_m(t) \tag{5.2.17}$$

$$\beta(t) = b_\beta + w_\beta \psi_\iota(t) \tag{5.2.18}$$

Here, b_α and b_β are intercepts determines the maximum and minimum value of α and β, and w_α and w_β are the slope value of lACh ψ_ι and mACh ψ_m. The level of mACh and

lACh release are determined by:

$$\psi_m(t) = \frac{1}{1 + \exp\left[\kappa\left(\mu - \xi_m(t)\right)\right]} \tag{5.2.19}$$

$$\psi_\iota(t) = \frac{1}{1 + \exp\left[\kappa\left(\mu - \xi_\iota(t)\right)\right]} \tag{5.2.20}$$

where $\psi_m(t)$ and $\psi_\iota(t)$ denotes the level of acetylcholine release based on IME ξ_m and ILE ξ_ι. Based on this equation, $\psi_m(t)$ and $\psi_\iota(t)$ reach the minimum value when the integrated error is little or zero, increase to 0.5 when the error is equal to μ and approach to 1.0 as the error becomes larger. The gain term κ defines the slope of the two functions. The integrated errors mentioned in the equation (5.2.19) are computed with neural integrator (Fig. 5.2):

$$\tau_m \frac{d\xi_m}{dt} = -\xi_m(t) + ||E_m(t)|| \tag{5.2.21}$$

$$\tau_\iota \frac{d\xi_\iota}{dt} = -\xi_\iota(t) + ||E_\iota(t)|| \tag{5.2.22}$$

Here, ξ_m and ξ_ι are integrated from ME $||E_m||$ and LE $||E_\iota||$ (L2-Norm of error vector) at each time step and decayed with time constant τ_m and τ_ι. The L2-norm of error vectors are neural computed (see Fig. 5.2) as below:

$$\begin{aligned} ||E_m(t)|| &= \rho \sum_{j=1}^{n_{gc}} C_{mj} \left[I_{gc}^{cpc}(t,j) - A_{gc}(t,j)\right]^2 \\ ||E_\iota(t)|| &= \rho \sum_{j=1}^{n_{avi}} C_{\iota j} \left[I_{avi}^{cpc}(t,j) - A_{avi}(t,j)\right]^2 \end{aligned} \tag{5.2.23}$$

where I_{gc}^{cpc} and I_{avi}^{cpc} are the recalled information of GCs and AVIs from the previous stored memory, introduced in the section 5.2.1. The error signals between recall and current information of GCs and AVIs are transported with neurons (see Fig. 5.2). The parameter ρ represents the level of acetylcholine degradation in the model. C_{mj} and $C_{\iota j}$ represent the acetylcholine dendrite is broken or not. The value of ρ, C_{mj} and $C_{\iota j}$ are correlated with aging.

5.2.4 Age-related degradation of cholinergic release

Aging related degradation in acetylcholine neuron is controlled by the parameter ρ. The value is set to 1.0 and 0.7 for the adult and aging model, respectively. According to Eqs. 5.2.23, ρ determines the amplitude of the error (novelty) signal delivered to medial septum. The parameter ρ is also the unbroken probability distribution of acetylcholine dendrite, determining the value of C_{mj} and C_{ij}, if the neural connection is broken, the value is 0.0 otherwise 1.0. Based on the above configuration, the aging model loss 30% of connections and the received error/novelty signals degrade 30%.

5.2.5 Simulations

Virtual environments for the two simulations presented in this paper were developed with Unity (`www.unity3d.com`).

In Simulation 1 (Figs. 5.3-5.6) two environments were used. First, a circular enclosure (diameter: 1 m) with a gray wall and three visual cues located on the wall. Second, a square room 1×1 m with gray walls. In the square room, the same three cues were used as in the circular room, but rotated 90°. The height of the walls in both rooms was 0.6 m. The simulation consisted of training the model for 15 minutes (9000 time steps) by moving quasi-randomly in the circular environment. After that the circular environment was replaced by the square environment, assuming that the simulated rat remained at the same spatial location. Then the model explored in the new environment for 15 minutes.

In Simulation 2 (Figs. 5.7-5.9), the experimental environment was a linear track (length: 2 m). A starting box and a barrier were located in the start and end of the track, respectively. The linear track was located in a large room 4×4 m (wall height: 1.2 m) with some additional visual cues the walls. At the start of a training trial, the model was first initialized inside the starting box. After the model has stabilized, the model rat was released to run the full length track and go back. After training, synaptic weights were then fixed to the learned values. During testing, the position of the starting box on the track was different for each testing trial, the rat was initialized in the box and the ran back and forth along the shortened track. This testing procedure is the same as was used in classical linear track experiments by Gothard et al. (1996b). In Rosenzweig et al. (2003),

the position of the starting box was also modified during training.

Twenty different animals were simulated, which means that the whole training-testing sequence in the simulations below was repeated 20 times and the data was averaged. For all the simulations, it took about 40 s to stabilize loop dynamics upon entering the experimental room. All model parameters are listed in Table 5.1.

Parameter	Value	Description
θ_{vpc}	0.80	recruiting threshold for VPCs
θ_{mpc}	0.85	recruiting threshold for MPCs
θ_{cpc}	0.60	recruiting threshold for CPCs
μ	0.5	Mean term
κ	10	Gain term
τ	5 second	Time decay constant
b_α	0.050	the maximum value of α
w_α	0.045	the decline slope value of α
b_β	0.50	the minimum value of β
w_β	0.20	the increasing slope value of β
E_{vpc}	5%	E%-max winner-take-all
E_{mpc}	20%	E%-max winner-take-all
E_{cpc}	50%	E%-max winner-take-all
ρ	70%	The unbroken acetylcholine dendrite and the degradation of acetylcholine release

Table 5.1: Parameters of the acetylcholine-modulated entorhinal-hippocampal loop model.

5.3 Results

5.3.1 Learning of novel environments by aged rats

Wilson et al. (2005a) studied how adult and aged rats represent novel environments by recording CA3/CA1 place cells while the animals explored a familiar and a novel environment. The familiar environment (denoted C1) was a circular room with three visual landmarks on the wall, in which the animals foraged for food during several weeks. After this familiarisation period, place cells were recorded first in the familiar environment C1 and than in a novel environment (S1). The novel environment was a square room with three original landmarks from C1 in a 90°-rotated positions. Recording of neural activities in the hippocampus suggested that in adults rats, place cells from both CA1 and CA3 areas expressed global remapping, such that spatial locations of place fields were highly different

in the two environments. In contrast, in aged rats only CA1, but not CA3 cells expressed remapping. CA3 place fields in aged rats remained at the same spatial location in both environments. These results suggested that aged place cells in CA3 were impaired in learning novel spatial information.

According to the cholinergic account of aging, release of ACh is increased with novelty (Ranganath and Rainer, 2003; Giovannini et al., 2001), levels of ACh control the switch between learning and recall (Hasselmo et al., 2002) and aging causes a decrease of ACh (Shen and Barnes, 1996; Fischer et al., 1989; Wilson et al., 2006). In our model these effects are simulated by aging- and sensory-error-induced cholinergic release and through ACh-controlled strength of hippocampal input to the EC (See Methods, section 5.2.3). Moreover, simulated aged rats are biased towards recall as opposed to encoding of new information (Section 5.2.4). In order to see whether our model can reproduce place-cell activity changes observed in aged rats, we simulated the experiment of Wilson et al. (2005a). Since our model includes grid cells, our simulations naturally provide experimental predictions of grid-cell activities in old rats. We thus trained the model in a simulated circular environment (C1). We then examined changes in ACh release in the novel environment (S1). After learning the new environment, the model was again placed in the familiar room (C2) and the neural activities were recorded.

In the simulated adult rats, place cells expressed global remapping of their firing fields by firing in different positions in the two environments (C1 and S1) or by activating only in one of the two environments (Fig. 5.3A, familiar-C1 vs novel-S1). Moreover, after subsequent learning of the novel environment, place cells retained spatial information from the previous one (Fig. 5.3A, familiar-C2). In order to quantify hippocampal remapping in the population of place cells, Pearson correlation was used to assess place-field overlap for each place cell by comparing spatial firing patterns of this cell in C1, relative to S1 and C2. Correlation values close to zero (no place-field overlap) or one (complete place-field overlap) indicate global or no remapping, respectively, while intermediate correlation values correspond to partial remapping (see Fig. 5.5D(i)). The three different types of place cells in the model (i.e. VPCs, MPCs and CPCs) had low correlation values in C1 compared to to S1 and high correlation values in C1 compared to C2, suggesting that these

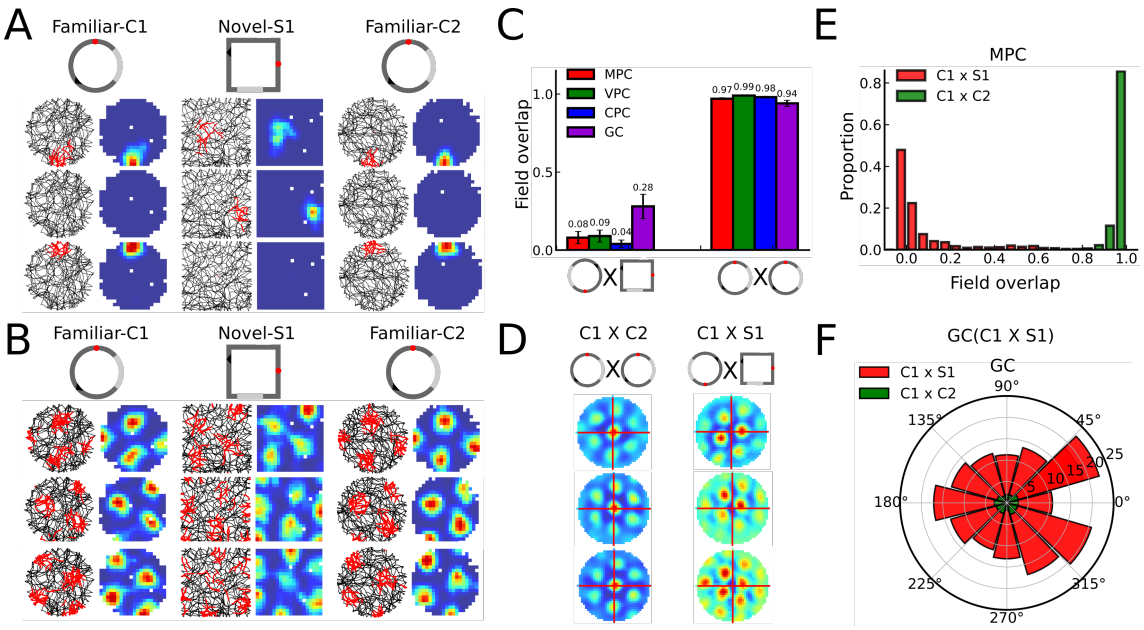

Figure 5.3: Global remapping and grid realignment in adult rats. A, B. Firing fields of three simultaneously recorded place cells (A) and realigned grid cells (B) in the familiar and novel environments. Each row corresponds to one cell. Left column: locations corresponding to firing rate >0.5 (red), superimposed on the simulated rat trajectory. Right column: firing rate color map (dark blue is zero, red is the maximal firing rate). C, Average changes in spatial firing fields quantified by the Pearson correlation of firing fields in the two environments. Left side of the bar plot shows field overlap between the familiar vs novel environments (C1 x S1). Right side of the bar plot shows the overlap between two trials in is the same environment (C1 x C2). Red, greed, blue and purple bars represent MPCs, VPCs, CPCs and grid cells, respectively. D. Color-coded cross-correlation matrices of three grid cells in B indicate the grid shift from C1 to C2 (left column) and from C1 to S1 (right column). The origin corresponds to zero displacement. The position of the peak indicates the grid displacement. E. Distribution of place field overlap in MPCs. Red and green bars represent the different (C1 x S1) and same environments (C1 and C2). F. Polar plot of grid-cell displacements at different direction over 20 trials. Red: C1 x S1, Green: C1 x C2)

cells were able to learn a representation of a novel environment in adult simulated rats (Fig. 5.3C,E).

Coherently with remapping of place cells, grid cells expressed realignment of their firing patterns (Fig. 5.3B). To quantify grid-cell realignment, cross-correlograms were computed for each grid cell between the two environments. The displacement between the origin and the location of peak correlation value in a cross-correlogram indicates the offset of the grid cell (Fig. 5.3D). In the whole population of grid cells, the displacement size due to grid realignment in C1 relative to S1 was in the range between 10 and 20cm (Fig. 5.3F, see Fyhn et al., 2007 for corresponding experimental data). No grid realignment occurred in C1 relative to C2.

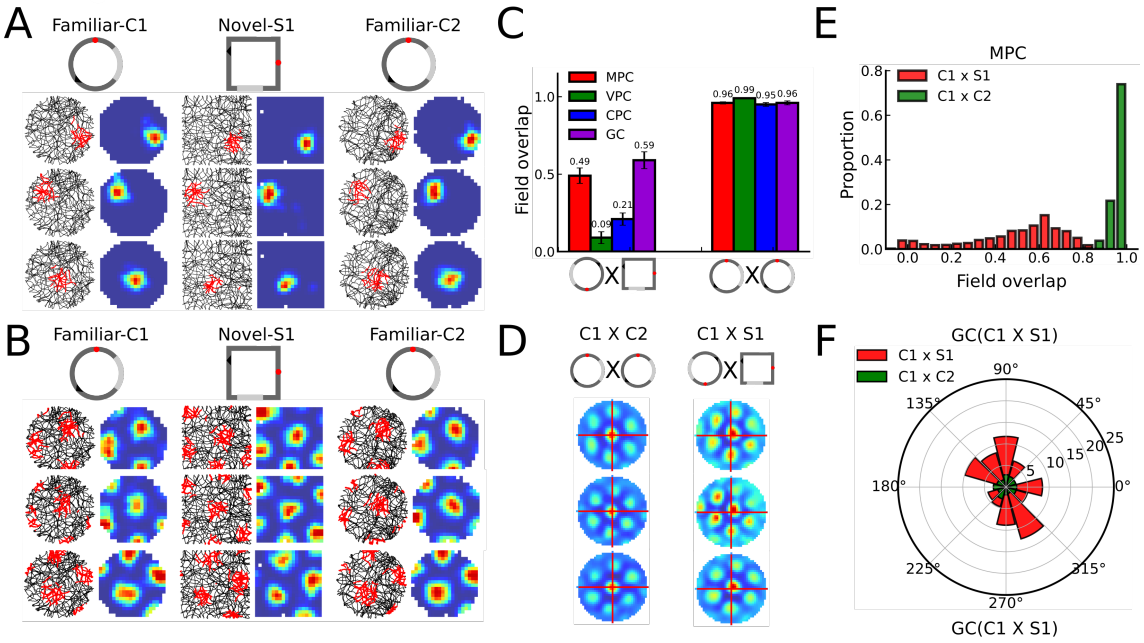

Figure 5.4: No place cell remapping and grid realignment was observed in aged rats. See the legend of Fig. 5.3.

In contrast to the above results, in simulated aged rats MPCs in CA3 expressed only partial remapping and similar firing fields in C1, relative to S1 and C2 (Fig. 5.4A,C,E). The position of grid fields changed only weakly in C1 relative to S1 (Fig. 5.4B,D) as shown by displacement statistics of grid cells over 20 trials (average displacement from 0 to 7.5 cm, Fig. 5.4B,F). Thus, simulated aged rats retained the spatial representation from the familiar room in the novel room, associated with a similar grid-field distribution. On the other hand, VPCs were not influenced by aging in our model and therefore expressed global remapping in the novel environment similarly to adult rats above. Because CPCs are driven by combined input from VPCs and MPCs, they were only partially influenced by aging and their remapping level was higher than in MPCs but lower than in VPCs. Thus, in contrast with adult rats, self-motion-driven cells, including GCs, MPCs, and CPCs, were unable to construct a novel representation of a novel environment (Fig. 5.5A–C). As mentioned earlier, in the study with real rats aging had a weaker influence on CA1 place cells in contrast CA3 (Wilson et al., 2005a), which corresponds to our results for the MPC population. While grid cells were not recorded in this experiment, our model predicts that grid cells in aged rats do not express grid realignment

The above results are explained by reduced ACh modulation from the medial septum in

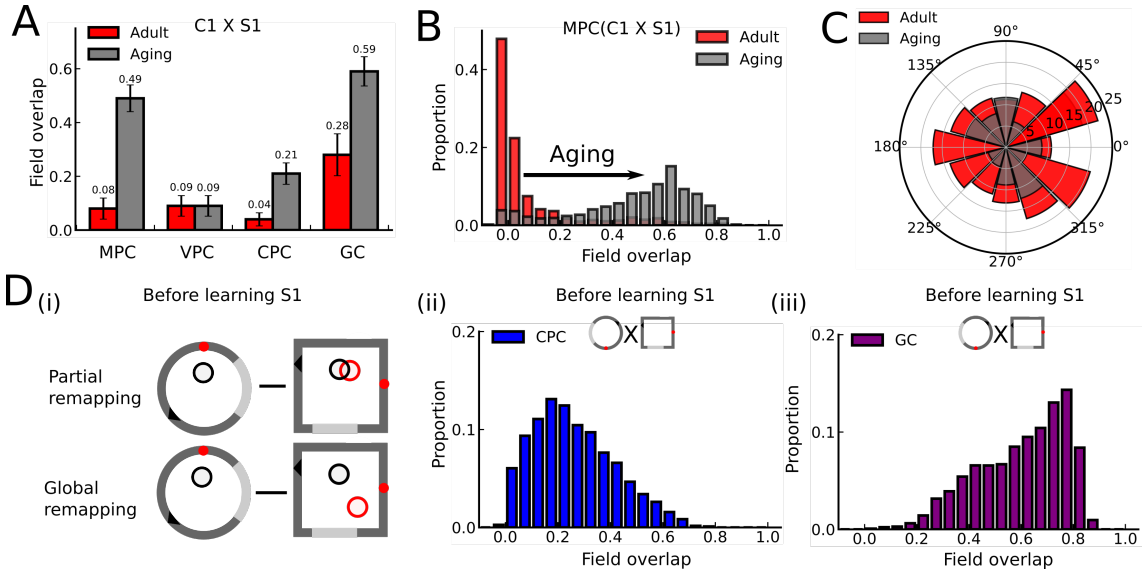

Figure 5.5: Comparison between adult and aged simulated rats. A. Comparison between place cells of adult and aged rats in terms of field overlap (red: adults rats, gray: aged rats). B. The impact of aging on the distribution of field overlap in MPCs. C. A polar plot comparing grid displacement distributions in adult and aged rat models. D. Partial vs global remapping of place cells. (i) Top: example of partial remapping. Bottom: example of global remapping. (ii and iii). Partially overlapped firing fields in CPCs and GCs between C1 and S1 before learning in S1.

our model. When simulated adult rats were placed in the familiar environment (C1), the level of lACh and mACh activation was low (Fig. 5.6B, 1st column), because the error between the recalled and current sensory information was low (Fig. 5.6C–E, 1st column). For adult rats, the strength of the recall-related input to the EC was elevated (Eq. 5.2.17). Before learning the novel environment (S1), the activity of lACh and mACh increased to the maximum as the model was placed into S1 (Fig. 5.6C–E, 2nd column). This activity tuned the hippocampal loop into the encoding state through reducing the hippocampal recall-related input, since the comparison error between the recalled and current sensory information (i.e. the novelty signal) was high. After learning the S1 environment, the recalled memory matched with current sensory input, giving rise to the reduction of ACh release (Fig. 5.6B–E, 3rd column). Thus, in the condition of a high novelty, the EC received less input from CPCs to reset the activity of grid cells, and therefore the activity of grid cells depended strongly on the current sensory input in this case. This in turn results in a realignment of entorhinal grids and hippocampal global remapping.

The impact of aging causes the reduction of ACh release due to the loss in neural connections (Section 5.2.4). As a result, the amount of ACh release stayed at a low level when

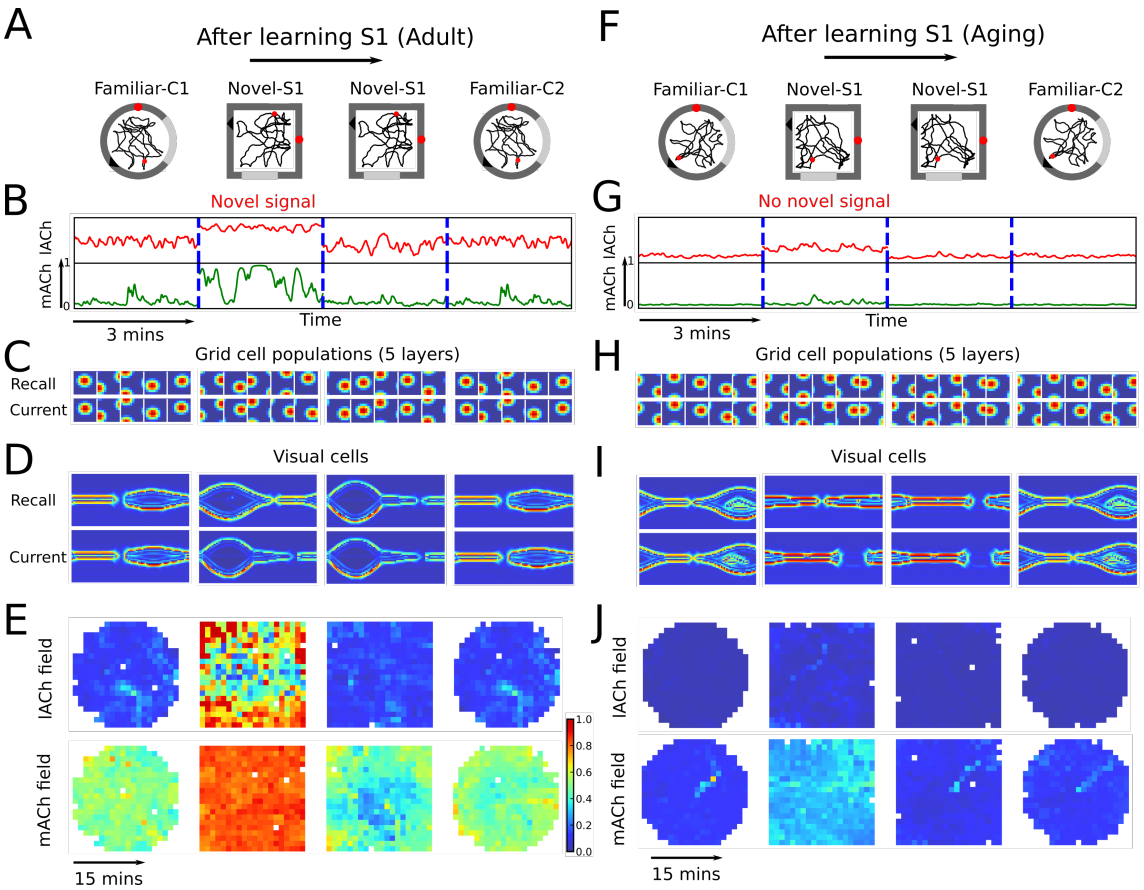

Figure 5.6: Properties of simulated acetylcholine activity in aged and adult rats. A. Simulated environments into which the simulated rats were introduced during simulations. The black line is the trajectory of the rat. The red dot marks the the position of the simulated rat in which the visual and grid-cell input was recorded in C and D. B. The mACh (green line) and lACh (red line) activity as a function of time upon the entry to the corresponding environment. C. Comparison of population activity in 5 grid-cell layers between the one induced by the sensory input (top row) and recalled from the hippocampal input (bottom row). D. Top row: visual information perceived from external environment. Bottom row: Visual information recalled from the hippocampal input. E. Color map of lACh and mACh activities (rows) in the corresponding environment during 15 minutes of exploration. F-J. Same as A-E but for aged simulated rats.

the aged simulated rats were placed in the novel environment (Fig. 5.6G, 2nd column). Because of a strong recall-related input to grid cells, the GC population activities were reset by the projection from CPCs (Fig. 5.6H, 2nd column). A subset of CPCs partially remapped between C1 and S1 (see Fig. 5.5D(i and ii)), and CPCs strongly reset the grid cell population activities with the encoded spatial representation from C1. Therefore, grid cell activities in S1 were highly similar with C1 (Fig. 5.5D(iii)), which in turn influenced the activation of MPCs and CPCs.

5.3.2 Age-related effects on the switch between idiothetic and allothetic cues

In a task requiring the rats to switch from self-motion to visual cues, Rosenzweig et al. (2003) found that aged rats were delayed, compared to adults rats, in the time of switch, leading to the conclusion that the ability of using visual cues to correct self-motion declines with age. In this task rats ran back and forth along a linear track (Fig. 5.7A). At the start of a trial, an animal was placed into the starting box, and once the box was opened the rat ran toward a barrier at the end of the track. The rat was motivated by a neural stimulation reward provided in a fixed position near the end of the track. After reaching the barrier, the rat ran back to the starting box. Upon the placement of the rat into the starting box and before the box was opened, the position of the box on the track was changed on some trials (Fig. 5.7B). If the rat estimates its location on the track based on the distance from the box after leaving it, the hippocampal spatial representation should be driven by self-motion signals irrespective of distal room cues and the distance to the barrier. On the other hand, if the rat takes into account these external cues, hippocampal representation should be aligned with the room cues irrespective from the distance to the box. Rosenzweig et al. (2003) recorded the activity of place cells in the hippocampus and found that in the beginning of the track, place fields were aligned with the box, until a transition point where the firing fields became aligned with the room cues (Fig. 5.8A). In the aged rats this transition point occurred later in the track than in the adult rats.

In our model, the release of mACh (see Methods, Section 5.2.3) controls the strength of visual input to the hippocampal loop. More specifically, if the value of mACh is relatively high, the influence of visual information in the entorhinal-hippocampal loop processing is stronger. Since aging reduces the release of mACh, aged simulated rats are expected to rely more on self-motion than adults rats. This was verified in a computer simulation of the linear track experiment. At the start of a trial, the model was initialized using visual features of the starting box. One the dynamics of the entorhinal-hippocampal loop was stabilized, the simulated rat was displaced from the box to the end of the (full length) track and back. Since we use one-shot learning, only one passage was sufficient for learning. The weights were then fixed and the model was tested in 20 trials with different starting

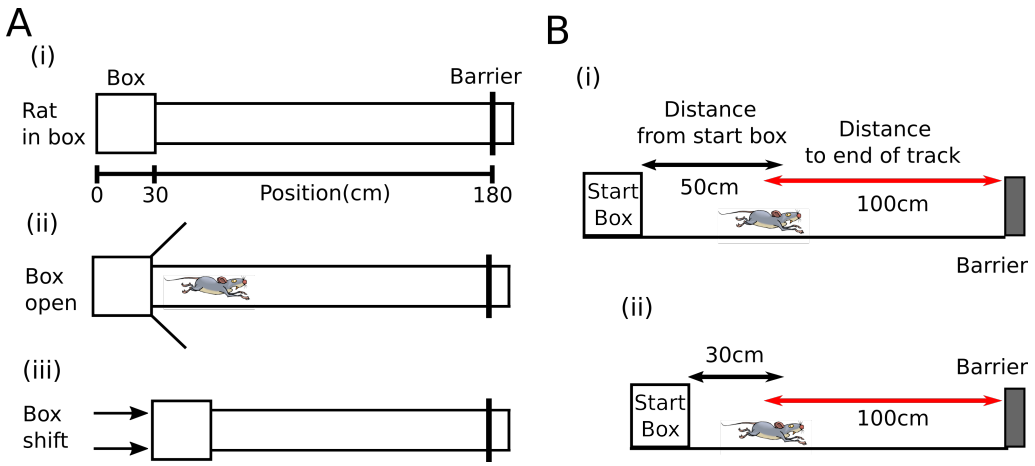

Figure 5.7: The linear track experiment and simulation. A. The experimental environment consisted of linear track (182 x 16 cm), a start box (30 cm width), an unmarked goal zone (not simulated) and the barrier. (i) At the start of a trial, the rat was placed in the box. (ii) Upon box opening, rat ran towards to the barrier and returned to the box. (iii) During recording, the position of box was pseudo-randomly selected from 20 different track configurations separated by 2.5 cm. B. Mismatch between self-motion and visual cues induced by changing the position of the box. (i) The estimation of the rat position based on self-motion cues (path integrated distance from the box, black line) and based on visual cues (distal room cues and the barrier, red line) in the full-length configuration learned during training. (ii) After moving the start box closer to the end of the track, there is a mismatch between the two position estimates.

box positions on the linear track, while the activities of VPCs, MPCs and CPCs were recorded. As in the experiment, place fields of cells with preferred locations close to the starting box were aligned with the distance from it (Fig. 5.8B–D). For place cells with preferred locations farther from the box, place fields progressively realigned from the box to the room cues. The transition speed of VPCs was faster than that of MPCs and CPCs. In particular, the transition of MPCs was slowest, because MPCs integrate information from grid cells, in turn driven by self-motion input. In order to measure the transition point between the box- and room-cues, the slope of the dependence of place-field center as a function of starting box position was computed for each place cell. If a place cell is completely controlled by the box cues, its place field shifts together with the box (slope unity). In contrast, if the place cell is controlled by the room cues alone, its position is independent from the box (slope zero). Comparison of the mean (over all cells) slopes for MPCs and CPCs in the aged vs adult model shows that the transition slopes in the aged model are slower (Fig. 5.9 A,B) as was observed by Rosenzweig et al. (2003).

As the simulated animal moved out from the shifted box, the visual cues from the room

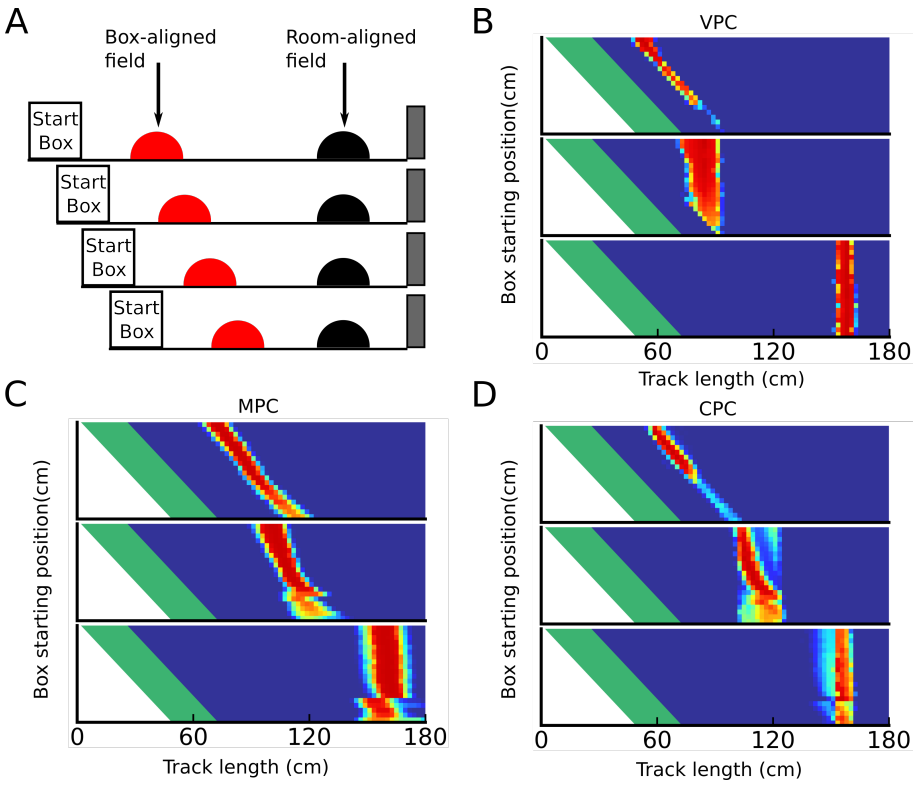

Figure 5.8: Mismatch correction between idiothetic and allothetic cues. A. Depending on the preferred location of a place cell, its firing field can either be aligned with the starting box (red) or with the room and barrier (black). B-D. Place field position along the linear track of three simultaneously recorded place cells (rows) in the VPC (B), MPC (C) and CPC (D) population, as a function of time (horizontal axis) and box position (vertical axis). If the change in place field position (in red) is equal to the change in box position (green), the slope of the cell is 1. If place field position is independent from the box position, its slope if 0. Cells in the middle of the rack express intermediate slopes.

signalled a position that was different from that encoded by hippocampal place cells, which are initially driven by the spatial representation initialized in the box. Thus, in the adult model the level of lACh release was higher (Fig. 5.9C) compared to the aged model (Fig. 5.9D), as a consequence of age-related reduce in cholinergic release. This difference resulted in a slower alignment of hippocampal place cells to visual cues in the aged model. More specifically, when the distance of the simulated rat from the box was between 20 and 80 cm, the level of mACh in the adult model was the same as in the aged model (Fig. 5.9C,D), and therefore the strength of hippocampal input to grid cells was the same in the two models. Since lACh in the adult model is higher in the aged during this period, the former uses gradually more visual information. During this period, the transition between the self-motion and visual cues did not occur, because the self-motion

cues from the starting box exerted a strong control over the hippocampal representation. When the distance from the box was between 80 and 140 cm, the impact of room cues reached its peak, and the adult model experienced a transition from self-motion to visual cues. In the aged model, the value of lACh was lower leading to a weaker effect of visual information on grid cells and to the delayed transition. Even though the mACh release has also increased in adult rat, resulting in a weaker correction of grid cells by the hippocampal input, this increase was delayed with respect to the lACh release so that the overall effect of visual cues was stronger during this delay period. Finally, closer to the end of the track, the lACh and mACh release reached the equilibrium in both models, so that that effect of visual information on place cells became the same in the two models.

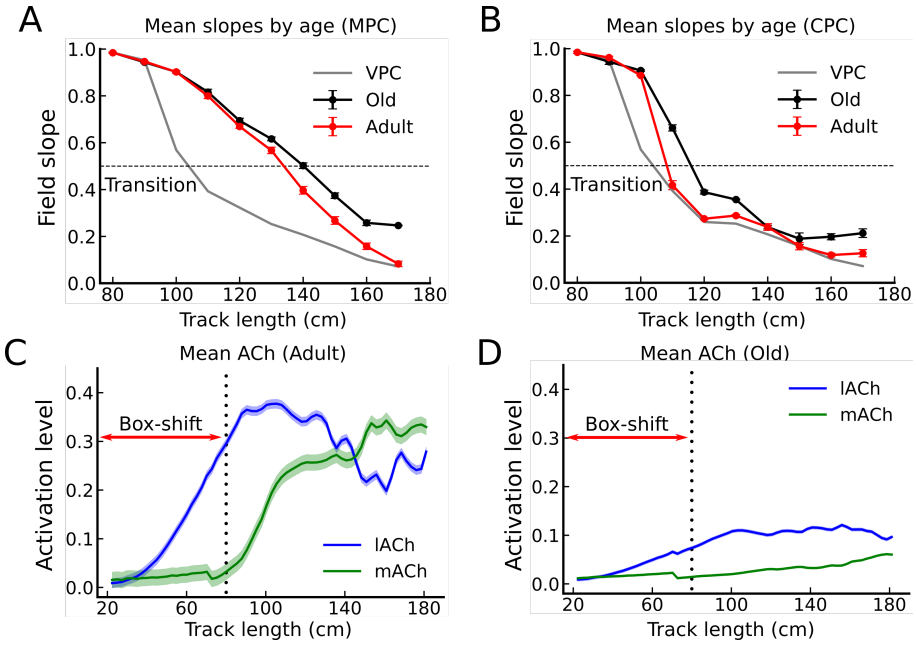

Figure 5.9: Cholinergic influence on the transition between self-motion and visual cues.. A,B. Mean transition slopes of MPCs, CPCs and VPC along the linear track (10 cm/bin) in the adult and aged models. The horizontal axis represents the position of the place-field center in the full-length track. The vertical axis represents the slope value. The transition point from self-motion to visual cues was defined as the point where the transition slopes cross the value of 0.5: box-aligned fields have slopes > 0.5, while room-aligned fields have slopes <0.5. Red and black lines represent adult and aged models, respectively. The gray line represents the mean slope of VPCs. C,D. Mean activation level ±SD of lACh (in blue) and mACh (in green) as a function of position on the linear track in the adult (C) and aged (D) models. The red arrow denotes the maximal shift of the starting box.

5.4 Discussion

The main novelty of the present model with respect to the model of Chapter 4 is the inclusion of cholinergic modulation of synaptic transmission from the CA1 area of the hippocampus to grid cells in the EC. This modulation biases the dynamics of the entorhinal-hippocampal processing loop between learning a novel environment or recalling a familiar one. Past physiological studies have shown an increase in cholinergic release from the MS to EC in response to an entry to a novel environment (Acquas et al., 1996), resulting a reduction mEC theta frequency (Givens and Olton, 1995; Carpenter et al., 2017). These changes in turn give rise to grid field expansion and realignment in entorhinal grid cells (Fyhn et al., 2007; Barry et al., 2012a). In our model, the mACh release, that depends on sensory error from grid cells, modulates the synaptic transmission from CA1 to grid cells and influences the strength of the hippocamal (reset) signal to grid cells (Bonnevie et al., 2013). In particular, in a familiar environment, the low mACh release causes strong recall of spatial information, resetting the activities of the grid cell populations to previously stored values (Section 5.3.1). As a result, firing fields of grid cells and place cells are maintained at the same position. On the other hand, in the novel environment, grid cells receive weak feedback output from CA1 because of high level of mACh release, leading to remapping of hippocampal place cells and grid cell realignment. Previously, Hasselmo and Schnell (1994) simulated CA1 activity, based on the input from EC and CA3. In this neural network model CA1 output was regulated by cholinergic activity and the model was tests in a non-spatial context of simple low-dimensional pattern learning. Barry et al. (2012b) studied the effects of cholinergic modulation on regulating theta rhythm in grid cells.

In our model aging is simulated by reduced cholinergic activity, resulting in a preferential recall of previously stored environment representation instead of encoding of a new one. A number of theoretical accounts of aging suggested that age-related synaptic loss in DG/CA3 together with age-induced augmentation of auto-associative dynamics in CA3 give rise to an impairment of DG-mediated pattern separation and excessive pattern completion, respectively (Wilson et al., 2005b, 2006; Yassa et al., 2011; Thomé et al., 2016). Our results (Fig. 5.4) propose a different explanation of the age-related impairment of spatial

learning in a novel environment. In our model, the reduction of cholinergic modulation biases the entorhinal-hippocampal loop processing from the learning state to a recall state. The recalled spatial representation, retrieved based on the back-projected signal from CA1 to grid cells, leads to a recall-induced reset of grid-cell population activity. The reset of grid-cell activities in turn leads to a partial reinstallment of recalled place cell representation in CA3 (MPCs) and CA1 (CPCs) and the absence of global remapping. As a subset of place cells in our model is based purely on vision (VPCs), their firing fields express global remapping also in the aged model, predicting that vision-based place cells will be affected by aging to a smaller degree than self-motion based. Recent data suggests the existence of place cells differentially sensitive to these two cue types (Chen et al., 2013, 2019; Fattahi et al., 2018).

The associative recall of spatial information in our model occurs within the EC based on spatial input from CA1 in agreement with past studies linking recollection of with CA1-EC-cortex projection (Naber et al., 2001; Kloosterman et al., 2003; Slomianka et al., 2011; Suzuki and Naya, 2011; Goshen et al., 2011). More specifically, CPCs input provides information about currently active spatial position code to the grid-cell population, while realignment of grid fields according to this position signal performs the recall of grid cell population activity. This activity in turn leads to the recall of associated visual input by the AVI cells. As suggested by our model in Chapter 3, the parieto-retrosplenial network can be the biological locus of an allocentric visual representation encoded by AVI cells in the present model. In agreement with the cholinergic accounts of novelty processing (Giovannini et al., 1998; Miranda et al., 2000; Giovannini et al., 2001; Ranganath and Rainer, 2003), ACh release in our model is controlled by the error resulting from a comparison between the recalled information and the actual sensory input. In various behavioral tasks, such an error (or novelty) signal can drive learning by adjusting synaptic weights in the hippocampus so to minimize the error (O'Reilly and Rudy, 2000). In our model, the feedback error signals (LE and ME, Eqs. 5.2.23) are used to regulate the dynamics of entorhinal-hippocampal loop and control the balance idiothetic and allothetic cues.

As our simulations suggest (Section 5.3.2), age-related decrease in cholinergic modula-

tion causes a delay in the transition between self-motion-based and vision-based spatial representations. In particular, acetylcholine release, controlled by the visual error/novelty signal (LE), is proposed to dynamically regulate the relative strength of visual input with respect to self-motion one. A high level of acetylcholine release corresponds to a highly novel visual stimulus, so that CPCs are biased to integrate more visual cues in a larger proportion relative to self-motion cues. As a result of age-related reduction of cholinergic modulation, CPCs in the aged model receive less visual information so that the transition of the spatial representation is delayed in simulated aged animals. The separation between self-motion-based and vision-based behavior is just one example of strategies used by animals for navigation (Barnes et al., 1980; Nicolle et al., 2003; Rosenzweig et al., 2003; Schuck et al., 2013; Bécu et al., 2019). Experimental studies in rodents and humans suggested a particular strong effect of age in switching from egocentric to an allocentric strategy (Harris and Wolbers, 2014) and from self-motion to vision (Rosenzweig et al., 2003). Our modeling results suggest that the bias towards self-motion-based egocentric strategies is causes by impaired novelty processing in the hippocampus, which manifests itself in a reduced cholinergic signal.

In summary, this work described a computation model of how spatial information processing in the entorhinal-hippocampal loop can be self-regulated by computing the sensory errors in the from of neural novelty signals. The neuromodulator acetylcholine is proposed to mediate the novelty signalling and balance hippocampal processing state between learning and recall, leading to the expression of egocentric and allocentric strategies. Age-related impairment of novelty processing leads, via reduced cholinergic signal, to strategy switching deficits. It is proposed that the novelty signal reflects the difference between a stored and a current sensory information and is important for spatial behaviour, as it can gradually tune spatial memory networks based on the memory demands of the current task.

Chapter 6

General discussion

6.1 Thesis summary and conclusions

The main motivation for this thesis was the development of an integrated computational model of human visuospatial cognition providing a simulation platform for studying age-related spatial memory deficits. The modeling work presented here focused on several important issues towards this objective. In particular, I studied neural mechanisms underlying the integration of visual and self-motion cues important for the formation of a mental environment representation and proposed how age-related neurobiological alterations may affect this process. The main methodological approach adopted in this work consisted in computer simulations of biological neural networks aimed at reproducing key experimental results in primates and rodents. Computational modeling of animal data on both behavioral and neural levels and formulation of model-based experimental predictions has proven an effective way to advance the understanding of biological processes underlying cognitive phenomena.

In Chapter 2, I reviewed available anatomical and physiological data in primates and rodents by focusing on the neural-level studies of the role of vision, spatial memory and aging in navigation behaviour. These data provide the basis and delimit the constraints of the modeling work in subsequent chapters. In addition we have presented the architecture of our neural simulation platform – Aging Human Avatar – that was conceived as a

proof-of-concept for future human avatar applications.

Chapter 3 described a spiking neural network implementation of the dorsal visual pathway implicated in scene processing and a transformation between egocentric visual representations to allocentric spatial memories. We have shown that neurocomputational properties of the simulated dorsal visual pathway network, including gain modulation by head direction and existence of head-fixed as well as world-fixed visual representations in the parietal-medial temporal circuit correspond to available experimental evidence from these structures. We then proposed the existence of a panoramic representation of the surrounding visual space in topographic visual coordinates that can serve as a proxy between visual and mnemonic brain areas instrumental for reorientation and planning of eye movements. Further, our modeling results linked visual and memory-related neural activities in the associated brain areas and suggested a novel interpretation of general novelty signals observed in the hippocampus in response to the presentation of visual stimuli. Finally, we outlined a neural architecture of a reorientation network that is proposed to perform correction of head direction based on view-based egocentric activities, and we have suggested how the existence of such a network in the brain manifests itself in behavioral tasks such as spatial reorientation and memory-based visual search.

Chapter 4 presented a neural-level model of spatial information processing in the entorhinal-hippocampal, focused on the bidirectional interactions between hippocampal place cells and entorhinal grid cell during learning of multi-compartment environments. We proposed a novel role for biological place cells that are exclusively driven by visual input: in our model they express properties that are different from place cells combining visual and self-motion cues in that they are not affected by progressive integration of the latter into spatial representation. We propose that these vision-based place cells progressively bias spatial processing in the hippocampal loop towards positions signalled by external sensory cues. We further proposed that the strength of the hippocampal input to the entorhinal cortex plays a critical role in governing the balance between idiothetic and allothetic cues. We have shown that when these cue types provide conflicting information about spatial location, as it occurs in multi-compartment environment with a high degree of visual aliasing, the correct balance between neural integration of these cues play a key role in

efficient construction of the environment representation.

Finally, in Chapter 5, spatial learning impairments caused by aging were studied in the framework of the entorhinal-hippocampal circuit model. Motivated by the evidence relating age-related cholinergic decrease and synaptic plasticity deficits in the hippocampal networks we proposed that acetylcholine balances the interplay between idiothetic and allothetic cues. The acetylcholine release is in turn modulated by novelty, implemented by computing the sensory error between the stored and actual states of the entorhinal attractor network and between the actual and stored visual inputs. Age-related decreases in the cholinergic signal lead to impaired novelty processing, in turn biasing spatial processing towards idiothetic cues and a recall of previously stored information, at the expense of inefficient learning of novel spatial stimuli. By simulating neurophysiological data from experiments in aged rodents, we have shown how such an age-related effect leads to an impaired spatial learning during exploration of a novel environment and to a preferential reliance in idiothetic cues during spatial navigation.

Overall, this thesis contributes to further understanding of the role of vision, self-motion and aging during spatial navigation and of the neural mechanisms governing the creation of cognitive maps. In subsequent sections I provide further details about specific contributions of our work that go beyond current state-of-the-art models of spatial orientation and propose principal directions of future work.

6.2 Contributions of the thesis and related work

One of the main contributions of the thesis, the model the dorsal visual path, builds on previous accounts of the involvement of parietal networks in coordinate transformations (Zipser and Andersen, 1988; Deneve et al., 2001; Pouget et al., 2002). The previous models have shown how the coordinate of a point-like stimulus, whose position was observed in a retinal frame of reference, can be converted to the head-fixed coordinates of the position of the stimulus is encoded by a population of cells with Gaussian tuning functions. Byrne et al., 2007 (see also Becker and Burgess, 2001) presented a rate-based model of coordinate conversion between egocentric information about distances to environmental boundaries an allocentric representation by so-called boundary-vector cells,

that in turn drive location-sensitive hippocampal neurons. In contrast to these models, our proposed network transforms the full-field visual stream in topographic visual coordinates into an allocentric world-fixed reference frame using spiking neurons. Moreover, our model is designed to work with limited visual fields, similar to that in primates, whereas previous models were tuned to rodent panoramic view. A smaller visual fields limit the amount of spatial information accessible to the system at any moment in time and reduce the sensitivity to scene-like processing and environmental geometry. This limitation is proposed to be overcome by a short-term synaptic memory mechanisms linking successive views in a single allocentric representation of surrounding visual space.

We proposed that spatial reorientation is performed by a network organized similarly to head-direction network and which is driven by the input from hippocampal place cells. This reorientation network is proposed to be active all the time and (subconsciously) correct orientation errors based on the comparison between memorized and actual spatial information. Previous models proposed view matching accounts of reorientation that either matched the current view with a single view of the desired goal location (Cheung et al., 2008) or implemented the memory-based view matching algorithmically (Sheynikhovich et al., 2009). Our results also provided an indication of how the reorientation network may affect behavior in spatial and non-spatial tasks.

An important novel property of our model of the entorhinal-hippocampal circuit is that grid cells and place cells continuously and dynamically interact with each other during spatial behavior. It is thus different from existing models based on the feed-forward input from grid cells to place cells (Solstad et al., 2006; O'Keefe and Burgess, 2005; Blair et al., 2008; Sheynikhovich et al., 2009; Pilly and Grossberg, 2012) and based on feed-forward input from place cells to grid cells (Bonnevie et al., 2013). In these earlier models, the role of the hippocampal input was only to reset the path integrator upon the entry to a novel environment and or to provide unspecific excitation to grid cells, in contrast to continuous dynamic mutual interaction between self-motion and vision in our model. These previous models are also at difficulty in explaining multi-sensory integration data as observed by grid- and place-cell recordings in multi-compartment environments. One previous computational study suggested how the interaction between place cells and grid

cells give rise to spatial remapping in a morphed environment (Rennó-Costa and Tort, 2017). Our model suggested in addition that in order to create a spatial representation of a novel environment, the hippocampal input to entorhinal cortex should decrease, reducing the impact of previously memorized representations. A second novel proposal related to our entorhinal-hippocampal circuit model is that the main locus of the neural mechanism combining idiothetic and allothetic cues has been shifted from the CA3 area of the hippocampus to the attractor network of the entorhinal cortex in our model. It thus provides a novel view on multisensory integration in the hippocampus, that is different from a long-standing idea that such integration is performed by the CA3 attractor network (McNaughton et al., 1996; Samsonovich and McNaughton, 1997).

We propose that CA1 plays an important role in memory retrieval via its feedback projection to EC. It is different from previous proposals stating that the role of CA1 is pattern comparison between EC and CA3 inputs (Hasselmo and Schnell, 1994). One potential problem of their theory is that EC and CA3 inputs to CA1 can not be compared directly, because CA3 projections transform the EC input via sparse coding in DG and pattern completion in CA3 (Yassa and Stark, 2011). Thus, it is not clear how such different representations can be compared by the CA1 circuit. In terms of spatial memory in CA1, it is also not clear how multi-sensory information in the EC can be compared with spatial representation in CA3. In our model, we suggested that CA1 represents the position code and that the feedback projection from CA1 to EC serves to recall the information in the EC by retrieving the previous encoded memory of that position. Our suggestion thus goes in line with studies suggesting that memory recall is evoked in CA1 via its projection to the EC and to the neocortex (Naber et al., 2001; Kloosterman et al., 2003; Slomianka et al., 2011; Suzuki and Naya, 2011; Goshen et al., 2011; Bartsch et al., 2011). The recalled EC can then be directly compared with current EC activity to provide an error/novelty signal.

Our model of age-related decrease of cholinergic release was motivated by neurophysiological studies demonstrating the role of this neuromodulator for hippocampal processing (Shen and Barnes, 1996; Wilson et al., 2006; Sava and Markus, 2008; Schliebs and Arendt, 2011). No previous models, to our knowledge, have addressed this question. The idea

that cholinergic release switches the hippocampal processing between encoding and recall was proposed by Hasselmo and Schnell (1994), but their model of this process was tested on a small number of low-dimensional patterns. We extended this model and linked the encoding/recall cycles of hippocampal processing to cholinergically-modulated idiothetic/allothetic cue switches during spatial behavior. Our proposal that age-related cholinergic bias towards recall is mediated by the CA1 projection to the EC provides a neurocomputational account of the role of aging in the hippocampal formation that is different from previous proposals. A number of previous theoretical and experimental studies suggested that aging effect on spatial navigation is caused by pattern separation impairment and excessive pattern completion in DG/CA3 (Wilson et al., 2005b, 2006; Yassa et al., 2011; Thomé et al., 2016). While our results do not exclude the involvement of DG-CA3 circuit in age-related deficits, we show that it is possible to simulate the key experimental data without it.

6.3 Experimental predictions

From our results in Chapter 3 we predict the existence of a panoramic representation in visually topographic coordinates in the parieto-retrosplenial network, which is likely to be stored in a world-fixed directional reference frame (see e.g. Robertson et al., 2016 for related data). This representation is further predicted to be necessary for directing eye movement outside of the current visual field. Moreover, we also predict that reorientation of head direction in reorientation experiments in empty rooms with geometrically polarized layout require an intact hippocampus. We hypothesize that a network organized similarly to the retrosplenial head-direction circuit encodes the reorientation error. For instance, Jacob et al. (2017) observed retrosplenial head-direction-like cells that have a doubly-peaked activity in symmetric environments, going in line with our hypothesis. Further, we predict slight but reliable changes in head direction cells in purely visual tasks in which, unexpectedly by the observer, a portion of visual features has been displaced, as in the experiment by Fiehler et al. (2014).

From our results in Chapter 4, we predict that place cells that are purely driven by external cues (Chen et al., 2013), potentially located in the deep sublayer of CA1 pyramidal layer

(Fattahi et al., 2018), have a number of properties different from other place cells, in particular those that rely on self-motion information. These vision-based place cells are predicted (i) to be unaffected by learning; and (ii) to possess repetitive place fields in spatially separated but identically oriented and otherwise similarly-looking rooms, even when a global representation has been established to distinguish between the rooms. Moreover, our results predict that the remapping of place cells close to the entry to a room (see Carpenter et al., 2015) should occur faster than for the cells far from the entrance, since the largest mismatch between the visual and self-motion representations occurs near the entrance. Finally, we predict that the mismatch between the visual and self-motion cues, as measured by the correlation between grid cells (see e.g. Fig. 4.6D) should be larger in animals who rely stronger on self-motion, as a result of training as as a natural consequence of aging. As experimental data (Tanila, 1999; Rosenzweig et al., 2003) and our simulations suggest, these animals are biased towards the use of self-motion cues.

Lastly, from our results in Chapter 5, we predict that intact CA1 and EC with potentially other *output* structures are sufficient for recall (Zeineh et al., 2003). This prediction is in line with the studies suggesting that CA1 plays an important role during memory retrieval (Rolls, 1996; Naber et al., 2001; Goshen et al., 2011). Another prediction is that age should be correlated both with novelty processing and with the reduce in cholinergic release within the same animal, as our model suggests. The final prediction from our results from Chapters 4 and 5 is that in aged rats, in conditions of the experiments of Wilson et al. (2005b) and Rosenzweig et al. (2003), only a subset of CA3 cells that project to deep sublayer of CA1 should remap or be progressively corrected by vision. Vision-based place cells should not be affected according to our proposal of the differential role of these cells in spatial memory.

6.4 Limitations and future work

Future efforts will be required to make the Aging Human Avatar platform in its current implementation to be a valuable tool for simulating visuospatial human behavior. Currently, the detailed model of the retina (Huth et al., 2018) can be linked directly to the spatial

memory module (not described in the present work). Additional work will be required to link the cerebellar model of vestibular-ocular reflex (Luque et al., 2019; Naveros et al., 2019) with the vision- and self-motion-based integrated model of spatial memory. Integration of eye movements is a long-term future objective. Together, integration of these modules within the Avatar platform are expected to provide a promising tool for visuospatial behavior simulation in realistic environments, modeled with the 3D environment simulator of the Avatar platform.

In terms of constituent networks of visual and spatial memory network, several potential improvements can be of use. Visual information delivered to the model uses a full-field visual stream and is thus sensitive to geometric and distal visual, but landmarks do not have special meaning in the model. Landmarks have been shown to be important for navigation in both rodents and primates (Wilber et al., 2014; Harris and Wolbers, 2014). Several computational models have addressed the role of landmarks for spatial memory and can be included in the model (Bicanski and Burgess, 2016, 2018). An adaptive integration theory is proposed to determine the weight of different cues while these cues are combined (Cheng et al., 2013). This improvements will permit reorientation based on different available cues according to their spatial information content.

Our current theoretical framework lacks the dentate gyrus, proposed to mediate pattern separation in the hippocampal network (de Almeida et al., 2009a,b) and CA3. Pattern separation reduces interference between similar visual input coming from the EC and increases spareness of neural activity (Leutgeb et al., 2007; Yassa et al., 2011). Classical view of CA3 is that it acts as and auto-associative network for pattern completion (Hunsaker and Kesner, 2013), but recent studies question this view as CA3 inherits integrated spatial information from EC (Colgin et al., 2010). The exact role of CA3 in hippocampal processing, and in particular its role in trajectory generation (Colgin et al., 2010) is an important question for future work.

Our model suggested an explanation for the age-related impairment of learning a novel environment, but it does not explain why aged animals can learn a novel spatial representation after a repeated presentation to the same novel environment (Wilson et al., 2004). In our model, once a spatial representation is created, it will be maintained in memory. The

future work should address the question of forgetting and relearning, related to the question memory maintenance and consolidation and the effect of age on these processes (Foster, 1999). In particular, in our current framework, the error/novelty signal originating from EC is used to fine tune the strength of recall in the EC and adjust the relative strength of self-motion and visual input. This error signal can also serve other purposes, for example for fine tuning the synapses along the trisynaptic circuit. Such an error back-propagation signal can affect spatial memory in a task-related manner (O'Reilly and Rudy, 2000). Since feedback error learning is long-term learning with a very low learning rate, it might explain aged animals progressively learn novel environments, even if they are strongly biased to the recollection of previously visited ones.

Appendix A

List of contributions

List of contributions

Papers

Tianyi Li, Angelo Arleo and Denis Sheynikhovich *(submitted)*. A model of panoramic visual representation in the dorsal visual pathway: the case of spatial reorientation and memory-based search. *eLife*.

Tianyi Li, Angelo Arleo and Denis Sheynikhovich *(2020)*. Modeling place cells and grid cells in multi-compartment environments: entorhinal-hippocampal loop as a multisensory integration circuit. *Neural Networks*, 121:37-51.

Tianyi Li, Angelo Arleo and Denis Sheynikhovich *(in preparation)*. Impact of Aging on the Entorhinal-Hippocampal Network.

Patent

Sheynikhovich, D., Carrillo, R., Bologna, L. L., Cherifi, Y., **Li, T.**, Arleo, A., Baranton, K., Scherlen, A.-C., and Tranvouez-Bernardin, D. (2019). Device for simulating a physiological behaviour of a mammal using a virtual mammal, process and computer program. Eur. Pat. Off., Patent App(n°EP19305363.4):March 22.

Oral Presentations

Tianyi Li, Angelo Arleo and Denis Sheynikhovich (2018). Bidirectional interactions between place-cells and grid-cells in the vision- and self-motion driven spatial representation model. Oral presentation at Spatial Cognition 2018, Tübingen, Germany.

Poster presentations

Tianyi Li, Angelo Arleo and Denis Sheynikhovich (2017) Coordinate-transformation spiking neural network for spatial navigation. In HBP 2017: Collaborative and Integrative Modeling of Hippocampus, Paris, France.

Tianyi Li, Angelo Arleo and Denis Sheynikhovich (2017) Coordinate-transformation spiking neural network for spatial navigation. In 3e Symposium des Neurosciences Computationnelles de l'UPMC, Paris, France.

Tianyi Li, Angelo Arleo and Denis Sheynikhovich (2017) Coordinate-transformation spiking neural network for spatial navigation. In 26th Annual Computational Neuroscience Meeting (CNS2017), vol. 18 (Suppl), pages P239, BMC Neuroscience 18 (Suppl), Antwerp, Belgium.

Tianyi Li, Angelo Arleo and Denis Sheynikhovich (2018) Bidirectional interactions between place-cells and grid-cells in the vision- and self-motion driven spatial representation model. In 11th FENS Forum of Neuroscience, Berlin, Germany.

Tianyi Li, Angelo Arleo and Denis Sheynikhovich (2018) Bidirectional interactions between place-cells and grid-cells in the vision- and self-motion driven spatial representation model. In Spatial Cognition 2018, Tübingen, Germany.

Tianyi Li, Angelo Arleo and Denis Sheynikhovich (2018) Loop-like bidirectional interactions between place-cells and grid-cells in a vision- and self-motion driven spatial representation model. In Neuralnet2018 - Understanding neural networks: from dynamics to functions, Paris, France.

Bibliography

Abdulrahman, H., Fletcher, P. C., Bullmore, E., and Morcom, A. M. (2017). Dopamine and memory dedifferentiation in aging. *Neuroimage*, 153:211–220.

Acquas, E., Wilson, C., and Fibiger, H. C. (1996). Conditioned and unconditioned stimuli increase frontal cortical and hippocampal acetylcholine release: effects of novelty, habituation, and fear. *J. Neurosci.*, 16(9):3089–96.

Agster, K. L. and Burwell, R. D. (2009). Cortical efferents of the perirhinal, postrhinal, and entorhinal cortices of the rat. *Hippocampus*, 19(12):1159–1186.

Amaral, D. G., Dolorfo, C., and Alvarez-Royo, P. (1991). Organization of Ca1 projections to the subiculum: a PHA-L analysis in the rat. *Hippocampus*, 1:415–435.

Amaral, D. G. and Witter, M. P. (1989). The three-dimensional organization of the hippocampal formation: A review of anatomical data. *Neuroscience*, 31(3):571–591.

Amaral, D. G. and Witter, M. P. (1995). Hippocampal formation. In Paxinos, G., editor, *The Rat Nervous System*, chapter 21, pages 443–493. Academic Press, second edition.

Andersen, P., Morris, R., Amaral, D., Bliss, T., and O'Keefe, J. (2006). *The Hippocampus Book*. Oxford Neuroscience Series. Oxford University Press, USA.

Andersen, R., Snyder, L. H. L., Li, C.-S. C., and Stricanne, B. (1993). Coordinate transformations in the representation of spatial information. *Curr. Opin. Neurobiol.*, 3:171–176.

Arleo, A. and Rondi-Reig, L. (2007). Multimodal sensory integration and concurrent navigation strategies for spatial cognition in real and artificial organisms. *J Integr Neurosci*, 6(3):327–366.

Aronov, D. and Tank, D. W. (2014). Engagement of Neural Circuits Underlying 2D Spatial Navigation in a Rodent Virtual Reality System. *Neuron*, 84(2):442–456.

Avillac, M., Denève, S., Olivier, E., Pouget, A., and Duhamel, J.-R. (2005). Reference frames for representing visual and tactile locations in parietal cortex. *Nat. Neurosci.*, 8(7):941–9.

Bachevalier, J., Nemanic, S., and Alvarado, M. C. (2015). The influence of context on recognition memory in monkeys: Effects of hippocampal, parahippocampal and perirhinal lesions. *Behav. Brain Res.*, 285:89–98.

Barnes, C. A., Nadel, L., and Honig, W. K. (1980). Spatial memory deficit in senescent rats. *Canadian journal of psychology*, 34 1:29–39.

Barnes, C. A., Suster, M. S., Shen, J., and McNaughton, B. L. (1997). Multistability of cognitive maps in the hippocampus of old rats. *Nature*, 388(6639):272–275.

Barry, C., Ginzberg, L. L., O'Keefe, J., and Burgess, N. (2012a). Grid cell firing patterns signal environmental novelty by expansion. *Proc. Natl. Acad. Sci. U. S. A.*, 109(43):17687–92.

Barry, C., Heys, J. G., and Hasselmo, M. E. (2012b). Possible role of acetylcholine in regulating spatial novelty effects on theta rhythm and grid cells. *Front. Neural Circuits*, 6(FEBRUARY):5.

Bartsch, T., Döhring, J., Rohr, A., Jansen, O., and Deuschl, G. (2011). CA1 neurons in the human hippocampus are critical for autobiographical memory, mental time travel, and autonoetic consciousness. *Proceedings of the National Academy of Sciences of the United States of America*, 108(42):17562–17567.

Bartunov, S., Santoro, A., Richards, B., Marris, L., Hinton, G. E., and Lillicrap, T. (2018). Assessing the Scalability of Biologically-Motivated Deep Learning Algorithms and Architectures. In S, B., Wallach, H., Larochelle, H., Grauman, K., Cesa-Bianchi, N., and Garnett, R., editors, *Adv. Neural Inf. Process. Syst. 31*, pages 9368–9378.

Becker, S. and Burgess, N. (2001). Modelling spatial recall, mental imagery and neglect. *Adv. Neural Inf. Process. Syst.*, 13.

Bécu, M., Sheynikhovich, D., Tatur, G., Agathos, C., Bologna, L. L., Sahel, J.-A., and Arleo, A. (2019). Age-related preference for geometric spatial cues during real-world navigation. *Nat. Hum. Behav.*, page In press.

Bicanski, A. and Burgess, N. (2016). Environmental Anchoring of Head Direction in a Computational Model of Retrosplenial Cortex. *J. Neurosci.*, 36(46):11601–11618.

Bicanski, A. and Burgess, N. (2018). A neural-level model of spatial memory and imagery. *Elife*, 7(7052):e33752.

Blair, H. T., Gupta, K., and Zhang, K. (2008). Conversion of a phase- to a rate-coded position signal by a three-stage model of theta cells, grid cells, and place cells. *Hippocampus*, 18(12):1239–1255.

Bonnevie, T., Dunn, B., Fyhn, M., Hafting, T., Derdikman, D., Kubie, J. L., Roudi, Y., Moser, E. I., and Moser, M.-B. (2013). Grid cells require excitatory drive from the hippocampus. *Nat. Neurosci.*, 16(3):309–317.

Bousquet, O., Balakrishnan, K., and Honavar, V. (1997). Is the Hippocampus a Kalman Filter? *Comput. Sci. Tech. Reports*, page Paper 19.

Boussaoud, D., Ungerleider, L. G., and Desimone, R. (1990). Pathways for motion analysis: Cortical connections of the medial superior temporal and fundus of the superior temporal visual areas in the macaque. *J. Comp. Neurol.*, 296(3):462–495.

Brandner, C. and Schenk, F. (1998). Septal lesions impair the acquisition of a cued place navigation task: Attentional or memory deficit? *Neurobiology of Learning and Memory*, 69(2):106–125.

Brandon, M. P., Koenig, J., Leutgeb, J. K., and Leutgeb, S. (2014). New and Distinct Hippocampal Place Codes Are Generated in a New Environment during Septal Inactivation. *Neuron*, 82(4):789–796.

Brandt, S. A. and Stark, L. W. (1997). Spontaneous Eye Movements During Visual Imagery Reflect the Content of the Visual Scene. *J. Cogn. Neurosci.*, 9(1):27–38.

Brodbeck, D. R. and Tanninen, S. E. (2012). *Place Learning and Spatial Navigation*, pages 2639–2641. Springer US, Boston, MA.

Brotchie, P. R., Andersen, R. A., Snyder, L. H., and Goodman, S. J. (1995). Head position signals used by parietal neurons to encode locations of visual stimuli. *Nature*, 375(6528):232–235.

Brun, V. H., Leutgeb, S., Wu, H.-Q., Schwarcz, R., Witter, M. P., Moser, E. I., and Moser, M.-B. (2008a). Impaired Spatial Representation in CA1 after Lesion of Direct Input from Entorhinal Cortex. *Neuron*, 57(2):290–302.

Brun, V. H., Otnaess, M. K., S., M., Steffenach, H.-A., Witter, M. P., Moser, M.-B., and Moser, E. I. (2002). Place Cells and Place Recognition Maintained by Direct Entorhinal-Hippocampal Circuitry. *Science*, 296(5576):2243–2246.

Brun, V. H., Solstad, T., Kjelstrup, K. B., Fyhn, M., Witter, M. P., Moser, E. I., and Moser, M.-B. (2008b). Progressive increase in grid scale from dorsal to ventral medial entorhinal cortex. *Hippocampus*, 18(12):1200–1212.

Burak, Y. and Fiete, I. R. (2009). Accurate path integration in continuous attractor network models of grid cells. *PLoS Comput. Biol.*, 5(2):e1000291.

Burgess, N. (2006). Spatial memory: how egocentric and allocentric combine. *Trends Cogn. Sci.*, 10(12):551–557.

Burgess, N. (2008). Spatial cognition and the brain. *Ann. N. Y. Acad. Sci.*, 1124:77–97.

Burgess, N. (2014). The 2014 Nobel Prize in Physiology or Medicine: A Spatial Model for Cognitive Neuroscience. *Neuron*, 84(6):1120–1125.

Burgess, N., Jeffery, K. J., and O'Keefe, J. (1999). Integrating hippocampal and parietal functions: a spatial point of view. In N. Burgess, K. J. J. and O'Keefe, J., editors, *The Hippocampal and Parietal Foundations of Spatial Cognition*, chapter 1, pages 3–29. Oxford University Press.

Burgess, N., Recce, M., and O'Keefe, J. (1994). A model of hippocampal function. *Neural Networks*, 7:1065–1081.

Burke, S. N. and Barnes, C. A. (2006). Neural plasticity in the ageing brain. *Nat. Rev. Neurosci.*, 7(1):30–40.

Burwell, R. D. and Amaral, D. G. (1998). Cortical afferents of the perirhinal, postrhinal, and entorhinal cortices of the rat. *J Comp Neurol*, 398(2):179–205.

Busch, N. A. and VanRullen, R. (2010). Spontaneous EEG oscillations reveal periodic sampling of visual attention. *Proc. Natl. Acad. Sci. U. S. A.*, 107(37):16048–53.

Buzsáki, G. (1984). Feed-forward inhibition in the hippocampal formation. *Progress in Neurobiology*, 22:131–153.

Buzsáki, G. (2002). Theta oscillations in the hippocampus. *Neuron*, 33(3):325–340.

Byrne, P. and Becker, S. (2008). A principle for learning egocentric-allocentric transformation. *Neural Comput.*, 20(3):709–37.

Byrne, P., Becker, S., and Burgess, N. (2007). Remembering the past and imagining the future: A neural model of spatial memory and imagery. *Psychol. Rev.*, 114(2):340–375.

Carpenter, F., Burgess, N., and Barry, C. (2017). Modulating medial septal cholinergic activity reduces medial entorhinal theta frequency without affecting speed or grid coding. *Sci. Rep.*, 7(1):14573.

Carpenter, F., Manson, D., Jeffery, K., Burgess, N., and Barry, C. (2015). Grid Cells Form a Global Representation of Connected Environments. *Curr. Biol.*, 25(9):1176–1182.

Cavada, C. and Goldman-Rakic, P. S. (1989). Posterior parietal cortex in rhesus monkey: I. Parcellation of areas based on distinctive limbic and sensory corticocortical connections. *J. Comp. Neurol.*, 287(4):393–421.

Ceruti, C., Bassis, S., Rozza, A., Lombardi, G., Casiraghi, E., and Campadelli, P. (2014). DANCo: An intrinsic dimensionality estimator exploiting angle and norm concentration. *Pattern Recognit.*, 47(8):2569–2581.

Chafee, M. V., Averbeck, B. B., and Crowe, D. A. (2007). Representing Spatial Relationships in Posterior Parietal Cortex: Single Neurons Code Object-Referenced Position. *Cereb. Cortex*, 17(12):2914–2932.

Chen, G., King, J. A., Burgess, N., and O'Keefe, J. (2013). How vision and movement combine in the hippocampal place code. *Proc. Natl. Acad. Sci.*, 110(1):378–383.

Chen, G., Lu, Y., King, J. A., Cacucci, F., and Burgess, N. (2019). Differential influences of environment and self-motion on place and grid cell firing. *Nat. Commun.*, 10(1):630.

Chen, Y., Byrne, P., and Crawford, J. D. (2011). Time course of allocentric decay, egocentric decay, and allocentric-to-egocentric conversion in memory-guided reach. *Neuropsychologia*, 49(1):49–60.

Cheng, K. (1986). A purely geometric module in the rat's spatial representation. *Cognition*, 23(2):149–178.

Cheng, K. and Gallistel, C. R. (2005). Shape parameters explain data from spatial transformations: comment on Pearce et al. (2004) and Tommasi & Polli (2004). *J Exp Psychol Anim Behav Process*, 31(2):254–9; discussion 260–1.

Cheng, K., Huttenlocher, J., and Newcombe, N. S. (2013). 25 years of research on the use of geometry in spatial reorientation: A current theoretical perspective. *Psychon. Bull. Rev.*, 20(6):1033–1054.

Cheng, K. and Newcombe, N. S. (2005). Is there a geometric module for spatial orientation? Squaring theory and evidence. *Psychon. Bull. Rev.*, 12(1):1–23.

Cheng, S. and Frank, L. (2011). The structure of networks that produce the transformation from grid cells to place cells. *Neuroscience*, 197:293–306.

Cheung, A., Stürzl, W., Zeil, J., and Cheng, K. (2008). The Information Content of Panoramic Images II: The Rotational Errors and the Similarity of Views in Rectangular Experimental Arenas. *J. Exp. Psychol. Anim. Behav. Process.*, 34(1):15–30.

Cho, J. and Sharp, P. E. (2001). Head direction, place, and movement correlates for cells in the rat retrosplenial cortex. *Behav. Neurosci.*, 115(1):3–25.

Christou, C. G. and Bülthoff, H. H. (1999). View dependence in scene recognition after active learning. *Mem. Cognit.*, 27(6):996–1007.

Chrobak, J. J. and Buzsáki, G. (1996). High-frequency oscillations in the output networks

of the hippocampal-entorhinal axis of the freely moving rat. *Journal of Neuroscience*, 16(9):3056–3066.

Chrobak, J. J., Lörincz, A., and Buzsáki, G. (2000). Physiological patterns in the hippocampo-entorhinal cortex system. *Hippocampus*, 10:457–465.

Ciaroni, S., Cuppini, R., Cecchini, T., Ferri, P., Ambrogini, P., Cuppini, C., and Del Grande, P. (1999). Neurogenesis in the adult rat dentate gyrus is enhanced by vitamin e deficiency. *J Comp Neurol*, 411(3):495–502.

Claiborne, B. J., Amaral, D. G., and Cowan, W. M. (1986). A light and electron microscopic analysis of the mossy fibers of the rat dentate gyrus. *J Comp Neurol*, 246(4):435–58.

Colgin, L. L., Denninger, T., Fyhn, M., Hafting, T., Bonnevie, T., Jensen, O., Moser, M.-B., and Moser, E. I. (2009). Frequency of gamma oscillations routes flow of information in the hippocampus. *Nature*, 462(7271):353–357.

Colgin, L. L., Leutgeb, S., Jezek, K., Leutgeb, J. K., Moser, E. I., McNaughton, B. L., and Moser, M.-B. (2010). Attractor-Map Versus Autoassociation Based Attractor Dynamics in the Hippocampal Network. *J. Neurophysiol.*, 104(1):35–50.

Constantinidis, C. and Steinmetz, M. A. (1996). Neuronal activity in posterior parietal area 7a during the delay periods of a spatial memory task. *J. Neurophysiol.*, 76(2):1352–5.

Cox, B. and Krichmar, J. (2009). Neuromodulation as a robot controller. *IEEE Robot. Autom. Mag.*, 16(3):72–80.

Cressant, A., Muller, R. U., and Poucet, B. (1997). Failure of centrally placed objects to control firing fields of hippocampal place cells. *Journal of Neuroscience*, 17(7):2531–2542.

Cressant, A., Muller, R. U., and Poucet, B. (1999). Further study of the control of place cell firing by intra-apparatus objects. *Hippocampus*, 9:423–431.

Crutcher, M. D., Calhoun-Haney, R., Manzanares, C. M., Lah, J. J., Levey, A. I., and Zola, S. M. (2009). Eye Tracking During a Visual Paired Comparison Task as a Predictor of Early Dementia. *Am. J. Alzheimer's Dis. Other Dementiasr*, 24(3):258–266.

Csicsvari, J., Jamieson, B., Wise, K., and Buzsáki, G. (2003). Mechanisms of gamma oscillations in the hippocampus of the behaving rat. *Neuron*, 37(2):311–322.

da Silva, F. H. L., Witter, M. P., Boeijinga, P. H., and Lohman, A. H. M. (1990). Anatomical organization and physiology of the limbic cortex. *Physiological Reviews*, 70:453–511.

de Almeida, L., Idiart, M., and Lisman, J. E. (2009a). A Second Function of Gamma Frequency Oscillations: An E%-Max Winner-Take-All Mechanism Selects Which Cells Fire. *J. Neurosci.*, 29(23):7497–7503.

de Almeida, L., Idiart, M., and Lisman, J. E. (2009b). The Input-Output Transformation of the Hippocampal Granule Cells: From Grid Cells to Place Fields. *J. Neurosci.*, 29(23):7504–7512.

Deneve, S., Latham, P. E., and Pouget, A. (2001). Efficient computation and cue integration with noisy population codes. *Nat. Neurosci.*, 4(8):826–831.

Ding, S.-L., Van Hoesen, G., and Rockland, K. S. (2000). Inferior parietal lobule projections to the presubiculum and neighboring ventromedial temporal cortical areas. *J. Comp. Neurol.*, 425(4):510–530.

Diwadkar, V. A. and McNamara, T. P. (1997). Viewpoint Dependence in Scene Recognition. *Psychol. Sci.*, 8(4):302–307.

Duhamel, J. R., Bremmer, F., Ben Hamed, S., and Graf, W. (1997). Spatial invariance of visual receptive fields in parietal cortex neurons. *Nature*, 389(6653):845–8.

Durstewitz, D., Seamans, J. K., and Sejnowski, T. J. (2000). Dopamine-Mediated Stabilization of Delay-Period Activity in a Network Model of Prefrontal Cortex. *J. Neurophysiol.*, 83(3):1733–1750.

Eichenbaum, H., Yonelinas, A., and Ranganath, C. (2007). The Medial Temporal Lobe and Recognition Memory. *Annu. Rev. Neurosci.*, 30(1):123–152.

Ekstrom, A. D. (2015). Why vision is important to how we navigate. *Hippocampus*, 25(6):731–735.

Ekstrom, A. D., Kahana, M. J., Caplan, J. B., Fields, T. A., Isham, E. A., Newman, E. L., and Fried, I. (2003). Cellular networks underlying human spatial navigation. *Nature*, 425(6954):184–188.

El-Hayek, Y. H., Wu, C., Ye, H., Wang, J., Carlen, P. L., and Zhang, L. (2013). Hippocampal excitability is increased in aged mice. *Exp. Neurol.*, 247:710–719.

Epstein, R., Harris, A., Stanley, D., and Kanwisher, N. (1999). The Parahippocampal Place Area: Recognition, Navigation, or Encoding? *Neuron*, 23(1):115–125.

Epstein, R. and Kanwisher, N. (1998). A cortical representation of the local visual environment. *Nature*, 392(6676):598–601.

Epstein, R. a. (2008). Parahippocampal and retrosplenial contributions to human spatial navigation. *Trends Cogn. Sci.*, 12(10):388–396.

Epstein, R. A. and Vass, L. K. (2014). Neural systems for landmark-based wayfinding in humans. *Philos. Trans. R. Soc. Lond. B. Biol. Sci.*, 369(1635):20120533.

Etienne, A. S. and Jeffery, K. J. (2004). Path integration in mammals. *Hippocampus*, 14(2):180–192.

Etienne, A. S., Maurer, R., and Seguinot, V. (1996). Path integration in mammals and its interaction with visual landmarks. *J Exp Biol*, 199(Pt 1):201–9.

Fairhall, S. L., Schwarzbach, J., Lingnau, A., Van Koningsbruggen, M. G., and Melcher, D. (2017). Spatiotopic updating across saccades revealed by spatially-specific fMRI adaptation. *Neuroimage*, 147:339–345.

Fattahi, M., Sharif, F., Geiller, T., and Royer, S. (2018). Differential Representation of Landmark and Self-Motion Information along the CA1 Radial Axis: Self-Motion Generated Place Fields Shift toward Landmarks during Septal Inactivation. *J. Neurosci.*, 38(30):6766–6778.

Fiehler, K., Wolf, C., Klinghammer, M., and Blohm, G. (2014). Integration of egocentric and allocentric information during memory-guided reaching to images of a natural environment. *Front. Hum. Neurosci.*, 8(August):1–12.

Fiete, I. R., Burak, Y., and Brookings, T. (2008). What Grid Cells Convey about Rat Location. *J. Neurosci.*, 28(27):6858–6871.

Fischer, W., Gage, F. H., and Bjorklund, A. (1989). Degenerative Changes in Forebrain Cholinergic Nuclei Correlate with Cognitive Impairments in Aged Rats. *Eur. J. Neurosci.*, 1(1):34–45.

Foster, T. C. (1999). Involvement of hippocampal synaptic plasticity in age-related memory decline. *Brain Res. Brain Res. Rev.*, 30(3):236–49.

Freund, T. F. and Antal, M. (1988). Gaba-containing neurons in the septum control inhibitory interneurons in the hippocampus. *Nature*, 336(6195):170–3.

Fuhs, M. C. (2006). A Spin Glass Model of Path Integration in Rat Medial Entorhinal Cortex. *J. Neurosci.*, 26(16):4266–4276.

Fuhs, M. C., VanRhoads, S. R., Casale, A. E., McNaughton, B., and Touretzky, D. S. (2005). Influence of Path Integration Versus Environmental Orientation on Place Cell Remapping Between Visually Identical Environments. *J. Neurophysiol.*, 94(4):2603–2616.

Fyhn, M., Hafting, T., Treves, A., Moser, M.-B., and Moser, E. I. (2007). Hippocampal remapping and grid realignment in entorhinal cortex. *Nature*, 446(7132):190–4.

Fyhn, M., Molden, S., Witter, M. P., Moser, E. I., and Moser, M.-B. (2004). Spatial Representation in the Entorhinal Cortex. *Science*, 305(5688):1258–1264.

Galletti, C., Gamberini, M., Kutz, D. F., Fattori, P., Luppino, G., and Matelli, M. (2001). The cortical connections of area V6: an occipito-parietal network processing visual information. *Eur. J. Neurosci.*, 13(8):1572–1588.

Gallistel, C. R. (1990). *The organization of learning*. MIT Press, Cambridge, MA.

Garsoffky, B., Schwan, S., and Hesse, F. W. (2002). Viewpoint dependency in the recognition of dynamic scenes. *J. Exp. Psychol. Learn. Mem. Cogn.*, 28(6):1035–50.

Gaunet, F., Vidal, M., Kemeny, A., and Berthoz, A. (2001). Active, passive and snapshot

exploration in a virtual environment: Influence on scene memory, reorientation and path memory. *Cogn. brain Res.*, 11(3):409–420.

Gavrilov, V. V., Wiener, S. I., and Berthoz, A. (1996). Whole body rotations enhance hippocampal theta rhythm slow activity in awake rats passively transported on a mobile robot. *Annals of the New York Academy of Sciences*, 781:385–398.

Geinisman, Y., de Toledo-Morrell, L., Morrell, F., Persina, I. S., and Rossi, M. (1992). Age-related loss of axospinous synapses formed by two afferent systems in the rat dentate gyrus as revealed by the unbiased stereological dissector technique. *Hippocampus*, 2(4):437–444.

Gerstner, W., Kistler, W. M., Naud, R., and Paninski, L. (2014). *Neuronal Dynamics*. Cambridge University Press, Cambridge.

Giovannini, M. G., Bartolini, L., Kopf, S. R., and Pepeu, G. (1998). Acetylcholine release from the frontal cortex during exploratory activity. *Brain Res.*, 784(1-2):218–227.

Giovannini, M. G., Rakovska, A., Benton, R. S., Pazzagli, M., Bianchi, L., and Pepeu, G. (2001). Effects of novelty and habituation on acetylcholine, GABA, and glutamate release from the frontal cortex and hippocampus of freely moving rats. *Neuroscience*, 106(1):43–53.

Givens, B. and Olton, D. (1995). Bidirectional Modulation of Scopolamine-Induced Working Memory Impairments by Muscarinic Activation of the Medial Septal Area. *Neurobiol. Learn. Mem.*, 63(3):269–276.

Goldman-Rakic, P. S. (1995). Cellular basis of working memory. *Neuron*, 14(3):477–485.

Golomb, J. D., Albrecht, A. R., Park, S., and Chun, M. M. (2011). Eye movements help link different views in scene-selective cortex. *Cereb. Cortex*, 21(9):2094–102.

Goodale, M. A. and Milner, A. D. (1992). Separate visual pathways for perception and action. *Trends Neurosci.*, 15(1):20–25.

Goodridge, J. P., Dudchenko, P. A., Worboys, K. A., Golob, E. J., and Taube, J. S. (1998). Cue control and head direction cells. *Behav. Neurosci.*, 112(4):749–761.

Goshen, I., Brodsky, M., Prakash, R., Wallace, J., Gradinaru, V., Ramakrishnan, C., and Deisseroth, K. (2011). Dynamics of Retrieval Strategies for Remote Memories. *Cell*, 147(3):678–689.

Gothard, K. M., Skaggs, W. E., and McNaughton, B. L. (1996a). Dynamics of mismatch correction in the hippocampal ensemble code for space: Interaction between path integration and environmental cues. *J. Neurosci.*, 16(24):8027–8040.

Gothard, K. M., Skaggs, W. E., Moore, K. M., and McNaughton, B. L. (1996b). Binding of hippocampal CA1 neural activity to multiple reference frames in a landmark-based navigation task. *Journal of Neuroscience*, 16(2):823–835.

Gould, E., Tanapat, P., Hastings, N. B., and Shors, T. J. (1999). Neurogenesis in adulthood: a possible role in learning. *Trends Cogn. Sci.*, 3(5):186–192.

Gouteux, S., Thinus-Blanc, C., and Vauclair, J. (2001). Rhesus monkeys use geometric and nongeometric information during a reorientation task. *J. Exp. Psychol. Gen.*, 130(3):505–19.

Gracian, E. I., Shelley, L. E., Morris, A. M., and Gilbert, P. E. (2013). Age-related changes in place learning for adjacent and separate locations. *Neurobiol. Aging*, 34(10):2304–9.

Granata, D. and Carnevale, V. (2016). Accurate Estimation of the Intrinsic Dimension Using Graph Distances: Unraveling the Geometric Complexity of Datasets. *Sci. Rep.*, 6(1):31377.

Grieves, R. M., Duvelle, É., and Dudchenko, P. A. (2018). A boundary vector cell model of place field repetition. *Spat. Cogn. Comput.*, 18(3):217–256.

Grieves, R. M., Jenkins, B. W., Harland, B. C., Wood, E. R., and Dudchenko, P. A. (2016). Place field repetition and spatial learning in a multicompartment environment. *Hippocampus*, 26(1):118–134.

Guanella, A., Kiper, D., and Vershure, P. (2007). A model of grid cells based on a twisted torus topology. *Int. J. Neural Syst.*, 17(04):231–240.

Haas, O. V., Henke, J., Leibold, C., and Thurley, K. (2019). Modality-specific Subpopulations of Place Fields Coexist in the Hippocampus. *Cereb. Cortex*, 29(3):1109–1120.

Hafting, T., Fyhn, M., Molden, S., Moser, M. B., and Moser, E. I. (2005). Microstructure of a spatial map in the entorhinal cortex. *Nature*, 436:801–806.

Hales, J. B., Schlesiger, M. I., Leutgeb, J. K., Squire, L. R., Leutgeb, S., and Clark, R. E. (2014). Medial Entorhinal Cortex Lesions Only Partially Disrupt Hippocampal Place Cells and Hippocampus-Dependent Place Memory. *Cell Rep.*, 9(3):893–901.

Hardcastle, K., Ganguli, S., and Giocomo, L. M. (2015). Environmental Boundaries as an Error Correction Mechanism for Grid Cells. *Neuron*, 86(3):827–839.

Harris, M. A. and Wolbers, T. (2014). How age-related strategy switching deficits affect wayfinding in complex environments. *Neurobiol. Aging*, 35(5):1095–1102.

Hartley, T., Burgess, N., Lever, C., Cacucci, F., and Keefe, J. O. (2000). Modeling place fields in terms of the cortical inputs to the hippocampus. *Hippocampus*, 10:369–379.

Hartley, T., Trinkler, I., and Burgess, N. (2004). Geometric determinants of human spatial memory. *Cognition*, 94(1):39–75.

Hasselmo, M., Schnell, E., and Barkai, E. (1995). Dynamics of learning and recall at excitatory recurrent synapses and cholinergic modulation in rat hippocampal region CA3. *J. Neurosci.*, 15(7):5249–5262.

Hasselmo, M. E., Bodelon, C., and Wyble, B. P. (2002). A proposed function for hippocampal theta rhythm: separate phases of encoding and retrieval enhance reversal of prior learning. *Neural Comput.*, 14(4):793–817.

Hasselmo, M. E. and Bower, J. M. (1993). Acetylcholine and memory. *Trends in Neurosciences*, 16(6):218–222.

Hasselmo, M. E. and Schnell, E. (1994). Laminar selectivity of the cholinergic suppression of synaptic transmission in rat hippocampal region CA1: computational modeling and brain slice physiology. *J. Neurosci.*, 14(6):3898–3914.

Hasselmo, M. E. and Wyble, B. P. (1997). Free recall and recognition in a network model

of the hippocampus: simulating effects of scopolamine on human memory function. *Behav. Brain Res.*, 89(1-2):1–34.

Hastings, N. B., Seth, M. I., Tanapat, P., Rydel, T. A., and Gould, E. (2002). Granule neurons generated during development extend divergent axon collaterals to hippocampal area ca3. *J Comp Neurol*, 452(4):324–33.

Hayhoe, M. M., Shrivastava, A., Mruczek, R., and Pelz, J. B. (2003). Visual memory and motor planning in a natural task. *J. Vis.*, 3(1):6.

Hayman, R. M. and Jeffery, K. J. (2008). How heterogeneous place cell responding arises from homogeneous grids – A contextual gating hypothesis. *Hippocampus*, 18(12):1301–1313.

Hazama, Y. and Tamura, R. (2019). Effects of self-locomotion on the activity of place cells in the hippocampus of a freely behaving monkey. *Neurosci. Lett.*, 701:32–37.

Heeger, D. J. (1992). Normalisation of cell responses in cat striate cortex. *Vis. Neurosci.*, 9:181–197.

Hermer, L. and Spelke, E. S. (1994). A geometric process for spatial reorientation in young children. *Nature*, 370:57–59.

Herweg, N. A. and Kahana, M. J. (2018). Spatial Representations in the Human Brain. *Front. Hum. Neurosci.*, 12:297.

Hoffman, K. L., Dragan, M. C., Leonard, T. K., Micheli, C., Montefusco-Siegmund, R., and Valiante, T. A. (2013). Saccades during visual exploration align hippocampal 3–8 Hz rhythms in human and non-human primates. *Front. Syst. Neurosci.*, 7:43.

Hori, E., Tabuchi, E., Matsumura, N., Tamura, R., Eifuku, S., Endo, S., Nishijo, H., and Ono, T. (2003). Representation of place by monkey hippocampal neurons in real and virtual translocation. *Hippocampus*, 13(2):190–6.

Hubel, D. H. and Wiesel, T. N. (1962). Receptive fields, binocular interaction and functional architecture in the cat's visual cortex. *J. Physiol.*, 160(1):106–154.

Hunsaker, M. R. and Kesner, R. P. (2013). The operation of pattern separation and pattern completion processes associated with different attributes or domains of memory.

Huth, J., Masquelier, T., and Arleo, A. (2018). Convis: A Toolbox to Fit and Simulate Filter-Based Models of Early Visual Processing. *Front. Neuroinform.*, 12:9.

Hyman, B. T., Van Hoesen, G. W., Kromer, L. J., and Damasio, A. R. (1986). Perforant pathway changes and the memory impairment of Alzheimer's disease. *Ann. Neurol.*, 20(4):472–481.

Iijima, T., Witter, M. P., Ichikawa, M., Tominaga, T., Kajiwara, R., and Matsumoto, G. (1996). Entorhinal-Hippocampal Interactions Revealed by Real-Time Imaging. *Science*, 272(5265):1176–1179.

Ikonen, S., McMahan, R., Gallagher, M., Eichenbaum, H., and Tanila, H. (2002). Cholinergic system regulation of spatial representation by the hippocampus. *Hippocampus*, 12(3):386–397.

Insausti, R., Herrero, M. T., and Witter, M. P. (1997). Entorhinal cortex of the rat: Cytoarchitectonic subdivision and the origin and distribution of cortical efferents. *Hippocampus*, 7:146–83.

Jacob, P.-Y., Capitano, F., Poucet, B., Save, E., and Sargolini, F. (2019). Path integration maintains spatial periodicity of grid cell firing in a 1D circular track. *Nat. Commun.*, 10(1):840.

Jacob, P.-Y., Casali, G., Spieser, L., Page, H., Overington, D., and Jeffery, K. (2017). An independent, landmark-dominated head-direction signal in dysgranular retrosplenial cortex. *Nat. Neurosci.*, 20(2):173–175.

Jacobs, J., Weidemann, C. T., Miller, J. F., Solway, A., Burke, J. F., Wei, X.-X., Suthana, N., Sperling, M. R., Sharan, A. D., Fried, I., and Kahana, M. J. (2013). Direct recordings of grid-like neuronal activity in human spatial navigation. *Nat. Neurosci.*, 16(9):1188–90.

Jayakumar, R. P., Madhav, M. S., Savelli, F., Blair, H. T., Cowan, N. J., and Knierim,

J. J. (2019). Recalibration of path integration in hippocampal place cells. *Nature*, 566(7745):533–537.

Johansson, R. and Johansson, M. (2014). Look Here, Eye Movements Play a Functional Role in Memory Retrieval. *Psychol. Sci.*, 25(1):236–242.

Jones, J. P. and Palmer, L. A. (1987). An evaluation of the two-dimensional Gabor filter model of simple receptive fields in cat striate cortex. *J. Neurophysiol.*, 58(6):1233–1258.

Jung, M. W. and McNaughton, B. L. (1993). Spatial selectivity of unit activity in the hippocampal granular layer. *Hippocampus*, 3(2):165–182.

Jutras, M. J. and Buffalo, E. A. (2010a). Recognition memory signals in the macaque hippocampus. *Proc. Natl. Acad. Sci.*, 107(1):401–406.

Jutras, M. J. and Buffalo, E. A. (2010b). Synchronous neural activity and memory formation. *Curr. Opin. Neurobiol.*, 20(2):150–155.

Kauffmann, L., Ramanoël, S., Guyader, N., Chauvin, A., and Peyrin, C. (2015). Spatial frequency processing in scene-selective cortical regions. *Neuroimage*, 112:86–95.

Keinath, A. T., Julian, J. B., Epstein, R. A., and Muzzio, I. A. (2017). Environmental Geometry Aligns the Hippocampal Map during Spatial Reorientation. *Curr. Biol.*, 27(3):309–317.

Killian, N. J., Jutras, M. J., and Buffalo, E. A. (2012). A map of visual space in the primate entorhinal cortex. *Nature*, 491(7426):761–764.

Kloosterman, F., van Haeften, T., Witter, M. P., and Lopes da Silva, F. H. (2003). Electrophysiological characterization of interlaminar entorhinal connections: an essential link for re-entrance in the hippocampal-entorhinal system. *Eur. J. Neurosci.*, 18(11):3037–3052.

Knierim, J. J., Kudrimoti, H. S., and McNaughton, B. L. (1995). Place Cells, Head Direction Cells, and the Learning of Landmark Stability. *J. Neurosci.*, 15(3):1648–1659.

Knierim, J. J., Kudrimoti, H. S., and McNaughton, B. L. (1998). Interactions between idiothetic cues and external landmarks in the control of place cells and head direction cells. *J. Neurophysiol.*, 80(1):425–46.

Kobayashi, Y. and Amaral, D. G. (2007). Macaque monkey retrosplenial cortex: III. Cortical efferents. *J. Comp. Neurol.*, 502(5):810–833.

Koenig, J., Linder, A. N., Leutgeb, J. K., and Leutgeb, S. (2011). The Spatial Periodicity of Grid Cells Is Not Sustained During Reduced Theta Oscillations. *Science*, 332(6029):592–595.

Kondo, H., Saleem, K. S., and Price, J. L. (2005). Differential connections of the perirhinal and parahippocampal cortex with the orbital and medial prefrontal networks in macaque monkeys. *J. Comp. Neurol.*, 493(4):479–509.

Kosel, K. C., Hoesen, G. W. V., and West, J. R. (1981). Olfactory bulb projections to the parahippocampal area of the rat. *Journal of Comparative Neurology*, 198:467–482.

Kravitz, D. J., Saleem, K. S., Baker, C. I., and Mishkin, M. (2011). A new neural framework for visuospatial processing. *Nat. Rev. Neurosci.*, 12(4):217–230.

Kriegeskorte, N. and Douglas, P. K. (2018). Cognitive computational neuroscience. *Nat. Neurosci.*, 21(September).

Krupic, J., Bauza, M., Burton, S., Barry, C., and O'Keefe, J. (2015). Grid cell symmetry is shaped by environmental geometry. *Nature*, 518(7538):232–235.

Kubie, J. L. and Ranck, J. B. (1983). Sensory-behavioral correlates in individual hippocampus neurons in three situations: Space and context. In Seifert, W., editor, *Neurobiology of the Hippocampus*, pages 433–447. Academic Press, New York.

Kuhn, H. G., Dickinson-Anson, H., and Gage, F. H. (1996). Neurogenesis in the dentate gyrus of the adult rat: age-related decrease of neuronal progenitor proliferation. *J. Neurosci.*, 16(6):2027–33.

Laeng, B., Bloem, I. M., D'Ascenzo, S., and Tommasi, L. (2014). Scrutinizing visual images: The role of gaze in mental imagery and memory. *Cognition*, 131(2):263–283.

Land, M., Mennie, N., and Rusted, J. (1999). The Roles of Vision and Eye Movements in the Control of Activities of Daily Living. *Perception*, 28(11):1311–1328.

Land, M. F. (2014). Do we have an internal model of the outside world? *Philos. Trans. R. Soc. Lond. B. Biol. Sci.*, 369:20130045.

Lavenex, P. and Schenk, F. (1996). Integration of olfactory information in a spatial representation enabling accurate arm choice in the radial arm maze. *Learning & Memory*, 2(6):299–319.

Leal, S. L. and Yassa, M. A. (2015). Neurocognitive Aging and the Hippocampus across Species. *Trends Neurosci.*, xx:1–13.

Legault, M., Rompré, P.-P., and Wise, R. A. (2000). Chemical stimulation of the ventral hippocampus elevates nucleus accumbens dopamine by activating dopaminergic neurons of the ventral tegmental area. *Journal of Neuroscience*, 20(4):1635–1642.

Lester, A. W., Moffat, S. D., Wiener, J. M., Barnes, C. A., and Wolbers, T. (2017). The Aging Navigational System.

Leutgeb, J. K., Leutgeb, S., Moser, M.-B., and Moser, E. I. (2007). Pattern Separation in the Dentate Gyrus and CA3 of the Hippocampus. *Science (80-.).*, 315(5814):961–966.

Li, T., Arleo, A., and Sheynikhovich, D. (2020). Modeling place cells and grid cells in multi-compartment environments: Entorhinal–hippocampal loop as a multisensory integration circuit. *Neural Networks*, 121:37–51.

Liu, P. and Bilkey, D. K. (1997). Parallel involvement of perirhinal and lateral entorhinal cortex in the polysynaptic activation of hippocampus by olfactory inputs. *Hippocampus*, 7(3):296–306.

Livingstone, M. S. and Hubel, D. H. (1984). Anatomy and physiology of a color system in the primate visual cortex. *J. Neurosci.*, 4(1):309–56.

Loomis, J. M., Klatzky, R. L., and Giudice, N. A. (2013). Representing 3D Space in Working Memory: Spatial Images from Vision, Hearing, Touch, and Language. In Lacey, S. and Lawson, R., editors, *Multisensory Imag.*, pages 131–155. Springer New York, New York, NY.

Loomis, J. M., Klatzky, R. L., Golledge, R. G., Cicinelli, J. G., Pellegrino, J. W., and Fry, P. A. (1993). Nonvisual Navigation by Blind and Sighted: Assessment of Path Integration Ability. *J. Exp. Psychol. Gen.*, 122(1):73–91.

Luo, Y., Zhou, J., Li, M.-X., Wu, P.-F., Hu, Z.-L., Ni, L., Jin, Y., Chen, J.-G., and Wang, F. (2015). Reversal of aging-related emotional memory deficits by norepinephrine via regulating the stability of surface AMPA receptors. *Aging Cell*, 14(2):170–179.

Luque, N. R., Naveros, F., Carrillo, R. R., Ros, E., and Arleo, A. (2019). Spike burst-pause dynamics of Purkinje cells regulate sensorimotor adaptation. *PLOS Comput. Biol.*, 15(3):e1006298.

Madl, T., Chen, K., Montaldi, D., and Trappl, R. (2015). Computational cognitive models of spatial memory in navigation space: A review. *Neural Networks*, 65:18–43.

Maguire, E. (2001). The retrosplenial contribution to human navigation: A review of lesion and neuroimaging findings. *Scand. J. Psychol.*, 42(3):225–238.

Manns, J. R., Stark, C. E., and Squire, L. R. (2000). The visual paired-comparison task as a measure of declarative memory. *Proc. Natl. Acad. Sci. U. S. A.*, 97(22):12375–9.

Mao, D., Kandler, S., McNaughton, B. L., and Bonin, V. (2017). Sparse orthogonal population representation of spatial context in the retrosplenial cortex. *Nat. Commun.*, 8(1):243.

Markus, E. J., Barnes, C. A., McNaughton, B. L., Gladden, V. L., and Skaggs, W. E. (1994). Spatial information content and reliability of hippocampal CA1 neurons: Effects of visual input. *Hippocampus*, 4(4):410–421.

Markus, E. J., Qin, Y., Leonard, B., Skaggs, W. E., McNaughton, B. L., and Barnes, C. A. (1995). Interactions between location and task affect the spatial and direction firing of hippocampal neurons. *Journal of Neuroscience*, 15:7079–7094.

Masquelier, T. and Thorpe, S. J. (2007). Unsupervised learning of visual features through spike timing dependent plasticity. *PLoS Comput. Biol.*, 3(2):e31.

Masurkar, A. V., Srinivas, K. V., Brann, D. H., Warren, R., Lowes, D. C., and Siegelbaum,

S. A. (2017). Medial and Lateral Entorhinal Cortex Differentially Excite Deep versus Superficial CA1 Pyramidal Neurons. *Cell Rep.*, 18(1):148–160.

McCloskey, M. and Cohen, N. J. (1989). Catastrophic Interference in Connectionist Networks: The Sequential Learning Problem. *Psychol. Learn. Motiv.*, 24:109–165.

McGregor, A., Hayward, A. J., Pearce, J. M., and Good, M. A. (2004). Hippocampal Lesions Disrupt Navigation Based on the Shape of the Environment. *Behav. Neurosci.*, 118(5):1011–1021.

McKee, R. D. and Squire, L. R. (1993). On the development of declarative memory. *J. Exp. Psychol. Learn. Mem. Cogn.*, 19(2):397–404.

McNaughton, B. L., Barnes, C. A., Gerrard, J. L., Gothard, K., Jung, M. W., Knierim, J. J., Kudrimoti, H., Qin, Y., Skaggs, W. E., Suster, M., and Weaver, K. L. (1996). Deciphering the hippocampal polyglot: the hippocampus as a path integration system. *J. Exp. Biol.*, 199(Pt 1):173–185.

McNaughton, B. L., Barnes, C. A., Meltzer, J., and Sutherland, R. J. (1989). Hippocampal granule cells are necessary for normal spatial learning but not for spatially-selective pyramidal cell discharge. *Exp Brain Res*, 76(3):485–96.

McNaughton, B. L., Barnes, C. A., and O'Keefe, J. (1983). The contributions of position, direction, and velocity to single unit activity in the hippocampus of freely-moving rats. *Experimental Brain Research*, 52:41–49.

McNaughton, B. L., Battaglia, F. P., Jensen, O., Moser, E. I., and Moser, M. B. (2006). Path integration and the neural basis of the 'cognitive map'. *Nat. Rev. Neurosci.*, 7(8):663–678.

Mehta, M. R., Barnes, C. A., and McNaughton, B. L. (1997). Experience-dependent, asymmetric expansion of hippocampal place fields. In *Proceedings Natl. Acad. Science USA*, volume 94, pages 8918–8921.

Meister, M. L. and Buffalo, E. A. (2016). Getting directions from the hippocampus: The neural connection between looking and memory. *Neurobiol. Learn. Mem.*, 134:135–144.

Melcher, D. and Morrone, M. C. (2015). Nonretinotopic visual processing in the brain. *Vis. Neurosci.*, 32:E017.

Miller, J., Watrous, A. J., Tsitsiklis, M., Lee, S. A., Sheth, S. A., Schevon, C. A., Smith, E. H., Sperling, M. R., Sharan, A., Asadi-Pooya, A. A., Worrell, G. A., Meisenhelter, S., Inman, C. S., Davis, K. A., Lega, B., Wanda, P. A., Das, S. R., Stein, J. M., Gorniak, R., and Jacobs, J. (2018). Lateralized hippocampal oscillations underlie distinct aspects of human spatial memory and navigation. *Nat. Commun.*, 9(1):2423.

Miller, J. F., Neufang, M., Solway, A., Brandt, A., Trippel, M., Mader, I., Hefft, S., Merkow, M., Polyn, S. M., Jacobs, J., Kahana, M. J., and Schulze-Bonhage, A. (2013). Neural activity in human hippocampal formation reveals the spatial context of retrieved memories. *Science*, 342(6162):1111–4.

Miller, R. (1991). *Cortico-Hippocampal interplay and the representation of contexts in the brain*. Springer-Verlag.

Miranda, M. I., Ramírez-Lugo, L., and Bermúdez-Rattoni, F. (2000). Cortical cholinergic activity is related to the novelty of the stimulus. *Brain Res.*, 882(1-2):230–235.

Mitchell, A. S., Czajkowski, R., Zhang, N., Jeffery, K., and Nelson, A. J. D. (2018). Retrosplenial cortex and its role in spatial cognition. *Brain Neurosci. Adv.*, 2:239821281875709.

Mittelstaedt, H. (1983). The role of multimodal convergence in homing by path integration. *Fortschritte der Zoologie*, 28:197–212.

Mittelstaedt, M. L. and Mittelstaedt, H. (1980). Homing by path integration in a mammal. *Naturwissenschaften*, 67:566–567.

Mizumori, S. J., McNaughton, B. L., Barnes, C. A., and Fox, K. B. (1989). Preserved spatial coding in hippocampal ca1 pyramidal cells during reversible suppression of ca3c output: evidence for pattern completion in hippocampus. *J Neurosci*, 9(11):3915–28.

Mizuseki, K., Diba, K., Pastalkova, E., and Buzsáki, G. (2011). Hippocampal CA1 pyramidal cells form functionally distinct sublayers. *Nat. Neurosci.*, 14(9):1174–1181.

Mizuseki, K., Sirota, A., Pastalkova, E., and Buzsáki, G. (2009). Theta Oscillations Provide Temporal Windows for Local Circuit Computation in the Entorhinal-Hippocampal Loop. *Neuron*, 64(2):267–280.

Moffat, S. D. (2009). Aging and spatial navigation: what do we know and where do we go? *Neuropsychol. Rev.*, 19(4):478–89.

Morris, R., Pandya, D. N., and Petrides, M. (1999). Fiber system linking the mid-dorsolateral frontal cortex with the retrosplenial]presubicular region in the rhesus monkey. *J. Comp. Neurol.*, 407(2):183–192.

Moser, E. I., Kropff, E., and Moser, M.-B. (2008). Place Cells, Grid Cells, and the Brain's Spatial Representation System. *Annu. Rev. Neurosci.*, 31(1):69–89.

Moser, E. I., Moser, M.-B., and McNaughton, B. L. (2017). Spatial representation in the hippocampal formation: a history. *Nat. Neurosci.*, 20(11):1448–1464.

Mountcastle, V. B., Andersen, R. A., Motter, B. C., Gnadt, J., and Fogassi, L. (1981). The influence of attentive fixation upon the excitability of the light-sensitive neurons of the posterior parietal cortex. *J. Neurosci.*, 1(11):1218–25.

Muessig, L., Hauser, J., Wills, T. J., and Cacucci, F. (2015). A Developmental Switch in Place Cell Accuracy Coincides with Grid Cell Maturation. *Neuron*, 86(5):1167–1173.

Müller, M. and Wehner, R. (1988). Path integration in desert ants, Cataglyphis fortis. *Proc. Natl. Acad. Sci.*, 85(14):5287–5290.

Muller, R. U. and Kubie, J. L. (1987). The effects of changes in the environment on the spatial firing of hippocampal complex-spike cells. *J. Neurosci.*, 7(7):1951–1968.

Muller, R. U., Kubie, J. L., and Ranck, J. J. B. (1987). Spatial firing patterns of hippocampal complex-spike cells in a fixed environment. *Journal of Neuroscience*, 7:1935–1950.

Murray, J. D., Anticevic, A., Gancsos, M., Ichinose, M., Corlett, P. R., Krystal, J. H., and Wang, X. J. (2014). Linking microcircuit dysfunction to cognitive impairment: Effects of disinhibition associated with schizophrenia in a cortical working memory model. *Cereb. Cortex*, 24(4):859–872.

Naber, P. A., Lopes da Silva, F. H., and Witter, M. P. (2001). Reciprocal connections between the entorhinal cortex and hippocampal fields CA1 and the subiculum are in register with the projections from CA1 to the subiculum. *Hippocampus*, 11(2):99–104.

Nadasdy, Z., Nguyen, T. P., Török, Á., Shen, J. Y., Briggs, D. E., Modur, P. N., and Buchanan, R. J. (2017). Context-dependent spatially periodic activity in the human entorhinal cortex. *Proc. Natl. Acad. Sci. U. S. A.*, 114(17):E3516–E3525.

Naveros, F., Luque, N. R., Ros, E., and Arleo, A. (2019). VOR Adaptation on a Humanoid iCub Robot Using a Spiking Cerebellar Model. *IEEE Trans. Cybern.*, pages 1–14.

Newell, F. N., Woods, A. T., Mernagh, M., and B\"ulthoff, H. H. (2005). Visual, haptic and crossmodal recognition of scenes. *Exp. Brain Res.*, 161(2):233–242.

Nicolle, M. M., Prescott, S., and Bizon, J. L. (2003). Emergence of a Cue Strategy Preference on the Water Maze Task in Aged C57B6 × SJL F1 Hybrid Mice. *Learn. Mem.*, 10(6):520–524.

O'Keefe, J. and Burgess, N. (1996). Geometric determinants of the place fields of hippocampal neurons. *Nature*, 381:425–428.

O'Keefe, J. and Burgess, N. (2005). Dual phase and rate coding in hippocampal place cells: Theoretical significance and relationship to entorhinal grid cells. *Hippocampus*, 15(7):853–866.

O'Keefe, J. and Conway, D. H. (1978). Hippocampal place units in the freely moving rat: Why they fire where they fire. *Experimental Brain Research*, 31:573–590.

O'Keefe, J. and Dostrovsky, J. (1971). The hippocampus as a spatial map. Preliminary evidence from unit activity in the freely-moving rat. *Brain Res.*, 34:171–175.

O'Keefe, J. and Nadel, L. (1978). *The hippocampus as a cognitive map*. Clarendon Press, Oxford.

O'Keefe, J. and Recce, M. (1993). Phase relationship between hippocampal place units and the EEG theta rhythm. *Hippocampus*, 3:317–330.

O'Keefe, J. and Speakman, A. (1987). Single unit activity in the rat hippocampus during a spatial memory task. *Exp. Brain Res.*, 68:1–27.

Oler, J. A. and Markus, E. J. (2000). Age-related deficits in the ability to encode contextual change: A place cell analysis. *Hippocampus*, 10(3):338–350.

Oliva, A., Wolfe, J. M., and Arsenio, H. C. (2004). Panoramic Search: The Interaction of Memory and Vision in Search Through a Familiar Scene. *J. Exp. Psychol. Hum. Percept. Perform.*, 30(6):1132–1146.

O'Regan, J. K. (1992). Solving the "real" mysteries of visual perception: the world as an outside memory. *Can. J. Psychol.*, 46(3):461–88.

O'Reilly, R. C., Herd, S. A., and Pauli, W. M. (2010). Computational models of cognitive control. *Curr. Opin. Neurobiol.*, 20(2):257–261.

O'Reilly, R. C. and Rudy, J. W. (2000). Computational principles of learning in the neocortex and hippocampus. *Hippocampus*, 10(4):389–397.

Park, S., Intraub, H., Yi, D.-J., Widders, D., and Chun, M. M. (2007). Beyond the Edges of a View: Boundary Extension in Human Scene-Selective Visual Cortex. *Neuron*, 54(2):335–342.

Pascalis, O., Hunkin, N., Bachevalier, J., and Mayes, A. (2009). Change in background context disrupts performance on visual paired comparison following hippocampal damage. *Neuropsychologia*, 47(10):2107–2113.

Paz-Villagrán, V., Save, E., and Poucet, B. (2006). Spatial discrimination of visually similar environments by hippocampal place cells in the presence of remote recalibrating landmarks. *Eur. J. Neurosci.*, 23(1):187–195.

Penny, W. D., Zeidman, P., and Burgess, N. (2013). Forward and Backward Inference in Spatial Cognition. *PLoS Comput. Biol.*, 9(12):e1003383.

Perry, E. K., Johnson, M., Kerwin, J. M., Piggott, M. A., Court, J. A., Shaw, P. J., Ince, P. G., Brown, A., and Perry, R. H. (1992). Convergent cholinergic activities in aging and Alzheimer's disease. *Neurobiol. Aging*, 13(3):393–400.

Pilly, P. K. and Grossberg, S. (2012). How Do Spatial Learning and Memory Occur in the Brain? Coordinated Learning of Entorhinal Grid Cells and Hippocampal Place Cells. *J. Cogn. Neurosci.*, 24(5):1031–1054.

Poucet, B., Chaillan, F., Truchet, B., Save, E., Sargolini, F., and Hok, V. (2015). Is there a pilot in the brain? Contribution of the self-positioning system to spatial navigation. *Front. Behav. Neurosci.*, 9:292.

Poucet, B., Sargolini, F., Song, E. Y., Hangya, B., Fox, S., and Muller, R. U. (2013). Independence of landmark and self-motion-guided navigation: a different role for grid cells. *Philos. Trans. R. Soc. B Biol. Sci.*, 369(1635):20130370–20130370.

Pouget, A., Deneve, S., and Duhamel, J.-r. (2002). A computational perspective on the neural basis of multisensory spatial representations. *Nat. Neurosci.*, 3(September):1–7.

Pouget, A. and Sejnowski, T. J. (1997). Spatial Transformations in the Parietal Cortex Using Basis Functions. *J. Cogn. Neurosci.*, 9(2):222–237.

Praxinos, G. and Watson, C. (1998). *The Rat Brain in stereotaxic coordinates*. Academic Press, fourth edition edition.

Quirk, G. J., Muller, R. U., Kubie, J. L., and Ranck Jr., J. B. (1992). The positional firing properties of medial entorhinal neurons: Description and comparison with hippocampal place cells. *Journal of Neuroscience*, 12(5):1945–1963.

Rajimehr, R., Devaney, K. J., Bilenko, N. Y., Young, J. C., and Tootell, R. B. H. (2011). The "Parahippocampal Place Area" Responds Preferentially to High Spatial Frequencies in Humans and Monkeys. *PLoS Biol.*, 9(4):e1000608.

Ranganath, C. and Rainer, G. (2003). Neural mechanisms for detecting and remembering novel events. *Nat. Rev. Neurosci.*, 4(3):193–202.

Redish, A. D. (1999). *Beyond the cognitive map. From place cells to episodic memory*. MIT Press-Bradford Books, London.

Redish, A. D., Rosenzweig, E. S., Bohanick, J. D., McNaughton, B. L., and Barnes,

C. A. (2000). Dynamics of hippocampal ensemble activity realignment: Time versus space. *Journal of Neuroscience*, 20(24):9298–9309.

Rennó-Costa, C. and Tort, A. B. (2017). Place and Grid Cells in a Loop: Implications for Memory Function and Spatial Coding. *J. Neurosci.*, 37(34):8062–8076.

Rensink, R. A. (2000). The Dynamic Representation of Scenes. *Vis. cogn.*, 7(1-3):17–42.

Robertson, C., Hermann, K., Mynick, A., Kravitz, D., and Kanwisher, N. (2016). Neural Representations Integrate the Current Field of View with the Remembered 360° Panorama in Scene-Selective Cortex. *Curr. Biol.*, 26(18):2463–2468.

Rockland, K. S. and Van Hoesen, G. W. (1999). Some Temporal and Parietal Cortical Connections Converge in CA1 of the Primate Hippocampus. *Cereb. Cortex*, 9(3):232–237.

Rodgers, M. K., Sindone, J. A., and Moffat, S. D. (2012). Effects of age on navigation strategy. *Neurobiol. Aging*, 33(1):202.e15–202.e22.

Rolls, E. T. (1996). A theory of hippocampal function in memory. *Hippocampus*, 6(6):601–620.

Rosenbaum, R. S., Winocur, G., Binns, M. A., and Moscovitch, M. (2012). Remote spatial memory in aging: all is not lost. *Front. Aging Neurosci.*, 4:25.

Rosenzweig, E. S., Redish, A. D., McNaughton, B. L., and Barnes, C. A. (2003). Hippocampal map realignment and spatial learning. *Nat. Neurosci.*, 6(6):609–15.

Rueckemann, J. W., DiMauro, A. J., Rangel, L. M., Han, X., Boyden, E. S., and Eichenbaum, H. (2016). Transient optogenetic inactivation of the medial entorhinal cortex biases the active population of hippocampal neurons. *Hippocampus*, 26(2):246–260.

Rutishauser, U., Mamelak, A. N., and Schuman, E. M. (2006). Single-Trial Learning of Novel Stimuli by Individual Neurons of the Human Hippocampus-Amygdala Complex. *Neuron*, 49(6):805–813.

Salinas, E. and Abbott, L. (1995). Transfer of coded information from sensory to motor networks. *J. Neurosci.*, 15(10):6461–6474.

Salinas, E. and Abbott, L. F. (2001). Coordinate transformations in the visual system: how to generate gain fields and what to compute with them. *Prog. Brain Res.*, 130:175–90.

Samsonovich, A. and McNaughton, B. L. (1997). Path integration and cognitive mapping in a continuous attractor neural network model. *J. Neurosci.*, 17(15):5900–5920.

Sanders, S. and Oberts, J. (2016). Booklet | Brain-inspired intelligent robotics: The intersection of robotics and neuroscience sciences. *Science (80-.).*, 354(6318):1445.2–1445.

Sargolini, F., Fyhn, M., Hafting, T., McNaughton, B. L., Witter, M. P., Moser, M. B., and Moser, E. I. (2006). Conjunctive representation of position, direction, and velocity in entorhinal cortex. *Science*, 312(5774):758–62.

Sasaki, T., Leutgeb, S., and Leutgeb, J. K. (2015). Spatial and memory circuits in the medial entorhinal cortex. *Curr. Opin. Neurobiol.*, 32:16–23.

Sava, S. and Markus, E. J. (2008). Activation of the medial septum reverses age-related hippocampal encoding deficits: a place field analysis. *J. Neurosci.*, 28(8):1841–53.

Save, E., Cressant, A., Thinus-Blanc, C., and Poucet, B. (1998). Spatial firing of hippocampal place cells in blind rats. *Journal of Neuroscience*, 18(5):1818–1826.

Save, E., Nerad, L., and Poucet, B. (2000). Contribution of multiple sensory information to place field stability in hippocampal place cells. *Hippocampus*, 10:64–76.

Schindler, A. and Bartels, A. (2013). Parietal cortex codes for egocentric space beyond the field of view. *Curr. Biol.*, 23(2):177–82.

Schlesiger, M. I., Boublil, B. L., Hales, J. B., Leutgeb, J. K., and Leutgeb, S. (2018). Hippocampal Global Remapping Can Occur without Input from the Medial Entorhinal Cortex. *Cell Rep.*, 22(12):3152–3159.

Schliebs, R. and Arendt, T. (2011). The cholinergic system in aging and neuronal degeneration. *Behav. Brain Res.*, 221(2):555–563.

Schuck, N. W., Doeller, C. F., Schjeide, B. M. M., Schröder, J., Frensch, P. A., Bertram,

L., and Li, S. C. (2013). Aging and KIBRA/WWC1 genotype affect spatial memory processes in a virtual navigation task. *Hippocampus*, 23(10):919–930.

Serre, T., Wolf, L., and Poggio, T. (2005). Object Recognition with Features Inspired by Visual Cortex. In *2005 IEEE Comput. Soc. Conf. Comput. Vis. Pattern Recognit.*, volume 2, pages 994–1000. IEEE.

Sharp, P. E. (1997). Subicular cells generate similar spatial firing patterns in two geometrically and visually distinctive environments: Comparison with hippocampal place cells. *Behavioral and Brain Research*, 85:71–92.

Sharp, P. E. (1999). Subicular place cells expand/contract their spatial firing pattern to fit the size of the environment in an open field, but not inthe presence of barriers: Comparison with hippocampal place cells. *Behavioral Neuroscience*, 113(4):643–62.

Sharp, P. E. and Green, C. (1994). Spatial correlates of firing patterns of single cells in the subiculum of freely moving rat. *Journal of Neuroscience*, 14(4):2339–2356.

Sharp, P. E., Kubie, J. L., and Muller, R. U. (1990). Firing properties of hippocampal neurons in a visually symmetrical environment: contributions of multiple sensory cues and mnemonic processes. *J Neurosci*, 10(9):3093–105.

Shelton, A. L. and McNamara, T. P. (1997). Multiple views of spatial memory. *Psychon. Bull. Rev.*, 4(1):102–106.

Shen, J. and Barnes, C. A. (1996). Age-related decrease in cholinergic synaptic transmission in three hippocampal subfields. *Neurobiol. Aging*, 17(3):439–451.

Shen, J., Barnes, C. A., McNaughton, B. L., Skaggs, W. E., and Weaver, K. L. (1997). The effect of aging on experience-dependent plasticity of hippocampal place cells. *J. Neurosci.*, 17(17):6769–82.

Sheynikhovich, D., Carrillo, R., Bologna, L. L., Cherifi, Y., Li, T., Arleo, A., Baranton, K., Scherlen, A.-C., and Tranvouez-Bernardin, D. (2019). Device for simulating a physiological behaviour of a mammal using a virtual mammal, process and computer program. *Eur. Pat. Off.*, Patent App(n° EP19305363.4):March 22.

Sheynikhovich, D., Chavarriaga, R., Strösslin, T., Arleo, A., and Gerstner, W. (2009). Is

there a geometric module for spatial orientation? Insights from a rodent navigation model. *Psychol. Rev.*, 116(3):540–566.

Skaggs, W. E. and McNaughton, B. L. (1998). Spatial Firing Properties of Hippocampal CA1 Populations in an Environment Containing Two Visually Identical Regions. *J. Neurosci.*, 18(20):8455–8466.

Skaggs, W. E., McNaughton, B. L., Wilson, M. A., and Barnes, C. A. (1996). Theta phase precession in hippocampal neuronal populations and the compression of temporal sequences. *Hippocampus*, 6(2):149–72.

Slomianka, L., Amrein, I., Knuesel, I., Sørensen, J. C., and Wolfer, D. P. (2011). Hippocampal pyramidal cells: the reemergence of cortical lamination. *Brain Struct. Funct.*, 216(4):301–317.

Smith, T. D., Adams, M. M., Gallagher, M., Morrison, J. H., and Rapp, P. R. (2000). Circuit-specific alterations in hippocampal synaptophysin immunoreactivity predict spatial learning impairment in aged rats. *J. Neurosci.*, 20(17):6587–93.

Snyder, L. H., Grieve, K. L., Brotchie, P., and Andersen, R. a. (1998). Separate body- and world-referenced representations of visual space in parietal cortex. *Nature*, 394(6696):887–91.

Sobotka, S., Nowicka, A., and Ringo, J. L. (1997). Activity Linked to Externally Cued Saccades in Single Units Recorded From Hippocampal, Parahippocampal, and Inferotemporal Areas of Macaques. *J. Neurophysiol.*, 78(4):2156–2163.

Solstad, T., Moser, E. I., and Einevoll, G. T. (2006). From grid cells to place cells: A mathematical model. *Hippocampus*, 16(12):1026–1031.

Spiers, H. J., Hayman, R. M. A., Jovalekic, A., Marozzi, E., and Jeffery, K. J. (2015). Place Field Repetition and Purely Local Remapping in a Multicompartment Environment. *Cereb. Cortex*, 25(1):10–25.

Stackman, R. W. and Taube, J. S. (1998). Firing properties of rat lateral mammillary single units: head direction, head pitch, and angular head velocity. *J. Neurosci.*, 18(21):9020–37.

Stark, M. (1996). Impairment of an Egocentric Map of Locations: Implications for Perception and Action. *Cogn. Neuropsychol.*, 13(4):481–524.

Stark, S. M., Yassa, M. A., and Stark, C. E. L. (2010). Individual differences in spatial pattern separation performance associated with healthy aging in humans. *Learn. Mem.*, 17(6):284–8.

Stein, J. F. (1992). The representation of egocentric space in the posterior parietal cortex. *Behav. Brain Sci.*, 15(04):691–700.

Stensola, T., Stensola, H., Moser, M.-B., and Moser, E. I. (2015). Shearing-induced asymmetry in entorhinal grid cells. *Nature*, 518(7538):207–212.

Stewart, M. and Fox, S. E. (1990). Do septal neurons pace the hippocampal theta rhythm? *Trends Neurosci.*, 13(5):163–169.

Stimberg, M., Brette, R., and Goodman, D. F. (2019). Brian 2, an intuitive and efficient neural simulator. *Elife*, 8.

Stroessner-Johnson, H. M., Rapp, P. R., and Amaral, D. G. (1992). Cholinergic cell loss and hypertrophy in the medial septal nucleus of the behaviorally characterized aged rhesus monkey. *J. Neurosci.*, 12(5):1936–44.

Sturz, B. R., Gurley, T., and Bodily, K. D. (2011). Orientation in trapezoid-shaped enclosures: implications for theoretical accounts of geometry learning. *J. Exp. Psychol. Anim. Behav. Process.*, 37(2):246–53.

Sturz, B. R., Kilday, Z. A., and Bodily, K. D. (2013). Does constraining field of view prevent extraction of geometric cues for humans during virtual-environment reorientation? *J. Exp. Psychol. Anim. Behav. Process.*, 39(4):390–396.

Sugaya, K., Greene, R., Personett, D., Robbins, M., Kent, C., Bryan, D., Skiba, E., Gallagher, M., and McKinney, M. (1998). Septo-hippocampal cholinergic and neurotrophin markers in age-induced cognitive decline. *Neurobiol. Aging*, 19(4):351–361.

Suzuki, W. and Naya, Y. (2011). Two Routes for Remembering the Past. *Cell*, 147(3):493–495.

Suzuki, W. A. and Amaral, D. G. (1994). Topographic organization of the reciprocal connections between the monkey entorhinal cortex and the perirhinal and parahippocampal cortices. *J Neurosci*, 14(3 Pt 2):1856–77.

Tanila, H. (1999). Hippocampal place cells can develop distinct representations of two visually identical environments. *Hippocampus*, 9(3):235–246.

Tanila, H., Shapiro, M., Gallagher, M., and Eichenbaum, H. (1997a). Brain aging: changes in the nature of information coding by the hippocampus. *J. Neurosci.*, 17(13):5155–66.

Tanila, H., Sipilä, P., Shapiro, M., and Eichenbaum, H. (1997b). Brain aging: impaired coding of novel environmental cues. *J. Neurosci.*, 17(13):5167–74.

Tapia-Arancibia, L., Aliaga, E., Silhol, M., and Arancibia, S. (2008). New insights into brain BDNF function in normal aging and Alzheimer disease. *Brain Res. Rev.*, 59(1):201–220.

Tatler, B. W., Gilchrist, I. D., and Rusted, J. (2003). The Time Course of Abstract Visual Representation. *Perception*, 32(5):579–592.

Tatler, B. W. and Land, M. F. (2011). Vision and the representation of the surroundings in spatial memory. *Philos. Trans. R. Soc. Lond. B. Biol. Sci.*, 366(1564):596–610.

Taube, J., Muller, R., and Ranck, J. (1990a). Head-direction cells recorded from the postsubiculum in freely moving rats. II. Effects of environmental manipulations. *J. Neurosci.*, 10(2):436–447.

Taube, J. S. (1995). Head direction cells recorded in the anterior thalamic nuclei of freely moving rats. *J. Neurosci.*, 15(1 Pt 1):70–86.

Taube, J. S. (2007). The Head Direction Signal: Origins and Sensory-Motor Integration. *Annu. Rev. Neurosci.*, 30(1):181–207.

Taube, J. S., Muller, R. U., and Ranck, J. B. (1990b). Head-direction cells recorded from the postsubiculum in freely moving rats. I. Description and quantitative analysis. *J. Neurosci.*, 10(2):420–435.

Tenenbaum, J. B., de Silva, V., and Langford, J. C. (2000). A global geometric framework for nonlinear dimensionality reduction. *Science (80-.).*, 290(5500):2319–23.

Thomé, A., Gray, D. T., Erickson, C. A., Lipa, P., and Barnes, C. A. (2016). Memory impairment in aged primates is associated with region-specific network dysfunction. *Mol. Psychiatry*, 21(9):1257–1262.

Thompson, L. T. and Best, P. J. (1989). Place cells and silent cells in the hippocampus of freely-behaving rats. *Journal of Neuroscience*, 9(7):2382–2390.

Tolman, E. C. (1948). Cognitive maps in rats and men. *Psychological Review*, 55:189–208.

Trullier, O., Wiener, S. I., Berthoz, A., and Meyer, J. A. (1997). Biologically-based artificial navigation systems: Review and prospects. *Progress in Neurobiology*, 51:483–544.

Van Cauter, T., Poucet, B., and Save, E. (2008). Unstable CA1 place cell representation in rats with entorhinal cortex lesions. *Eur. J. Neurosci.*, 27(8):1933–1946.

van der Maaten, L. and Hinton, G. (2008). Visualizing Data using t-SNE. *J. Mach. Learn. Res.*, 9(Nov):2579–2605.

Viskontas, I. V., Knowlton, B. J., Steinmetz, P. N., and Fried, I. (2006). Differences in Mnemonic Processing by Neurons in the Human Hippocampus and Parahippocampal Regions. *J. Cogn. Neurosci.*, 18(10):1654–1662.

Vogt, B. A., Finch, D. M., and Olson, C. R. (1992). Functional Heterogeneity in Cingulate Cortex: The Anterior Executive and Posterior Evaluative Regions. *Cereb. Cortex*, 2(6):435–443.

Vogt, B. A. and Pandya, D. N. (1987). Cingulate cortex of the rhesus monkey: II. Cortical afferents. *J. Comp. Neurol.*, 262(2):271–289.

Wernle, T., Waaga, T., Mørreaunet, M., Treves, A., Moser, M.-B., and Moser, E. I. (2018). Integration of grid maps in merged environments. *Nat. Neurosci.*, 21(1):92–101.

Wilber, A. A., Clark, B. J., Forster, T. C., Tatsuno, M., and McNaughton, B. L. (2014).

Interaction of Egocentric and World-Centered Reference Frames in the Rat Posterior Parietal Cortex. *J. Neurosci.*, 34(16):5431–5446.

Wilson, F. A. and Goldman-Rakic, P. S. (1994). Viewing preferences of rhesus monkeys related to memory for complex pictures, colours and faces. *Behav. Brain Res.*, 60(1):79–89.

Wilson, I., Ikonen, S., McMahan, R., Gallagher, M., Eichenbaum, H., and Tanila, H. (2003). Place cell rigidity correlates with impaired spatial learning in aged rats. *Neurobiol. Aging*, 24(2):297–305.

Wilson, I. A., Gallagher, M., Eichenbaum, H., and Tanila, H. (2006). Neurocognitive aging: prior memories hinder new hippocampal encoding. *Trends Neurosci.*, 29(12):662–670.

Wilson, I. A., Ikonen, S., Gallagher, M., Eichenbaum, H., and Tanila, H. (2005a). Age-Associated Alterations of Hippocampal Place Cells Are Subregion Specific. *J. Neurosci.*, 25(29):6877–6886.

Wilson, I. A., Ikonen, S., Gureviciene, I., McMahan, R. W., Gallagher, M., Eichenbaum, H., and Tanila, H. (2004). Cognitive Aging and the Hippocampus: How Old Rats Represent New Environments. *J. Neurosci.*, 24(15):3870–3878.

Wilson, I. A., Ikonen, S., Gurevicius, K., McMahan, R. W., Gallagher, M., Eichenbaum, H., and Tanila, H. (2005b). Place cells of aged rats in two visually identical compartments. *Neurobiol. Aging*, 26(7):1099–1106.

Wilson, M. A. and McNaughton, B. L. (1993). Dynamics of the hippocampal ensemble code for space. *Science*, 261:1055–1058.

Winson, J. (1978). Loss of hippocampal theta rhythm results in spatial memory deficits in the rat. *Science*, 201:160–163.

Witter, M. P. (1993). Organization of the entorhinal-hippocampal system: A review of current anatomical data. *Hippocampus*, 3:33–44.

Witter, M. P., Groenewegen, H. J., da Silva, F. H. L., and Lohman, A. H. M. (1989).

Functional organization of the extrinsic and intrinsic circuitry of the parahippocampal region. *Progress in Neurobiology*, 33:161–253.

Witter, M. P., Naber, P. A., van Haeften, T., Machielsen, W. C., Rombouts, S. A., Barkhof, F., Scheltens, P., and Lopes da Silva, F. H. (2000). Cortico-hippocampal communication by way of parallel parahippocampal-subicular pathways. *Hippocampus*, 10(4):398–410.

Yassa, M. A., Lacy, J. W., Stark, S. M., Albert, M. S., Gallagher, M., and Stark, C. E. L. (2011). Pattern separation deficits associated with increased hippocampal CA3 and dentate gyrus activity in nondemented older adults. *Hippocampus*, 21(9):968–79.

Yassa, M. A., Muftuler, L. T., and Stark, C. E. L. (2010). Ultrahigh-resolution microstructural diffusion tensor imaging reveals perforant path degradation in aged humans in vivo. *Proc. Natl. Acad. Sci. U. S. A.*, 107(28):12687–12691.

Yassa, M. A. and Stark, C. E. (2011). Pattern separation in the hippocampus. *Trends in Neurosciences*, 34(10):515–525.

Yeckel, M. F. and Berger, T. W. (1990). Feedforward excitation of the hippocampus by afferents from the entorhinal cortex: redefinition of the role of the trisynaptic pathway. *Proc Natl Acad Sci U S A.*, 87(15):5832–6.

Zeineh, M. M., Engel, S. A., Thompson, P. M., and Bookheimer, S. Y. (2003). Dynamics of the hippocampus during encoding and retrieval of face-name pairs. *Science*, 299(5606):577–80.

Zhang, K. (1996). Representation of spatial orientation by the intrinsic dynamics of the head-direction cell ensemble: a theory. *J. Neurosci.*, 16(6):2112–2126.

Zhang, S.-J., Ye, J., Miao, C., Tsao, A., Cerniauskas, I., Ledergerber, D., Moser, M.-B., and Moser, E. I. (2013). Optogenetic Dissection of Entorhinal-Hippocampal Functional Connectivity. *Science*, 340(6128):1232627.

Zipser, D. and Andersen, R. A. (1988). A back-propagation programmed network that simulates response properties of a subset of posterior parietal neurons. *Nature*, 331:679–684.

Zola, S. M., Manzanares, C. M., Clopton, P., Lah, J. J., and Levey, A. I. (2013). A Behavioral Task Predicts Conversion to Mild Cognitive Impairment and Alzheimer's Disease. *Am. J. Alzheimer's Dis. Other Dementiasr*, 28(2):179–184.

Zola, S. M., Squire, L. R., Teng, E., Stefanacci, L., Buffalo, E. A., and Clark, R. E. (2000). Impaired recognition memory in monkeys after damage limited to the hippocampal region. *J. Neurosci.*, 20(1):451–63.